Accurate Estimation of Precipitable Water Vapor Using Ground-Based GPS Observation Network and its Data Assimilation into a Mesoscale Numerical Weather Prediction Model

by

Yoshinori Shoji

Acknowledgments

I would like to express my sincere gratitude to Professor Toshitaka Tsuda of Research Institute for Sustainable Humanosphere, Kyoto University for his longstanding and unwavering guidance, as well as for watching over the development of my study with warmth and understanding. I am also profoundly grateful to Dr. Kazuo Saito of the Meteorological Research Institute (MRI) for his encouragement, stimulation to further research, and also his understanding and considerable support over the years.

The late Dr. Hajime Nakamura, the former director of the Numerical Prediction Division (NPD) of the Japan Meteorological Agency (JMA), gave me the overall picture and direction for this research. His knowledge, deep insight, passion, and warm heart promoted mutual understanding among participants of the interdisciplinary GPS/MET JAPAN project. I will never forget the days when I worked with him.

Professor Isao Naito of the National Astronomical Observatory taught me the concepts of space-based geodesy and GPS meteorology. Discussions with Professor Naito gave me a number of hints to improve GPS analysis. He also taught me the importance of having a broader view in my personal life as well as in my research.

I am fortunate to have good and excellent co-researchers in MRI. Dr. Tadashi Tsuyuki, the director of the Forecast Research Department, is our indispensable teacher on data assimilation. Observational studies with Dr. Kazumasa Aonashi generated my interest in water vapor behavior. Dr. Hiromu Seko inspires me with his progressive approaches not only to GPS meteorology but also to a wide range of mesoscale meteorological research. I can not feel anything but gratitude to Dr. Masahiro Hara, Dr. Takuya Kawabata, Dr. Tohru Kuroda, and Dr. Masaru Kunii for their kind support and fruitful discussions.

My results are based on the achievements of my predecessors. In particular, the data assimilation (DA) experiments in this study use the Meso 4D-Var DA system and GPS PWV observation operator that were developed by NPD/JMA. Long-term support and frank discussions with Dr. Nobutaka Mannoji, Dr. Ko Koizumi, and Dr. Yoshihiro Ishikawa of JMA played an essential role in this study. Dr. Koichi Yoshimoto established a practical near real-time (NRT) GPS analysis system. His efforts provided pragmatic information for improving the NRT procedure. Dr. Eiji Ozawa has developed

an operational DA system for GPS radio occultation data. His research brought to my notice the importance of bias correction for both observational data and NWP models.

I am convinced that the results of this research owe much to my research associates in the field of geodesy. Active research on GPS meteorology by Dr. Tetsuya Iwabuchi of the University Corporation for Atmospheric Research (UCAR) provided me with incentives. A review on the relation between GPS signal delay and water vapor by Dr. Ryu Ohtani of the National Institute of Advanced Industrial Science and Technology was the first article I read on GPS meteorology. I learned much from Dr. Hatanaka about issues that needed to be addressed for GPS analysis. I also found from his studies that ways of mitigating errors in GPS water vapor retrieval coincide with those for improving positioning accuracy. When I began my studies, Dr. Ryuichi Ichikawa of the National Institute of Information and Communication Technology was conducting a pioneering study to eliminate atmospheric delay using NWP outputs. His research gave me opportunities to rediscover the possibility of NWP. Through the Mt. Fuji GPS downward looking experiment, Dr. Yuichi Aoyama of the National Institute for Polar Research taught me the benefits of careful preparation.

Jet Propulsion Laboratory (JPL) provided the GIPSY OASIS II software package. This thesis describes the research results obtained by using this software. Dr. Yoaz Bar-Sever of JPL provides much useful advice and suggestions regarding GIPSY analyses. Dr. Jean O. Dickey of JPL always kindly arranged to have time for discussions.

I appreciate the long-lasting support and friendship of Dr. Ying-Hwa Kuo of UCAR. Despite his busy schedule, he always welcomed me and offered warm hospitality. His leadership really comforted and motivated me. Dr. Chris Rocken of UCAR also played a key role in the implementation of this study. Discussions at the COSMIC Office in UCAR were very exciting and fruitful.

Members of Tsuda Laboratory always greet me cordially. Meetings with Dr. Jun-ichi Furumoto and Dr. Hiroo Hayashi give me helpful suggestions.

I also would like to thank Ms. Nami Shibazaki and Ms. Sachiko Shikata for their accurate responses, supports, and kindness over the years.

This thesis is a tribute to all concerned that my study can be summarized here. Although I cannot include all their names, I would like to thank everyone who has contributed to GPS meteorology.

Abstract

This thesis presents a sequence of studies aimed at developing a practical method that uses Global Positioning System (GPS) observations for retrieving information about precipitable water vapor (PWV) in the atmosphere. Then, the results of impact studies of GPS-derived Precipitable Water Vapor (PWV) on mesoscale numerical weather predictions (NWP) in Japan are discussed.

In Japan, the Geographical Survey Institute (GSI) has established one of the densest (placed at a distance of 15–20 km) nationwide ground-based GPS network in the world, with more than 1,200 GPS stations. This network has been termed GEONET (GPS Earth Observation Network). Because of the capability of space-based geodetic techniques used to estimate signal delays caused by atmospheric gases, especially water vapor, GPS has been considered to be a valuable tool for meteorology and climate studies. To establish the use of GEONET as a giant water vapor sensor array, Japanese meteorologists and geodesists launched an interdisciplinary research project "GPS/MET Japan" in April 1997. However, at the start of the project, it was found that there were the following three issues associated with the GPS analysis method.

(1) Ohtani and Naito (2000) compared GPS PWV observations with radiosonde observations for a year and found a negative bias of 2.7 mm in the GPS PWV.

(2) They also found that the PWV derived from GPS agrees well with those derived from the morning launches (08:30 JST or 23:30 UTC) of the radiosonde, but has a negative correlation with an increasing PWV value for nighttime launches (20:30 JST or 11:30 UTC) of the radiosonde.

(3) Several studies have shown that GPS PWV has positive impacts on NWP (e.g., Nakamura et al., 2004a). Such previously conducted studies in Japan mainly used post-processing results in which precise final ephemerides (orbits and clocks) were used. The latency of final ephemerides was approximately 2 weeks. Therefore, there was a need for developing rapid retrieval procedures of GPS PWV, and it was essential to conduct a study to examine the statistical impacts of GPS PWV on NWP.

In the first half of this thesis, we present studies aimed at removing errors in GPS

analysis and at establishing a near real-time (NRT) PWV retrieval procedure. The results can be summarized as follows.

(1) Comparison of GPS PWV and Microwave Radiometer (MWR) observations revealed diurnal and semi-diurnal variations in errors in the GPS PWV results. Further, it was also found that incorporation of an ocean tidal loading (OTL) model in the GPS analysis reduced the amplitudes of these diurnal and semi-diurnal error variations by approximately 60% and 80%, respectively.

(2) Phase center variation (PCV) of a GPS antenna causes bias in GPS-derived PWV. The bias is specific to antenna types, and it sometimes approaches several millimeters. The US National Oceanic and Atmospheric Administration (NOAA) assesses PCV for each antenna type and provides their results as elevation-dependent antenna PCV models. We found that the use of NOAA's antenna PCV models removes most of the PWV biases specific to antenna types.

(3) However, GPS PWV retrieved from two different types of co-located GPS antennae revealed that the bias in GPS PWV varies with amplitude of approximately 1.5 mm and a cycle of several hours. We constructed new site-specific PCV correction maps (Multi-Path Stacking map; MPS map) by stacking one-way postfit phase residuals. The MPS maps describe the dependency of PCV on both the elevation and the azimuth of GPS satellites. The adoption of MPS maps reduced the site specific systematic biases in GPS PWV and resulted in better agreement between GPS PWV and radiosonde observations, with root mean square (RMS) differences of 2.0 mm or less.

(4) The International GNSS Service has been routinely providing ultra rapid orbit (IGU) information about GPS satellites. We found that the accuracy of predicted GPS satellite clock offsets in IGU is insufficient and needed to be corrected in order to retrieve PWV by using precise point positioning (PPP) method. A new satellite clock correction scheme was developed. The scheme utilizes clock information of a ground GPS station which is equipped with hydrogen maser atomic clock. The modified clock information of GPS satellites leads comparable accuracy in retrieved PWV with those obtained by post-processing using precise final ephemerides. This method enables the retrieval of PWV in near real-time (NRT), within several tens of minutes after the observation.

We applied these NRT-retrieved GPS PWV obtained from GEONET to a mesoscale four-dimensional DA (Meso 4D-Var) system of the Japan Meteorological Agency

(JMA). A 12-day continuous DA experiment, from September 1 to 12, 2006, and a DA experiment on the Hokuriku, Kinki heavy rainfall event of July 28, 2008 were performed. In the DA experiment of July 28, 2008, PWV derived from GPS stations in East Asia were assimilated together with the GEONET-derived PWV. Results of these impact studies are presented in the latter half of this thesis. The results can be summarized as follows.

(1) The results of the 12-day continuous DA experiment showed either neutral or some improvement in the precipitation threat score throughout the 18 h prediction period.

(2) The DA experiment of July 28, 2008 showed that assimilation of GEONET-derived PWV led to remarkable improvements in the precipitation predictions.

(3) When PWVs derived from both the GEONET and the GPS over East Asia were assimilated, further improvement in the precipitation predictions was observed. In this case, PWV derived from GPS stations in the Korean peninsula were seemed to play a significant role for water vapor analysis in the windward direction of the strong precipitation system.

(4) As a result of PWV DA, a surface wind and water vapor convergence zone extending from Wakasa Bay towards the west-northwest was enhanced and shifted southward. As a whole, more appropriate environment was reproduced for the formation of cumulus convective clouds around the observed precipitation system. Though GPS PWV is not a dynamical element and limited on land, by assimilate using the Meso 4D-Var, dynamical fields (wind field for example) can also be modified and the increment of water vapor propagates over the ocean. Further, the importance of water vapor information in the windward direction is highlighted.

By following the procedures described above, we have developed an NRT retrieval procedure of PWV from ground-based GPS observations and have confirmed its benefits for mesoscale NWP. On October 28, 2009, JMA started the operational use of PWV derived from GEONET in its mesoscale DA system. The NRT PWV retrieval method which is described in this thesis has been adopted for the operational GPS analysis system of JMA.

Contents

List of Figures

List of Tables

Acronyms and Abbreviations

Acronym	Abbreviation
4D-Var	Four-Dimensional Variational Data Assimilation
AMeDAS	Automated Meteorological Data Acquisition System
AO	Aerological Observatory (Upper sounding station adjacent to MRI)
CHAMP	Challenging Mini-satellite Payload (Germany, USA)
COSMIC/Formosat-3	Constellation Observing System for Meteorology, Ionosphere, and Climate (Taiwan, USA) (Formosat-3 is a name in Taiwan)
CR	Choke Ring
DA	Data Assimilation
DAEJ	IGS ground GNSS network station in Korea
DD	Double Difference
ECMWF	European Center for Medium Range Weather Forecasting
ERA40	ECMWF 40 year reanalysis data set
ERP	Earth Rotation Parameter
Formosat-3	Formosa Satellite Mission #3 (Nominal designation of COSMIC in Taiwan)
Galileo	European GNSS (EU/ESA)
GEONET	GPS Earth Observation Network
GFZ	German Research Center for Geosciences (formerly named Geo Foeschung Zentrum Potsdam)
GLONASS	GLObalnaya NAvigatsionnaya Sputnikovaya Sistema (Russia)
GMS	Geostationary Meteorological Satellite
GNSS	Global Navigation Satellite System (generic for GPS/GLONASS/Galileo)
GOTIC	A program for the computation of OTL effects
GP	Ground Plane
GPS	Global Positioning System (USA)
GPS RO	GPS Radio Occultation
GRACE	Gravity Recovery and Climate Experiment

Acronym	Abbreviation
GSI	Geographical Survey Institute
IGF	IGS final ephemerides
IGR	IGS rapid ephemerides
IGS	International GNSS Service
IGU	IGS Ultra rapid ephemerides
ITRF	International Terrestrial Reference Frame
JAXA	Japan Aerospace Exploration Agency
JMA	Japan Meteorological Agency
JNoVA	JMA Nonhydrostatic model-based 4D-Var system
JPF	JPL final ephemerides
JPL	Jet Propulsion Laboratory
JPR	JPL rapid ephemerides
K_1	Principal solar and lunar combined tidal constituent (angular velocity is 15.041069 degree/hour)
K_2	Principal solar semidiurnal tidal constituent (angular velocity is 30.082137 degree/hour)
LEO	Low Earth Orbit
M_2	Principal lunar semidiurnal tidal constituent (angular velocity is 28.981898 degree/hour)
Meso 4D-Var	JMA hydrostatic model-based 4D-Var system
MetOp	Meteorological Operational Satellite
M_f	Principal lunar long-term tidal constituent (angular velocity is 1.098033 degree/hour)
MIT	Massachusetts Institute of Technology
M_m	Principal lunar long-term tidal constituent (angular velocity is 0.544375 degree/hour)
MPS	Multi Path Stacking
MRI	Meteorological Research Institute
MSM	JMA hydrostatic mesoscale model
MWR	Microwave Water vapor Radiometer (sometimes referred to as "WVR")
N_2	Principal lunar semidiurnal tidal constituent (angular velocity is 28.439730 degree/hour)
NASA	National Aeronautics and Space Administration

Acronym	Abbreviation
NCEP	National Center for Environmental Prediction
NHM	JMA Non-Hydrostatic Model
NOAA	National Oceanic and Atmospheric Administration
NRT	Near-Real Time
NWP	Numerical Weather Prediction
O_1	Principal lunar diurnal tidal constituent (angular velocity is 13.943036 degree/hour)
OSN2	IGS ground GNSS network station in Korea
OTL	Ocean Tidal Loading
P_1	Principal solar diurnal tidal constituent (angular velocity is 14.958931 degree/hour)
PCV	Phase Center Variation (here used for GPS antenna)
PPP	Precise Point Positioning
PWV	Precipitable Water Vapor
Q_1	Principal lunar diurnal tidal constituent (angular velocity is 13.398661 degree/hour)
Radar-AMeDAS	Analyzed rainfall using meteorological radar calibrated surface rain gauge observation
RA-OB	Radiosonde observation
RINEX	Receiver independent exchange format for GPS data
RMS	Root Mean Square
S_2	Principal solar semidiurnal tidal constituent (angular velocity is 30.000000 degree/hour)
SAC-C	Satellite de Aplicaciones Cientificas-C (Argentina, USA)
SPD	Slant Path Delay
S_{sa}	Principal solar long-term tidal constituent (angular velocity is 0.082137 degree/hour)
SUWN	IGS ground GNSS network station in Korea
SYNOP	surface SYNOPtic observation
TZD	Total Zenith Delay
UCAR	University Corporation for Atmospheric Research (Boulder Co, US)
USUD	IGS ground GNSS network station in Saku, Nagano, Japan
UTC	Universal Time Co-ordinated (in practice the same as the Greenwich Mean Time)

Acronym	Abbreviation
UTC	Universal Time Co-ordinated (in practice the same as the Greenwich Mean Time)
WVR	Water Vapor Radiometer (sometimes referred to as "MWR")
ZHD	Zenith Hydrostatic Delay, a part of the zenith propagation delay accurately calculated from the total ground pressure
ZTD	Zenith Total Delay (sometimes referred to as "Total Zenith Delay" or TZD)
ZWD	Zenith Wet Delay (component of the ZTD leftover when the ZHD is removed from the ZTD)

Chapter 1

General Introduction

In this chapter, we first provide a brief overview of the principles and history of GPS meteorology. We then describe the special characteristics of GPS remote sensing and compare them to those of other water vapor observation methods. Third, we discuss the importance of water vapor observation for numerical weather prediction (NWP), and finally, we present the scope and structure of this thesis.

1.1 GPS Meteorology

1.1.1 Basic Principle of Global Navigation Satellite Systems

In recent years, global navigation satellite systems (GNSSs) have been widely used and have become a part of the basic infrastructure for navigation, time transfer, and positioning. The Global Positioning System (GPS) is a representative example of GNSSs and is the first operational GNSS in the world. GPS was developed during the period of 1970–1980 by the United States. Although the system was developed for military applications, GPS signals have been made available to the private sector since December 1993. Since then, the number of scientific and commercial GPS applications has been increasing.

The basic concept of the GPS involves performing range measurements between satellites and receivers by measuring the time required for the GPS signals to reach the receivers. For precise range measurements, GPS satellites are equipped with cesium (Cs) or rubidium (Rb) stable clock oscillators. As of November 2009, 30 GPS satellites have been arrayed in six orbital planes; they transmit timing information at 1.57542 GHz (L_1) and 1.2276 GHz (L_2). At present, because of advanced orbit determination technology, the GPS satellite orbit positions provided by the International GNSS Service (IGS) have accuracies higher than 2.5 cm. Therefore, if the distances of a GPS receiver from more than three GPS satellites are known, its position in three-dimensional space can be

estimated.

1.1.2 GPS Meteorology

Navigation signals are affected by the Earth's atmosphere including the ionosphere, and these effects cause positioning errors. The ionospheric effect depends on the frequency of the radio waves and most of the effect can be eliminated by forming a linear combination of two GPS carrier waves. The signal delay caused by a neutral atmosphere is estimated as one of the unknown parameters by carrying out a GPS analysis. The atmospheric delay is obtained by integrating the refractivity along the ray path, and this refractivity is expressed by an equation that includes the variables of pressure, temperature, and vapor pressure of the neutral atmosphere. Therefore, the possibility of sensing atmospheric conditions using GPS signal delay was advocated in several studies in the 1980s. For example, Askne and Nordius (1987) formulated a relationship between the vertically integrated water vapor amount (precipitable water vapor; PWV) and signal delay in the zenith direction (zenith total delay; ZTD). Davis et al. (1985) introduced the weighted mean temperature, which is used to calculate the proportional coefficient between the PWV and vertically integrated signal delay caused by water vapor (zenith wet delay; ZWD). These studies led to the establishment of a new interdisciplinary research field called "GPS Meteorology" (Bevis et al. 1992; Businger et al. 1996).

Atmospheric sensing by GPS is roughly classified into two primary methods. The first method utilizes data collected by ground-based GPS receivers to retrieve the PWV above a receiver or in the direction of each GPS ray path. The other method monitors the vertical profile of atmospheric refractivity using the signal delay caused when the radio path between a GPS satellite and a GPS receiver in the low Earth orbit (LEO) traverses the Earth's atmosphere. When a LEO satellite observes radio waves from GPS satellites that are occulted behind the Earth, the GPS radio waves transect successive layers of the atmosphere and the ray bending can be analyzed by using the time variations in the signal delays. By integrating the bending angles from the top of the atmosphere, profiles of the refractivity can be obtained. This method is known as the GPS radio occultation (GPS RO) method.

In the mid 1990s, two milestone projects were conducted in the US. One project used ground-based receivers, whereas the other used satellite-borne receivers. In 1994, a GPS observation campaign called "GPS/STORM" was conducted in the central part of the North American continent with six GPS receivers. It succeeded in estimating PWV with a

1.8 mm root mean square (RMS) difference against the observations by radiosondes and microwave water vapor radiometers (MWRs) (Rocken et al., 1995; Duan et al., 1996). In April 1995, "MicroLab 1," which was a small low Earth orbit (LEO) satellite equipped with a GPS receiver, was launched. This LEO satellite observed radio waves from GPS satellites that were occulting behind the Earth. The temperature profiles retrieved from refractivity profiles exhibited an accuracy of better than 0.5 ℃ at the tropopause, with a vertical resolution of approximately 1 km (Ware et al. 1996).

In June 2005, the National Center for Environmental Prediction (NCEP) started the operational use of GPS-derived PWV. With regard to the GPS RO method, following the successful results of GPS RO missions such as CHAMP (Germany) and SAC-C (Argentina), six LEO satellites were launched in April 2006 as a joint project between Taiwan and the US called FORMOSAT-3/COSMIC (F3/C). F3/C observes approximately 1,500–2,000 atmospheric profiles per day. In addition to F3/C, as of February 2010, several GPS RO satellites will be providing atmospheric profiles every day, for example GRACE (launched in 2006), MetOp-A (2008), and Oceansat-2 (2009). A considerable number of new GPS RO missions are now in the planning stages. Several numerical weather prediction (NWP) centers, for example the European Center for Medium-Range Weather Forecasts (ECMWF), NCEP, and Japan Meteorological Agency (JMA), use GPS RO data for operational data assimilation (DA) in the global analysis field of NWP.

1.1.3 GPS/MET JAPAN

To monitor crustal deformation in Japan, the Geographical Survey Institute (GSI) began establishing a nationwide GPS network called GEONET (GPS Earth Observation NETwork) in 1994. Prior to the start of the GEONET service, Japanese geodesists and meteorologists held the first workshop on "GPS Tropospheric Delay" in 1989 at the National Astronomical Observatory, Mizusawa (currently the Mizusawa VLBI Observatory), and recognized the importance of GPS meteorology, following a suggestion by N. Mannoji of JMA. After a year-long feasibility study based on a concept proposed by H. Tsuji of GSI, the Japanese GPS meteorology project "GPS/MET JAPAN" was launched as a five-year project, which continued from April 1997 to March 2002. The objective of this project was to achieve the following two advantages: the assimilation of PWV data obtained from GEONET to improve mesoscale NWP, and an improvement in the space geodetic accuracy based on NWP data (Figure 1.1).

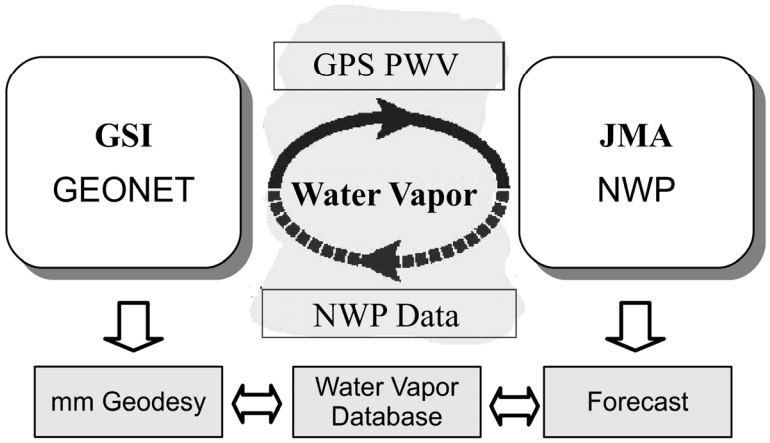

Figure 1.1: Basic concept of "GPS/MET JAPAN" project. The objective of this project was to achieve the following two objectives: the application of PWV data obtained from GEONET to a DA system for numerical weather predictions (NWP) and an improvement in the geodetic accuracy of GPS based on NWP data (Adapted from Shoji et al. 2009b).

At the dawn of the project, statistical evaluations of GEONET-derived PWV data were energetically carried out. From the results of a half-year comparison between GPS PWV data and the data obtained from nearby radiosonde observations, Ohtani and Naito (2000) found that the agreement between the two sets was 3.7 mm in terms of the root mean square (RMS) differences with a mean bias of -2.7 mm. They also found that the mean bias systematically differed, depending on whether the observation time was 12:00 UTC (21:00 JST) or 00:00 UTC (09:00 JST). Furthermore, another two years of comparison at Tsukuba, Japan, revealed seasonal variations in the mean bias. Such bias variations according to day or night and based on the season, are critical from the point of view of variational DA, because the method supposes a Gaussian distribution for the errors in observational data. The series of studies described in this thesis is aimed at reducing these errors to allow the GPS PWV to contribute to NWP.

In spite of the abovementioned issues, the applicability of GEONET-derived PWVs has been proven in studies on the water vapor variations associated with mesoscale meteorological phenomena, such as the passage of weather fronts (Iwabuchi et al. 1997) and thermally induced local circulation (Sasaki and Kimura, 2001). The relation between local circulation and precipitation has also been investigated (e.g., Iwasaki and Miki, 2001; Sato and Kimura, 2005). All of these analyses, however, have attested to the critical necessity of knowing the water vapor variations at the scale of a few kilometers to improve the accuracy of GPS positioning and PWV retrieval. This led researchers to

conduct a dense GPS network campaign with 75 receivers in a quadrate area of 400 km^2 around Tsukuba, Japan. The retrieval method of the slant path delay (SPD) of GPS signals was developed (Shoji et al. 2004; see Appendix B) and tomography analyses of SPD revealed the three-dimensional distribution of water vapor (Seko et al. 2004b; Noguchi et al. 2004).

The impact of GPS derived water vapor information on mesoscale NWP has been thoroughly investigated (Nakamura et al. 2004a; Koizumi and Sato, 2004; Seko et al. 2004c). These studies mainly used GPS PWV data retrieved by GPS analysis using IGS's precise final ephemerides. Shoji (2009) developed an NRT PWV analysis system, which retrieves the PWV data quickly enough to enable the JMA to use the data in the operational mesoscale DA. Using NRT-retrieved PWV, Shoji et al. (2009a) succeeded in predicting heavy rainfall events that JMA's operational mesoscale NWP model (MSM) could not predict well.

On the other hand, an impact assessment of the local-scale atmospheric phenomena on GPS positioning was also carried out using mesoscale NWP outputs (Shimada et al. 2002; Ichikawa et al. 2004; Seko et al. 2004a).

In the early phases of the project, an evaluation study of the temperature profiles retrieved from the first proof of concept GPS RO satellite, "Micro Lab 1," confirmed their high accuracy and high vertical resolution, which were comparable to radiosonde observations. The GPS RO method yielded a global-scale temperature distribution, which shed light on a vertical propagation process involving atmospheric gravity waves in the tropics (Tsuda et al. 2000; Nishida et al. 2000). These results attracted a great deal of international attention and called for the promotion of investigations into the energy sources of quasi-biennial oscillations in the equatorial stratosphere. Furthermore, it was found that atmospheric waves energized by convective activity in the tropics and by mountain regions in the mid-latitudes excited temperature variations in the stratosphere and plasma disturbances in the ionosphere (Hocke and Tsuda 2001a; Hocke and Tsuda 2001b).

Even after the termination of the "GPS/MET JAPAN" project, several other research projects focusing on GPS RO were conducted. In these follow-on projects, the GPS RO technique was applied to retrieve refractivity profiles using GPS signals from occulting satellites observed by receivers inside the atmosphere. This GPS downward-looking method was tested during the summers of 2001–2003 using GPS receivers located at the Mt. Fuji observatory. Aoyama et al. (2004) succeeded in retrieving the fine vertical structures of the refractivity, temperature, and humidity near a typhoon area at altitudes

lower than the receiver. A receiver for the airborne GPS downward-looking observation method was also developed and observation campaigns were conducted in 2004. Yoshihara et al. (2006) succeeded in retrieving refractivity profiles over the ocean. These two results are the world's first successful retrieval cases for GPS downward-looking observations by a receiver at the summit of an isolated mountain and onboard an aircraft, respectively.

DA experiments involving GPS RO data have been performed to evaluate their impacts on both the global and mesoscale NWP models. Ozawa (2007) developed a dynamic bias correction scheme for GPS RO refractivity and confirmed its positive impact on global analysis through continuous month-long DA experiments in summer and winter. To retrieve refractivity profiles from bending angle data, the Abel inversion scheme (Fjeldbo et al. 1971) is commonly used. However, because of the large inhomogeneity of water vapor in the lower troposphere, representative errors increase as the altitude of the signal tangent point decreases. In order to reduce the influence of atmospheric inhomogeneity, Syndargaard et al. (2005) developed a non-local observation operator that traces the refractivity inversion procedure of GPS RO observations using model first guesses. Shoji (2007) evaluated this operator and confirmed that it leads to smaller representative errors in the lower troposphere. Seko et al. (2009a) developed a non-local excess phase operator that assumes linear paths for GPS radio signals. They also took into account the vertical correlation of observational error and succeeded in reproducing a strong precipitation system in a heavy rainfall case that occurred in Hokuriku, Japan in July 2004. Kunii et al. (2009) conducted a DA experiment using GPS RO data acquired by FORMOSAT-3/COSMIC for typhoon USAGI of 2007. They adopted the procedure of Seko et al. (2009a) and succeeded with a realistic prediction of the typhoon development.

Following these results, JMA started using GPS PWV derived from GEONET for mesoscale analyses on October 28, 2009. In addition, JMA also started using GPS RO refractivity profiles in their operational global analyses on November 30, 2009. As of February 2010, 16 years after they became available to the private sector, GPS signals have established a solid position as atmospheric humidity sensors.

1.2 Significance of Water Vapor

Water is an important component of the Earth's environment and greatly affects our lives. Water emits and absorbs heat energy through changes in its temperature and form, i.e., solid, liquid, or gaseous states. Water vapor absorbs infrared thermal radiation from

the Earth and is responsible for approximately 65% of the total greenhouse effect. A global increase in temperature will result in an increase in atmospheric water vapor caused by increases in evaporation and the water vapor holding capacity of the atmosphere. Though water vapor by itself is not responsible for global warming, an increase in water vapor is likely to enhance global warming. Monitoring water vapor amounts over time is important in the study of global warming.

Further, water vapor is an important parameter for short-range weather forecasting. Nowadays, NWP models play an essential role in weather forecasting. NWP models consist of a number of equations that describe the time evolution of atmospheric phenomena expressed by, for example, atmospheric pressure, temperature, humidity, and wind speed. NWP is an initial value problem that requires the accurate initial state of the atmosphere. An increase in water vapor in the lower atmosphere implies an increase in atmospheric instability, which sometimes causes torrential rainfall. Because water vapor is one of the parameters that describe atmospheric conditions in NWP models, monitoring the variation in water vapor is important for weather forecasting and for the mitigation of disasters caused by hazardous heavy rainfall and/or snowfall.

Regardless of its significance, it is difficult to monitor variations in water vapor. The amount of water vapor in the atmosphere is highly variable in space and time. Conventional radiosonde observation has been the main in-situ method of water vapor monitoring, and it is indispensable for analyzing NWP initial fields. However, most of the radiosonde stations are arrayed on land with a horizontal spacing of approximately several hundred kilometers, and the time interval between each radiosonde observation is ordinarily 12 h. Therefore, there is a need and a hope for much denser observations in both time and space.

Methods for observing water vapor have undergone remarkable development during the last quarter century. Microwave and infrared radiation intensities contain information on water vapor and atmospheric temperature. Because of the advances in space-based remote sensing technology, accurate global water vapor observations have recently become available. These technologies are indispensable for both monitoring the Earth's environment and forecasting the daily weather. The practical application of the variational DA method in NWP enables us to use, not only the retrieved humidity information, but also the observed radiation intensity information directly. Further, the upgrading of the information and telecommunication networks facilitates the implementation of GPS in practical weather prediction. The characteristics of water vapor observation methods are summarized in Appendix-A.

1.3 Special Characteristics of GPS Remote Sensing

The theory of GPS remote sensing is described in Chapter 2. Here, we briefly discuss the unique characteristics of the GPS remote sensing method and compare them to those of other water vapor observation methods.

1.3.1 Availability under All Weather Conditions

The first favorable characteristic of GPS remote sensing that can be cited is its robustness. Unlike other remote sensing methods, GPS utilizes the phase of the carrier signal transmitted by GPS satellites, whereas MWR relies on amplitude measurements. This enables GPS remote sensing to utilize a much wider dynamic range of approximately 10^6.

The signal delay of the 19-cm and 24-cm wavelength carriers is affected only by atmospheric refractivity, and unlike in MWR remote sensing, the delay is not affected by liquid water or ice in the atmosphere. The delay due to water vapor is introduced by the permanent dipole moment of water molecules, which is caused by an asymmetric distribution of charge in the molecule. Therefore, in liquid water and ice, the hydrogen bond between water molecules greatly reduces the contribution of the dipole moment to the delay. Space-based MWR measurements are also affected by conditions on the Earth's surface. GPS remote sensing can measure signal delay without being affected by these noise sources for MWR measurements.

1.3.2 Calibration Free and of High Accuracy

The second favorable characteristic of GPS is its inherent stability, which enables it to provide long-term, high-accuracy monitoring without adjustment or calibration. A fundamental characteristic of the GPS system is a high-precision timing estimation method. The GPS carrier phase is referenced to a ground-based hydrogen maser atomic clock that has a stability ($\Delta f/f$) of less than 10^{-14} s. In a signal from a GPS satellite located at the zenith of a receiver, an error of 10^{-14} s is roughly equivalent to an error of 5×10^{-5} mm in PWV. This distinct principle enables GPS to measure PWV with an accuracy of 2–3 mm and allows the GPS RO method to measure the refractive index with an accuracy of 1 %. Meanwhile, space-based MWR sometimes requires frequent in-orbit calibration.

Nakamura et al. (2004b) conducted a cross validation of the PWV data obtained by GPS and two types of radiosondes (Vaisala RS80-A and Meisei RS2-91) and found a dry bias in the RS80-A data. They also tried to clarify the biases in the earlier types of humidity sensors using previously conducted simultaneous observations of GPS and radiosonde data. Their study suggests that the GPS observation method has the potential to be a standard that can be used to test the quality of radiosonde humidity sensors.

1.3.3 High Resolution

Ground-based GPS receivers can reproduce PWV information for every sampling epoch. For positioning purposes, a sampling epoch is commonly set at 30 s. In Japan, we can acquire PWV information with a 15–25 km spacing using GEONET, even though it is limited on land. Because PWV has no vertical information, studies have been conducted to analyze the 3-D water vapor structure by the tomographic technique using SPD (e.g., Seko et al. 2004b; Noguchi et al. 2004).

GPS RO, on the other hand, possesses a high vertical resolution of several tens of meters. The horizontal resolution varies with the height of the GPS signal and becomes several hundred kilometers in the lower troposphere. If we use the approximation that the atmosphere is spherically symmetric, each sample of occultation data can be associated with a point in space whose coordinates are known to within a few meters. However, the asymmetric property of the water vapor in the lower troposphere increases the representative errors in these inverted profiles, and this has become an issue associated with the use of a refractivity profile derived by the GPS RO method in the lower troposphere. Advanced variational DA technology enables the direct assimilation of the phase delay. Several studies have been conducted to develop an observation operator for GPS RO's excess phase delay, and these studies have succeeded in improving mesoscale NWP (e.g., Seko et al. 2009a).

1.3.4 Cost Effectiveness

Another benefit of the GPS measurement technique is its economic feasibility. Ground-based GPS remote sensing can be carried out using commercial dual frequency GPS receivers like ordinary surveying. Even in space-based GPS limb sounding, the payload is much smaller and lighter than those used in other space-based remote sensing instruments. In the Taiwan-US joint mission "Formosat-3/COSMIC," six small satellites with onboard GPS RO instruments were launched by one rocket in April 2006. It can be expected that observations of the global atmosphere by GPS RO will continue to increase

and will become the standard observation tool for climate monitoring as well as NWP.

1.4 Numerical Weather Prediction

The NWP technology is the core and essential for contemporary weather forecasting, as well as atmospheric research. This technology can be roughly divided into two parts: (1) NWP modeling methodologies and (2) DA systems for analyzing the initial state of the atmosphere. Our study's primary objective is to contribute toward the improving the accuracy of NWP. In this section, we briefly describe the outline of the NWP technology.

1.4.1 Numerical Weather Prediction Model

Because atmospheric conditions vary in accordance with physical and dynamical laws, if the atmospheric condition at a specific time is obtained, we can use it as the initial state for predicting future atmospheric conditions using governing equations. In practice, meteorological variables such as pressure, temperature, humidity, and wind velocities in three directions are analyzed and predicted at each spatially discretized finite grid point in the virtual space of computer memory. The method is called "numerical weather prediction (NWP)" because it uses numerical integration. The computer programs used to execute NWP are called NWP models.

Theoretical weather prediction based on physical laws was first proposed by Vilhelm Bjerkness (1862–1951) in the early 1900s and was first attempted by Lewis Fry Richardson (1881–1953) in the early 1920s. After the first success of NWP by Jule Gregory Charney (1917–1981) in 1950, which used a simplified model, NWP models that use fewer approximations have been developed to treat atmospheric phenomena more realistically. From the 1950s to the 1970s, NWP was mostly focused on the prediction of large-scale motions such as planetary waves by using quasi-geostrophic models or balanced models. In the early 1970s, less approximated models were applied for practical use. Though these models assumed hydrostatic equilibrium, they were applied widely to several phenomena at scales ranging from global to regional scales. However, the primitive models cannot be applied to small-scale atmospheric phenomena because the approximation of hydrostatic equilibrium does not hold in the atmosphere involving large vertical motion. Recent progress of computer power has enabled the use of higher horizontal resolutions in the operational mesoscale NWP. Non-hydrostatic models that eliminated the hydrostatic assumption were initially developed as a research tool for the simulation of small-scale meteorological phenomena such as cumulus convection or nonlinear mountain lee waves. Nowadays, several non-hydrostatic models

are used as operational mesoscale NWP models.

JMA started the operational use of mesoscale models (MSMs) in March 2001 using a hydrostatic model with a horizontal spacing of 10 km and 40 vertical layers. In September 2004, the model was updated to a non-hydrostatic model (NHM: Saito et al. 2006; 2007) with a horizontal spacing of 10 km and 40 vertical layers. In March 2006, the model was further updated to a finer grid spacing of 5 km and 50 vertical layers.

1.4.2 Data Assimilation

NWP is an initial value problem; hence, the initial state of the atmosphere is required. To realize a reliable initial state, the so-called "analysis-forecast cycle" is commonly adopted. In this cycle, the predicted state from previously analyzed initial states is modified by the assimilation of observational data to produce another state for subsequent analysis. The observational data density is very sparse compared to the NWP grid density. Furthermore, many in-situ observational data are located over land. The field of remote-sensing DA has advanced remarkably in recent decades. Operational assimilation of satellite-borne remote sensing data now compensates for the shortage of observational data over the oceans. The assimilation of these remotely sensed data became possible by development of variational assimilation methods.

Variational DA is one of the most popular methods of DA; several major world forecast centers have adopted this method for operational NWP. JMA has adopted a four-dimensional DA method for both global and regional analyses. In the variational assimilation method, the optimal atmospheric state is analyzed by minimizing the so-called cost function. The cost function of the three-dimensional variational assimilation (3D-Var) method is shown in equation (1.1). The cost function is defined as the sum of the (weighted) distance between $\boldsymbol{x}$ and background $\boldsymbol{x}^b$ and the (weighted) distance to the observation, $\boldsymbol{y}^o$, as follows:

$$J(\mathbf{x}) = \frac{1}{2}\left\{\left(\mathbf{x}-\mathbf{x}^b\right)^T \mathbf{B}^{-1}\left(\mathbf{x}-\mathbf{x}^b\right) + \left[\mathbf{y}^0 - H(\mathbf{x})\right]^T \mathbf{R}^{-1}\left[\mathbf{y}^0 - H(\mathbf{x})\right]\right\}, \tag{1.1}$$

where $\boldsymbol{x}$ is the model prognostic variable at the initial time and $\boldsymbol{x}^b$ is the first guess for $\boldsymbol{x}$. $\mathbf{B}$ is the background error covariance matrix, H is the observation operator, $\mathbf{y}^o$ is the observation, and $\mathbf{R}$ is the observation error covariance matrix. The first term in the parentheses of right-hand side measures the distance of forecast field $\boldsymbol{x}$ to background $\boldsymbol{x}^b$, and the second term measures the distance to observation $\boldsymbol{y}^o$. The analysis $\boldsymbol{x}$ is obtained by

adding the innovations to the model forecast with weights **W** based on the estimated statistical error covariance of forecast (**B**) and observations (**R**) as follows:

$$\mathbf{x} = \mathbf{x}^b + \mathbf{W}\left[\mathbf{y}^{\mathbf{0}} - H\left(\mathbf{x}^b\right)\right]. \tag{1.2}$$

Generally, observations are not given at model grid points but at observation locations. Satellites do not directly measure the NWP model variables (e.g., temperature, humidity, wind direction and speed, and pressure) but measure physical quantities as radiances, brightness, temperatures, and refractivity. A model equivalent of the observation needs to be calculated to enable a comparison in the observation space. This is done with the observation operator (H). In a simple case the operator, H, may be an interpolation from model grid to observation location, for example, in-situ observations of winds or temperature by radiosondes. In the more complex case, for example, satellite radiances, H may need sophisticated transformations of model variables with the radiative transfer equation.

The four-dimensional variational assimilation (4D-Var) finds the initial condition such that its forecast fits the observations within the assimilation period. In 4D-Var, the cost function $J(\mathbf{x})$ is generalized to include observations at different times, as shown in equation (1.3).

$$J\left(\mathbf{x}_{\mathbf{0}}\right) = \frac{1}{2}\left(\mathbf{x}_{\mathbf{0}} - \mathbf{x}_{\mathbf{0}}^b\right)^T \mathbf{B}^{-1}\left(\mathbf{x}_{\mathbf{0}} - \mathbf{x}_{\mathbf{0}}^b\right) + \sum_{k=0}^{N} \frac{1}{2}\left[\mathbf{y}_k^{\mathbf{0}} - H_k\left(\mathbf{x}_k\right)\right]^T \mathbf{R}_k^{-1}\left[\mathbf{y}_k^{\mathbf{0}} - H_k\left(\mathbf{x}_k\right)\right], \tag{1.3}$$

$$\mathbf{x}_{k+1} = M_k \mathbf{x}_k \quad (k = 0, \cdots, N), \tag{1.4}$$

where $\mathbf{x_0}$ is the model prognostic variables at the initial time and $\mathbf{x}_{\mathbf{0}}^{\boldsymbol{b}}$ is the first guess for $\mathbf{x_0}$. M represents the nonlinear model and k denotes the time steps within the DA period.

In the 4D-Var, the influence of an observation in space and time is controlled by the model dynamics, which increases its realism by disseminating observational information. This is achieved by having the background errors modified by the model dynamics over the assimilation period in a flow-dependent manner.

In March 2002, JMA started a mesoscale four-dimensional variational assimilation system (Meso 4D-Var; Ishikawa and Koizumi 2002; Koizumi et al. 2005). The dynamical core of this system was based on the mesoscale hydrostatic spectral model of JMA (MSM), and the system consisted of a nonlinear forward model and a simplified adjoint model whose horizontal resolution was 20 km. An incremental approach is

employed where the analysis field is formed by an outer model with a horizontal resolution of 10 km. The operational mesoscale DA system was replaced with a non-hydrostatic 4D-Var (JMA non-hydrostatic 4D-Var; JNoVA) system in April 2009 (Honda and Sawada 2009). We use the Meso 4D-Var system in Chapter 4. Specifications of the original system and those used in our study are listed in Table 4.1.

1.5 Scope and Structure of This Thesis

The objective of this thesis is to establish the GPS analysis procedures for a PWV sensor to compensate for the insufficiency in water vapor observations and to evaluate the impact of nationwide dense water vapor information on mesoscale NWP.

As described in subsection 1.1.3, a time varying negative bias was found in GEONET-derived PWV in the early 2000s even though the analysis used IGS final ephemerides (IGF). The latency of the IGF is approximately 2 weeks (12–18 days). The series of studies described in this thesis was aimed at reducing these biases and enabling the timely determination of the GPS PWV data for an operational DA system that contributes to mesoscale NWP. In order to achieve this goal, we examined several trials to remove the error sources in GPS analyses, including the site displacement effect due to ocean tidal loading, antenna phase center variation, multi-path effect, and satellite clock error.

Then, it is necessary to evaluate the impact of the GPS PWV retrieved by the above developed method on mesoscale NWP. Japan is surrounded by the ocean. Kato and Aranami (2005) insisted on the importance of water vapor observations over the ocean. Although the GEONET GPS stations are installed on land, by using 4D-Var and GEONET-derived PWV data, we can expect to modify the fields for the water vapor and other meteorological elements not only on land but also over the ocean.

The structure of this thesis is as follows. Chapter 2 describes the basic theory of GPS and how the atmospheric delay of GPS signals is modeled. Chapter 3 presents possible error sources in GPS remote sensing, along with studies to remove these error sources and validation results. This chapter is divided into three sections: an evaluation of the site displacement effect, construction of site-specific multipath correction tables, and procedure for GPS satellite clock error elimination. The results of these studies enable, not only nationwide, but also global NRT GPS PWV analyses. In Chapter 4, the impacts of GPS-derived PWV on NWP are described. In the first section, the impact of GPS PWV on precipitation prediction is statistically described. In the second section, a DA experiment using a heavy rainfall case from July 28, 2008 is introduced. Finally, in

Chapter 5, we summarize this study and present the conclusions.

In addition, Appendix-A summarizes the methods used for the measurement of water vapor in order to present a clear distinction between the GPS-based method and others. This study focuses on GPS-derived PWV; however, the results of our study are also being used in several research projects related to 3-D water vapor tomography. Therefore, we describe the retrieval procedure for the GPS signal delay along each ray path in Appendix-B.

Chapter 2

Measuring Water Vapor using Space Geodetic Technique

2.1 Basic Methods of Space Geodesy

The Global Positioning System (GPS) is a satellite system used for navigation and positioning. It is mainly designed for navigation, but because the GPS signals are affected by the atmosphere, it is possible to use the GPS system to study the atmosphere.

The system consisted of 24 satellites when the service started in December 1993, and as of February 2010, it consisted of 30 satellites orbiting the Earth at an altitude of approximately 20200 km and an inclination angle of 55°. The GPS satellites transmit at two frequencies: 1575.42 MHz (designated L_1) and 1227.60 MHz (L_2). Codes are modulated onto these carriers. The P-code is modulated on both the frequencies, whereas the C/A-code is modulated only on L_1 (Table 2.1).

Table 2. 1: Frequencies and wavelengths of GPS signals

Carrier		C/A code	P code
L_1	1575.42 MHz (19.0 cm)	1.023 MHz (293 m)	10.23 MHz (29.3 m)
L_2	1227.60 MHz (24.4 cm)	Not modulated	

The GPS carrier phase measurement (φ_i^l) between the receiver i and satellite l for either of the two carrier waves can be expressed by the following observation equation:

$$\varphi_i^l = \rho_i^l + N_i^l\lambda + dT_i^l - dI_i^l + c\times\left(\delta_i - \delta^l\right) + \varepsilon_i , \tag{2.1}$$

where ρ_i^l denotes the range between the GPS satellite l and receiver i; N_i^l, the integer bias referred to as the "phase ambiguity"; λ, the wavelength; c, the speed of light in vacuum; and ε_i, a residual that includes effects such as reflection (multipath reflection)

and phase center instability of the antenna. dT_i^l and dI_i^l represent the propagation delays caused by the neutral atmosphere and ionosphere, respectively, and δ_i and δ^l are the clock offsets of the receiver and satellite, respectively.

By using GPS carrier-phase measurements, GPS analysis software packages are used to estimate unknown parameters including station positions, constant biases, clock offsets, and the signal delay due to the neutral atmosphere. The ionospheric effect in equation (2.1) is eliminated by linearly combining two GPS carrier frequencies. The linear combination is usually referred to as L_c (or L_3). The phase of L_c is expressed as

$$\varphi_{L_C} = \left[\varphi_{L_1} - \frac{f_{L_2}}{f_{L_1}} \varphi_{L_2} \right] \frac{f_{L_1}^2}{f_{L_1}^2 - f_{L_2}^2}, \tag{2.2}$$

where φ_{L_1} (φ_{L_2}) and f_{L_1} (f_{L_2}) are the phase and frequency of L_1 (L_2), respectively. To reduce the number of unknown parameters, GPS software packages assume the atmosphere to be horizontally homogeneous or homogeneous with a first-order gradient term (MacMillan 1995). This simplification allows the atmospheric delay to all visible satellites to be described with a single zenith value (ZTD) and sometimes with two gradient terms.

2.1.1 Two Analysis Strategies

There are two major GPS analysis procedures for unknown parameter estimation: the double difference (DD) procedure (e.g., Hofmann et al. 2000) and the precise point positioning (PPP) procedure (e.g., Zumberge et al. 1997). These two procedures differ in their treatment of the effects of the clock offsets of GPS satellites and receivers.

The DD procedure uses a linear combination of observations from two stations (i, j) and two satellites (l, m) as follows:

$$dd_{i,j}^{l,m} = \left(\varphi_i^l - \varphi_j^l\right) - \left(\varphi_i^m - \varphi_j^m\right). \tag{2.3}$$

This linear combination enables us to cancel out the clock offsets of the abovementioned receivers (i, j) and satellites (l, m). In the PPP procedure, on the other hand, all the satellite clock offsets are estimated once in advance, and the receiver clock offsets are added to receiver-specific unknown parameters. When receiver-specific parameters are analyzed, the pre-estimated satellite clock offsets are fixed as a known

parameter.

In both the procedures, one can estimate the GPS signal delay caused by the neutral atmosphere as an unknown parameter. In the DD procedure, when we analyze a small network of GPS receivers with the distance between the GPS receivers at each end being less than several hundred kilometers, the differential delay is sensitive only to the relative value of the zenith delay at each receiver position. However, by forming a wide network of GPS receivers (covering a distance larger than 500 km), we can resolve the absolute value of the atmospheric delay at each receiver. Duan et al. (1996) adopted the DD strategy and derived the precipitable water vapor (PWV) at GPS stations with root-mean-square (RMS) differences of 1.0~1.5 mm in comparison with the values recorded by water vapor radiometers. In the PPP procedure, the accuracy of the derived PWV highly depends on the accuracy of the predetermined satellite positions and satellite clock offsets. Shoji et al. (2004) estimated the PWV at GPS stations by using PPP with the final orbits and clocks provided by the International GNSS Service (IGS). Comparison with a nearby radiosonde observation showed RMS differences of 2.0 mm or less. However, as described later, the PPP procedure retrieves the PWV with poor accuracy when using the ultra rapid orbit of the IGS (IGU).

With regard to the computational cost, the PPP procedure is economically feasible. In the DD procedure, all observation equations are coupled through GPS satellite orbits, GPS satellite clocks, and Earth orientation parameters. Hence, to estimate unknown parameters such as site coordinates and signal delays, a design matrix of parameter estimations must include all parameters at all sites. Therefore, the computational cost increases dynamically with the number of GPS sites. On the other hand, in the PPP procedure, by setting the satellite clock offsets to previously estimated values, each observation equation is uncoupled and this enables us to determine unknown parameters at each site independently. According to Zumberge et al. (1997), the computational cost of the DD procedure is order of the third power of the number of GPS stations, whereas that of the PPP procedure increases linearly with the number of GPS stations. Therefore, in view of the computational burden of analyzing more than 1200 GPS stations, we adopt the PPP procedure in this study.

2.1.2 Basic Concept of PPP Procedure

Suppose that n satellites are simultaneously observed from a GPS receiver i and an ionosphere-free linear combination of L_1 and L_2 is used. The observation model of the PPP is then given as

$$\begin{pmatrix} \varphi_i^1 \\ \varphi_i^2 \\ \vdots \\ \varphi_i^n \end{pmatrix} = \begin{pmatrix} \rho_i^1 + N_i^1\lambda + dT_i^1 + c\times\left(\delta_i - \delta^1\right) + \varepsilon_i \\ \rho_i^2 + N_i^2\lambda + dT_i^2 + c\times\left(\delta_i - \delta^2\right) + \varepsilon_i \\ \vdots \\ \rho_i^n + N_i^n\lambda + dT_i^n + c\times\left(\delta_i - \delta^n\right) + \varepsilon_i \end{pmatrix}. \tag{2.4}$$

The unknown parameters estimated in this study are

$$x = \left(r_i,\ \delta_i,\ ZWD_i,\ G_{ni},\ G_{ei},\ N_i^1,\ N_i^2,\ \ldots\ ,\ N_i^n\right), \tag{2.5}$$

where r_i is the receiver position and G_n and G_e are the first-order gradients of atmospheric delay in the north-south direction and east-west direction, respectively. In this study, the time variation of δ_i is modeled as a white-noise process and those of *ZWD*, G_n, and G_e are modeled as random-walk processes. Hereafter, we refer to these three parameters as atmospheric parameters. The random-walk sigma is set as 0.17 mm/s$^{1/2}$ for *ZWD* and 0.03 mm/s$^{1/2}$ for G_n and G_e. Atmospheric delay (dT_i^l) is expressed as

$$dT_i^l = m\left(\theta^l\right)\cdot\left(ZTD_i + cot\theta^l\left(G_{ni}cos\phi^l + G_{ei}sin\phi^l\right)\right), \tag{2.6}$$

where θ and ϕ denote the elevation and azimuth angle of each satellite, respectively. m(θ) is the mapping function.

ZTD can be expressed as a sum of *ZWD* and *ZHD*:

$$ZTD = ZWD + ZHD\ . \tag{2.7}$$

ZHD is calculated from the station altitude and is regarded as a constant throughout the analysis.

$$ZHD\ = 1.012\ \cdot 2.27\ \cdot \exp\left(-\ 0.116\ \cdot 10^{-3}\ \cdot\ Alt\right), \tag{2.8}$$

where *Alt* denotes the station altitude in meters.

In the PPP analysis, satellite clock offsets (δ^l) are treated as known parameters. One simple approach to acquire these data is to use the IGS final ephemerides (IGF). In practice, the relative clock differences of all satellite pairs should be predetermined accurately but absolute satellite clock offsets are not necessarily needed. Furthermore, as described in section 3.4, our study shows that even if the relative clock differences of satellites have some biases, as long as the time variation of the relative clock differences

are maintained constant during the analysis period, it is possible to retrieve the PWV with an accuracy comparable to that obtained by GPS analysis using final precise orbits and clocks.

2.2 Radio Wave Propagation

The atmosphere is a dielectric medium. When a dielectric is placed in an electric field, only a slightly shift of electric charges from the average equilibrium positions causes dielectric polarization. In the neutral atmosphere, the dielectric constant of air (ε) is greater than 1 and the magnetic permeability of air (μ) is approximately 1. Hence, the speed of a radio wave in the atmosphere is less than that in a vacuum. The effect can be described using the refractive index n, which is defined as

$$n = \sqrt{\varepsilon\mu} = \frac{c_0}{c} > 1, \tag{2.9}$$

where c_0 and c represent the speed of light in a vacuum and that in the atmosphere, respectively. Therefore, it takes δt longer for the signal to traverse the atmosphere than it would take the signal to traverse the same distance in a vacuum. The delay is often measured in a unit of length as $\Delta T = c_0 \delta t$. The delay varies primarily with the elevation (θ) and to some extent with the azimuth (ϕ) of the signal as

$$dT_i^l(\theta,\phi) = \int n ds - G = \int (n-1) ds + S - G, \tag{2.10}$$

where S is the true path of the refracted signal and G is the geometric path. The first term on the right-hand side of equation (2.10) is the delay of the signal due to the reduced speed, whereas the second term is the "geometric delay" due to the bending of the signal. The geometric delay can be ignored for an elevation angle above 15° but is 10 cm for an elevation angle of 5°. Both the terms are taken into account through a mapping function discussed in section 2.3.

The refractive index n is often expressed for convenience by means of the refractivity N as

$$N = 10^6 (n-1), \tag{2.11}$$

and thus, ignoring the geometric delay term, equation (2.10) can be rewritten in the form

$$dT_i^l(\theta,\phi) = 10^{-6}\int N(s)ds\,. \tag{2.12}$$

The refractive index of a mixture of nonpolar gases is given by the Lorentz-Lorenz equation as

$$\frac{n^2-1}{n^2+2} = \sum_i \frac{N_i\alpha_i}{3\varepsilon_0}, \tag{2.13}$$

where N_i is the number of molecules per unit volume and α_i is the mean polarizability of the ith component of the mixture. The left-hand side of equation (2.13) can be approximated as

$$\frac{n^2-1}{n^2+2} \approx (n-1)\left[1-\frac{n-1}{6}\right]^{\frac{2}{3}} \approx n-1. \tag{2.14}$$

The general equation for the radio refractivity of air becomes

$$N = (n-1)\cdot 10^6 = K_1\frac{P_d}{T}Z_d^{-1} + K_2\frac{P_w}{T}Z_w^{-1} + K_3\frac{P_w}{T^2}Z_w^{-1}, \tag{2.15}$$

where P_d (hPa) is the partial dry air pressure, P_d is the partial water vapor pressure, and T (K) is the temperature. Z_d^{-1} and Z_w^{-1} are the inverse compressibility factors for dry air and water vapor, respectively, introduced by Owens (1967) to account for the nonideal behavior of the atmospheric constituents. The first term of equation (2.15) accounts for the induced dipole moment of dry constituents of the atmosphere. The second and third terms account for the induced and permanent dipole moments of the water vapor in the atmosphere, respectively (Davis et al. 1985). Thayer (1974) noted that the omission of compressibility factors leads to errors in the radio wave refractivity of 0.04 ppm in the dry term and 0.1 ppm in the wet term at high humidity.

Several values for the constants K_1, K_2, and K_3 have been determined theoretically or by fitting observed atmospheric data. For example, Boudoris (1963) measured indices of refraction for both dry air and water vapor using a cavity spectrometer for pressures between 0 and 1013 hPa and temperatures between 273 and 323 K. The resulting coefficients were

$$\left.\begin{array}{ll} K_1 : 77.60 \pm 0.008 & \text{K/hPa} \\ K_2 : 71.98 \pm 10.82 & \text{K/hPa} \\ K_3 : (3.754 \pm 0.036) \times 10^5 & \text{K}^2\text{/hPa} \end{array}\right\}. \tag{2.16}$$

In this thesis, we derive the PWV from the estimated ZTD using equation (2.15) with coefficients (2.16) and ignoring the compressibility factors. Details are given in section 2.4.

2.3 Modeling of Atmospheric Effect

When working with atmospheric delays, it is often convenient to normalize all delays to a common direction, normally the zenith direction. If we assume that there are no horizontal variations in the atmospheric refractivity, we can relate the delay experienced by a radio signal from a satellite observed at elevation angle θ to the delay the signal would have experienced if the satellite was located in the zenith direction of a receiver. The relation is often expressed using a mapping function $m(\theta)$:

$$dT_i^l(\theta) = m(\theta) ZTD \,, \tag{2.17}$$

where *ZTD* is the atmospheric delay in the zenith direction. If we make the approximation that the earth is flat, it is easily shown that $m(\theta) = 1 / \sin\theta$. Because this simple mapping function does not consider the earth's curvature, there will be a large error in the slant delay for a low elevation angle.

On the basis of ray tracing using a global radiosonde profile, Niell (1996) developed a new mapping function that takes into account the seasonal and latitudinal dependences of the mapping function. The Niell mapping function (NMF) is divided into wet and dry parts. The total delay can be written as

$$dT_i^l(\theta) = m_w(\theta) ZWD + m_h(\theta) ZHD \,, \tag{2.18}$$

where *ZWD* and *ZHD* are the zenith wet delay and zenith hydrostatic delay, respectively (Details are described in section 2.4.). These delays are transformed into delays in the zenith direction by using a wet mapping function (m_w) and hydrostatic mapping function (m_h) as independent mapping functions. These two mapping functions utilize the same form of equation as shown below:

$$m(\theta) = \frac{1 + \dfrac{a}{1 + \dfrac{b}{1 + c}}}{\sin\theta + \dfrac{a}{\sin\theta + \dfrac{b}{\sin\theta + c}}}. \tag{2.19}$$

In the Niell hydrostatic mapping function (NMF_h), the coefficients a, b, and c are functions of the site latitude, site altitude, and day of year, whereas in the Niell wet mapping function (NMF_w), these coefficients are functions only of the site latitude. The NMF_h and NMF_w are accurate to approximately 1% down to an elevation angle of approximately 3° (Niell, 1996).

Recently, on the basis of ray tracing using the 40-year re-analysis atmospheric field product (ERA-40) produced by the European Center for Medium-Range Weather Forecasting (ECMWF), Boehm et al. (2006) constructed a new mapping function that expresses dependencies of the mapping function on the site latitude, site altitude, day of year, and site longitude. The mapping function is named the global mapping function (GMF) and its use has spread rapidly in the field of space geodesy.

Under certain atmospheric conditions such as the passage of weather fronts or other mesoscale phenomena, it is more appropriate to model the distribution of the refractivity due to the locally asymmetric atmosphere. MacMillan (1995) developed the gradient mapping function, which takes into account the effect of the horizontal gradient of refractivity. The slant path delay (SPD) then becomes

$$dT_i^l(\theta,\phi) = m(\theta)\cdot\left[ZTD + \cot\theta\left(G_n\cos\phi + G_e\sin\phi\right)\right], \tag{2.20}$$

where G_n and G_e are the delay gradients in the north and east directions, respectively.

In this thesis, we mainly use the gradient mapping function, which takes the NMF as $m(\theta)$.

2.4 Relation Between Signal Delay and Water Vapor

According to Askne and Nordius (1987), the *ZTD* can be expressed as

$$ZTD = 10^{-6}\left[\frac{K_1 R}{g_m M_d}P_s + \int_H^{\infty}\left[\left(K_2 - K_1\frac{M_w}{M_d}\right)\frac{P_w}{T} + K_3\frac{P_w}{T^2}\right]dz\right], \tag{2.21}$$

where P_s is the total surface pressure, R is the molar gas constant (8.314 J/(mol K)), and M_d and M_w are the molar masses of dry air and water, respectively. g_m (m/s^2) is the gravitational acceleration at the mass center of a vertical column of the atmosphere, and is expressed as

$$g_m = \frac{9.784}{1 - 0.00266\cos 2\Phi - 0.00028H}, \tag{2.22}$$

where Φ is the latitude and H is the height in kilometers with respect to the geoid.

Thus, the *ZHD* (the first term on the right-hand side of equation (2.21)) can be expressed as a function of surface pressure (P_s), Φ, and H:

$$ZHD(P_s, \Phi, H) = \frac{0.0022768 P_s}{1 - 0.00266\cos 2\Phi - 0.00028H}. \tag{2.23}$$

The *ZWD* can then be calculated by substituting $ZHD(P_s,\Phi,H)$ from the GPS-derived ZTD.

The *PWV* is the vertically integrated water vapor and is a quantity often used in meteorology. It is defined as

$$PWV = \frac{\int_0^\infty \rho_v(z)dz}{\rho_w}, \tag{2.24}$$

where $\rho_v(z)$ is the water vapor density at height z and ρ_w is the density of water.

According to Askne and Nordius (1987), the *ZWD*, which can be estimated by GPS analysis, is proportional to the *PWV*:

$$PWV = \Pi \cdot ZWD, \tag{2.25}$$

$$\Pi = \frac{10^5}{R_v\left(k_2 - k_1\frac{m_v}{m_d} + \frac{k_3}{T_m}\right)}, \tag{2.26}$$

$$T_m = \frac{\int \frac{P_v}{T} dz}{\int \frac{P_v}{T^2} dz}, \tag{2.27}$$

where R_v is the water vapor gas constant, m_v and m_d are the numbers of moles of water vapor and dry air, respectively, T is the temperature at a given height, and T_m is the mean temperature of the atmospheric column weighted by the amount of water vapor at that height.

The proportional coefficient Π averages out to 0.15, but it varies by approximately 15% depending on the geographical and weather conditions at the site of a GPS antenna. Because a major amount of water vapor exists in the lower troposphere, it is expected that T_m is highly correlated with the surface temperature at the site of a GPS antenna. On the basis of results obtained from two years of radiosonde observations, Bevis et al. (1992) concluded that T_m can be estimated from the surface temperature, with an accuracy sufficient for practical purposes, as $T_m = 0.72Ts + 70.2$ (Figure 2.1). Their result is based on radiosonde observations in North America including Alaska. We evaluated the relation obtained by Bevis et al. using data from 20 Japanese radiosonde stations to determine a more appropriate relation for Japan (Figure 2.2). The results show certain differences between the linear regressions. As shown in Figure 2.1, when the surface temperatures are lower than 260 K, the inclination of the regression equation is reduced. Most of these data may have been obtained in Alaska. The result suggests that using the relation of Bevis et al. for Japanese GPS stations may result in an underestimation of the *PWV* when the surface temperature is higher than 290 K and may result in an overestimation when the surface temperature is lower than 280 K.

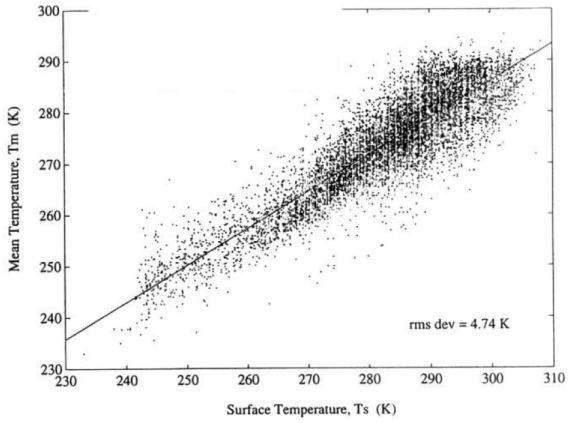

Figure 2. 1: Relationship between T_m and $T_{surface}$ determined from analysis of radiosonde profiles acquired from fall of 1989 to fall of 1991. The solid line represents the linear regression through all the data points. The profile is based on data obtained from 13 stations in the United States; the latitudes range includes regions from Fairbanks, Alaska, to West Palm Beach, Florida. (Adapted from Bevis et al. 1992.)

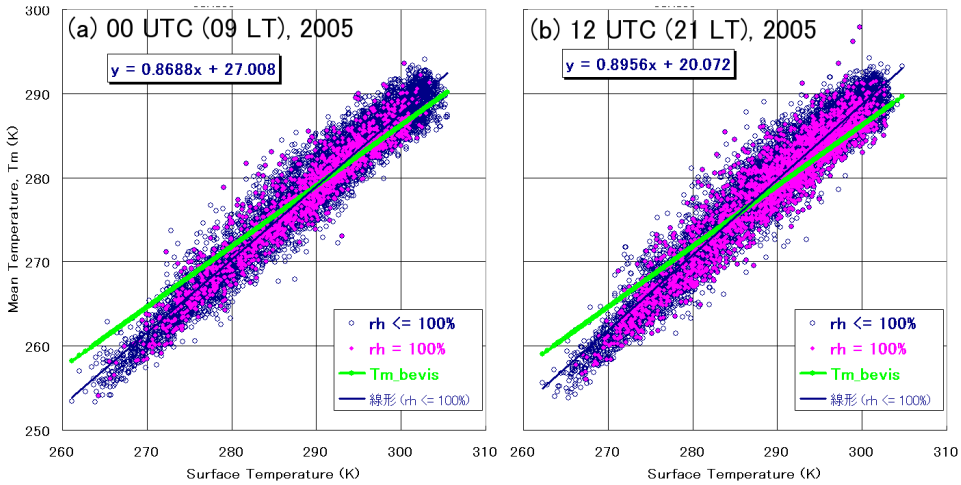

Figure 2. 2: Relationship between T_m and $T_{surface}$ determined from analysis of radiosonde profiles acquired in Japan in 2005. Blue open circles represent all data, whereas peach-colored filled circles highlight the cases with 100% relative humidity at the surface. Panel (a) represents the results obtained from daytime (09:00 h in Japan) observations, whereas panel (b) shows nighttime (21:00 h) data. The solid blue line in each panel represents the linear regression derived from the scatter plot. The green line represents the relationship acquired by Bevis et al. (1992).

Chapter 3

Improvements in GPS-derived PWV

3.1 Introduction

The Japanese GPS meteorology project "GPS/MET JAPAN" was launched in 1997 as a five-year project that would extend from April 1997 to March 2002. At the start of the project, the accuracy of PWV data obtained from GEONET was statistically tested by comparing it with PWV data derived from GPS and other observations, such as the data obtained from radiosonde and ground-based microwave water vapor radiometers (MWR).

At the start of the project, the following three issues were associated with GPS analysis.

(1) Ohtani and Naito (2000) compared GPS PWV observations with radiosonde observations for a year and found a negative bias of 2.7 mm in the GPS PWV.

(2) They also found that the PWV derived from GPS agreed well with those derived from the morning launches (08:30 JST or 23:30 UTC) of the radiosonde; however, it had a negative correlation with an increasing PWV value for nighttime launches (20:30 JST or 11:30 UTC) of the radiosonde.

(3) Several studies have shown that GPS PWV has positive impacts on NWP (e.g., Nakamura et al., 2004a). Such previously conducted studies in Japan mainly used post-processing results in which precise final ephemerides (orbits and clocks) were used. The latency of final ephemerides was approximately 2 weeks. Therefore, there was a need for developing rapid retrieval procedures for GPS PWV, and it was essential to conduct a study to examine the statistical impacts of GPS PWV on NWP.

In this chapter, we present studies aimed at eliminating errors in GPS analysis and at establishing a near real-time (NRT) PWV retrieval procedure. This chapter is divided into three sections. In section 3.2, the evaluation results of the effect of site displacement due to ocean tidal loading (OTL) are presented. In section 3.3, the construction of

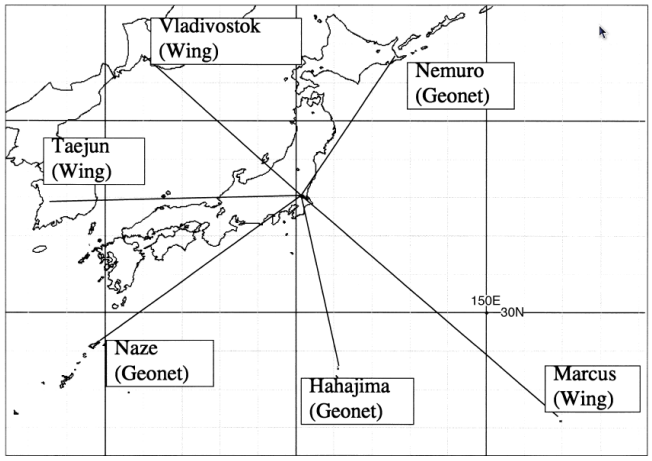

Figure 3. 1: GPS analysis network used in Bernese Ver. 4.0. GEONET is the operational GPS network site of the Geographical Survey Institute, and Wing is the Western Pacific Integrated Network of GPS. (Adapted from Shoji et al. 2000)

Table 3. 1: Specifications of GPS analysis

Ionosphere Correction	LC combination.
GPS satellite orbits and clocks	JPL final analysis
Earth-rotation parameters	IGS
Antenna PCV correction	IGS's PCV model
Elevation cut-off	15°
Sampling rate	30 s
Mapping function	NMF (Niell, 1996)
A priori sigma for L1 and L2	1cm
Elevation dependent weight	Not assigned
Solid earth tide model	Williams 1970
Ocean Tidal Loading	No model | Shwiderski 1981 (Calculated by GOTIC)
Interval of ZTD estimation	5-min.

site-specific multipath correction tables and validation results are described. In section 3.4, the procedure for GPS satellite clock error elimination is presented. The results of these studies clearly indicate an improvement in PWV accuracy and the applicability of GPS PWV for operational NWP.

3.2 Evaluation of Positioning Error Effect on PWV Analysis

3.2.1 Result of the Campaign Observation from July 22 to August 1, 1997

In order to evaluate the accuracy of GPS-estimated PWV and to diagnose its temporal variations, the GPS/MET Japan" project conducted a series of preliminary

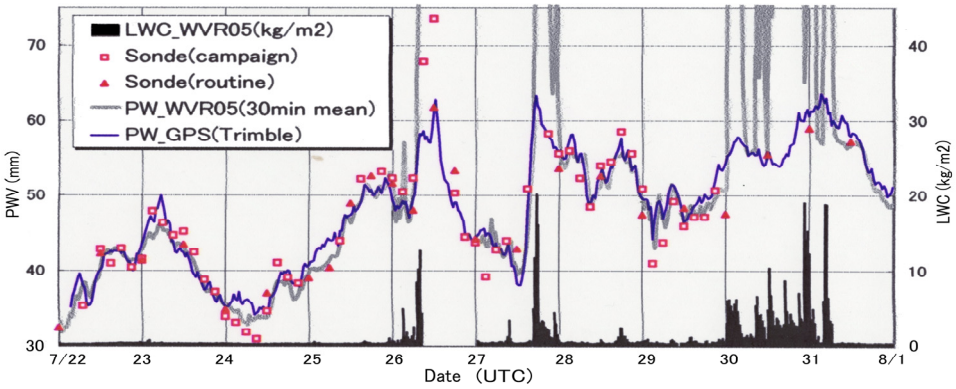

Figure 3. 2: Time series of PWVs obtained using observations by radiosondes (open triangles and open squares), MWR (gray thick line) and GPS (blue line) at MRI from July 22 to 31 1997. (Reproduced from Shoji et al. 1999)

GPS observations from July 22 to August 1, 1997 in which observations by GPS, radiosondes, and a water vapor radiometer were performed. MRI launched a RS80-A radiosonde every 3 h at around 00:00, 03:00, 06:00, 09:00, 12:00, 15:00, 18:00, and 21:00 UTC, and the Aerological Observatory (AO), which is located adjacent to MRI, cooperated by launching an operational JMA RS2-91 radiosonde every 6 h at 00:00, 06:00, 12:00, and 18:00 UTC.

The first GPS analysis attempted the use of the so-called “absolute method (Duan et al. 1996)” with the Bernese Ver. 4.0 software (Rothacher and Mervart 1996). To separate ZTDs at each station, 7 baselines longer than 900 km were added to the analysis network (Figure 3.1).

In this analysis, the ocean tidal loading (OTL) effect was not considered (Table 3.1) because the Bernese Ver. 4.0 did not include any OTL model. GPS PWV showed good agreement with those observed by radiosonde and MWR (Figure 3.2), however, on closer inspection, a periodic variation in the differences was found (Figure 3.3).

To clarify the cause of the periodic difference, we conducted a two month collocated observation of GPS and MWR from May 1 to June 30, 1998 at MRI.

3.2.2 Result of a Two Months Collocated Observation of GPS and MWR

In order to detect the characteristics of PWV difference between GPS and MWR, simultaneous observations involving GPS and an MWR were conducted at the Meteorological Research Institute (MRI) in Tsukuba for 2 months from May 1 to June 30, 1998.

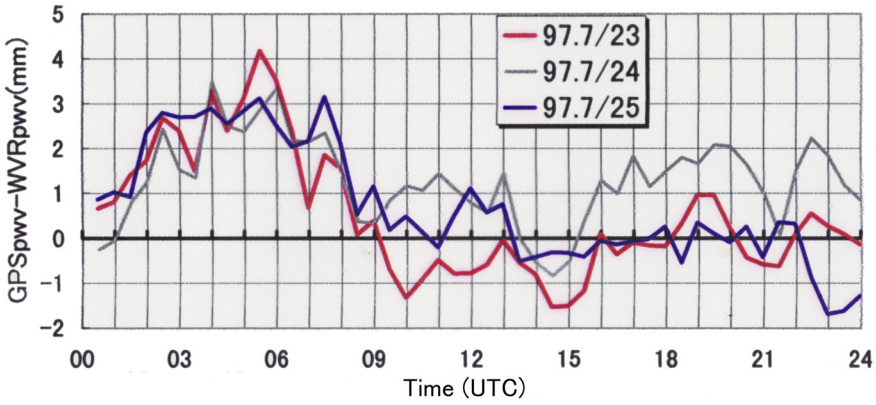

Figure 3. 3: Composite time series of GPS PWV differences against MWR from 23 to 25 July 1997. (Reproduced from Shoji et al. 1999)

Table 3. 2: Amplitude and phase of 11 main tidal components of site displacement due to OTL at MRI calculated by GOTIC. (Adapted from Shoji et al. 2000)

	U-D	N-S	E-W	U-D	N-S	E-W	
	amplitude (mm)			phase (degree)			period
Ssa	0.97	0.07	0.29	285.63	99.37	260.31	4382.911 h
Mm	0.49	0.08	0.08	223.99	24.91	208.02	661.309 h
Mf	0.17	0.04	0.04	170.52	237.14	148.08	327.859 h
Q_1	1.72	0.23	0.35	198.04	−122.09	−12.84	26 h 52 m 06.1 s
O_1	8.44	1.27	1.72	203.33	−108.30	−10.09	25 h 49 m 09.6 s
P_1	3.33	0.52	0.69	−137.58	−86.95	9.82	24 h 03 m 57.2 s
K_1	10.77	1.72	2.17	−137.51	−88.81	10.01	23 h 56 m 04.1 s
N_2	1.25	0.36	0.37	69.77	−91.63	−200.69	12 h 39 m 30.1 s
M_2	8.27	1.91	3.01	55.14	−83.21	−187.22	12 h 25 m 14.2 s
S_2	4.25	0.76	1.40	77.74	−67.14	−146.80	12 h 00 m 00.0 s
K_2	1.20	0.24	0.38	−279.08	−61.60	−145.07	11 h 58 m 02.0 s

The ZTD was estimated every 5 min using the precise point positioning method with the GIPSY/OASIS-II software package (GIPSY) (Webb and Zumberge, 1993). Specifications of the GPS analysis are listed in Table 3.1. At first, no OTL model was used. GPS PWV was then derived from ZTD with observed surface pressure and temperature. The GPS PWV was compared to the MWR-derived PWV (hereafter referred to as MWR PWV). The root mean square (RMS) difference between the GPS PWV and the MWR PWV was less than 1.5 mm during the project period for no-rain cases.

However, it was found that the difference between GPS PWV and MWR PWV

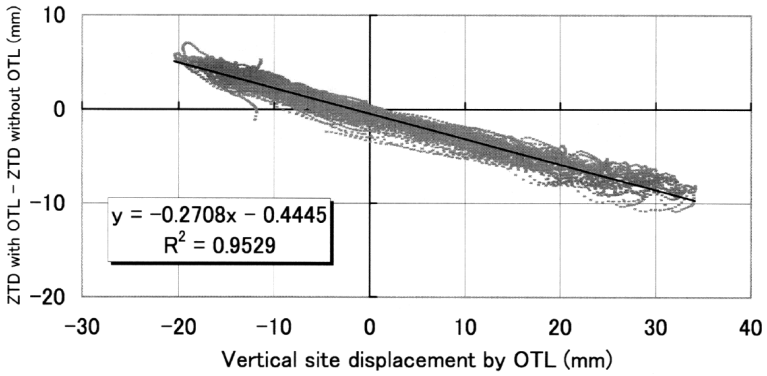

Figure 3. 4: A scatter diagram of difference in ZTDs (with OTL - without OTL) to vertical site displacement for project data from May 1 to June 30, 1998 at MRI. The straight black line represents the result of linear regression. (Adapted from Shoji et al. 2000)

(hereafter referred to as dPWV) sometimes increased, reaching 3–4 mm. This large amplitude of dPWV constitutes a serious problem for meteorological application. It was found that the temporal variation pattern of the dPWV with 3–4 mm amplitude can be classified into (1) semi-diurnal and diurnal oscillations and (2) shorter time variations of 2 to 3 hours.

Ocean tides induce periodic deformations of the Earths surface which is referred to as ocean tide loading (OTL). In Japan, the treatment of the OTL effect is crucial when modeling site position because the Japan Islands are surrounded by ocean. Spatial variation of site displacement due to OTL effect is very large because of its sensitivity to the distance from the ocean, depth of the sea and geographical features of the shore. For example, amplitudes of M_2 component range from 5 mm to 2 cm within Japan (Sengoku and Sato 1995). In GIPSY, the displacement of a site coordinate Z_j (t) due to OTL at a station j at arbitrary time t can be given as the sum of the OTL components as follows,

$$\Delta Z_j(t) = \sum_{i=1}^{N} A_i^j \cos\left(\omega_i t + V_i - \delta_i^j\right), \tag{3.1}$$

where ω_i is the frequency of i-th tidal component, V_i is the astronomical argument, and A_j^i and δ_j^i are amplitudes and Greenwich phase lag, respectively. The amplitude and phase lag at our project site in Tsukuba was calculated with a program for OTL effect computation named “GOTIC” (Sato and Hanada 1984). The GOTIC can evaluate the loading effects for 11 main tidal constituents by using Schwiderski’s ocean tidal model (Schwiderski, 1981). The accuracy of topographic maps employed in GOTIC is about

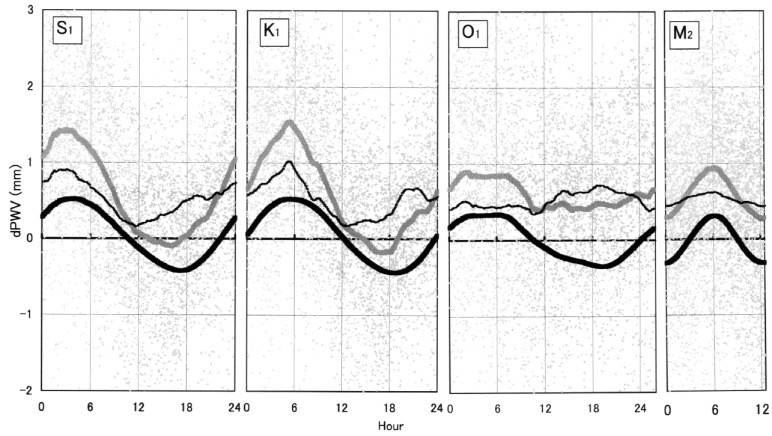

Figure 3. 5: Composite time series of dPWV and the $dPWV_{simulated}$ by S_1, K_1, O_1, and M_2 periods. Thick gray lines are composite time series of dPWV without OTL, thin black lines are composite time series of dPWV with OTL, and thick black lines are composite time series of $dPWV_{simulated}$. Gray dots are dPWV without OTL before averaging. (Adapted from Shoji et al. 2000)

0.5 minutes of arc (roughly about 1 km) for any place in Japan. The integral method is used to take into account the effect of the finite area of the meshes near the station. Table 3.2 gives A_j^i and δ_j^i computed for MRI.

Beutler et al. (1988) showed that in case of satellite elevation cut off angle is set to 20 degrees, 1 mm estimation error of ZTD causes 2.9 mm error in the estimation of vertical site coordinate. This also implies that, if there is an error in the vertical coordinate due to neglect of the OTL effect, an error will result in ZTD. To confirm this relation for our case, we calculated the difference in the ZTDs analyzed with and without OTL. Then we compared it to the vertical component of site displacement calculated from 11 OTL components. Figure 3.4 shows that a good linear relationship exists between them. The magnitudes of ZTD difference were 27% of those of the vertical site displacement due to OTL. Hereafter, as a reference for error evaluation, we will use "$dPWV_{simulated}$" which was calculated from vertical site displacement due to 11 components of the OTL,

$$dPWV_{\text{simulated}} = \text{UD} \times 0.27 \times \Pi\,, \tag{3.2}$$

where UD is the vertical site displacement due to OTL effect, and Π is the conversion coefficient from ZWD to PWV.

To study the relation between dPWV and the effects of each component of the OTL, we separate the two months of data into small time series data with a period of an OTL component and then average the small time series data to get a composite time series

Table 3. 3: Comparison of GPS PWV to WVR PWV during the project period from May 1 to June 30, 1998. “slope of linear regression” and “y-intercept of linear regression” are tilt and y-intercept of a line resulting from fitting by linear regression, respectively. (Adapted from Shoji et al. 2000)

	without OTL	with OTL
slope of linear regression	0.9732	0.9748
y-intercept of linear regression	1.3247	1.2006
GPS-WVR bias (mm)	0.59	0.51
GPS-WVR bias removed rms (mm)	1.28	1.09

data with the OTL component period. For composition, we chose K_1, O_1, M_2, and S_1 components. K_1, O_1, and M_2 have large vertical amplitudes. The vertical amplitude of the S_1 component is small, but the component period is 24 hours. There can be other sources besides OTL, which cause 24-hour periodic variations in dPWV. For example, variation in atmospheric surface temperature from day to night may cause error in GPS PWV during the process of converting ZTD to PWV as well as during the retrieval process of PWV in MWR.

Figure 3.5 shows composite time series data for S_1, K_1, O_1, and M_2 components. There are biases between the dPWV data and the $dPWV_{simulated}$. The dPWV without OTL (thick gray lines) generally shows pure sinusoidal curves, which resemble those of the $dPWV_{simulated}$ (solid black lines). The agreement of the M_2 component is especially remarkable. The curves of other components have some high frequency irregularities. When the OTL was included in the GIPSY analysis, the amplitudes of the dPWV curves were reduced for all components (thin solid lines). The improvement of the M_2 component is remarkable (about 80 percent).

To evaluate the accuracy of GPS PWV, we constructed a scatter diagram for MWR PWV and GPS PWV (not shown). We also calculated linear regression coefficients and bias removed RMS difference between GPS PWV and MWR PWV. The results are summarized in Table 3.3. It shows that 5-minute estimation of the GPS PWV without OTL agreed well with MWR PWV with RMS difference of 1.3 mm. When the OTL is included in the analysis, a positive impact is observed reducing RMS difference to 1.1 mm.

3.2.3 Summary

The results suggest that the OTL components calculated by the GOTIC succeeded in simulating the actual site displacement by OTL effects in Japan. On the other hand, in

K_1 components, the amplitude of dPWV without OTL in GIPSY is 1.5 times larger than the simulated GPS PWV error, with considerable error remaining even in the case of GIPSY analysis with OTL. The error may be due to multi-path effect, temperature dependency on conversion from Zenith Wet Delay to PWV, or instrument dependency of MWR on temperature. Analysis utilizing much longer data periods than the present two months is required to overcome these difficulties.

3.3 Correction of Multipath Effect

3.3.1 Introduction

In order to study small-scale water vapor variations over distances from a few kilometers to 20 km, two campaign observations with a dense GPS network were carried out for 2.5 months at Tsukuba, Japan. For these observations, 79 GPS antennas were installed at 75 sites within a 20 km × 20 km square area at intervals of 1 to 3 km.

The PCV models provided by the US National Oceanic and Atmospheric Administration (NOAA) were applied to remove unmodeled phase center variations (PCVs) specific to the GPS antenna type. In addition, new PCV maps (MPS maps) were constructed for all the antennas by stacking one-way postfit residuals over both campaign periods; this helped to eliminate not only the azimuth-dependent PCV but also the errors due to multipath effects.

After MPS maps were introduced into the analysis, the strong elevation dependence as well as azimuth dependence of the postfit phase residuals disappeared almost completely for all the antennas. The improvement of the postfit residuals following the application of MPS maps also exhibited a positive impact on PWV estimation. Systematic biases of GPS-derived PWVs between different antenna types (Trimble and Ashtech) were reduced, resulting in a better agreement of GPS PWVs, with RMS errors of 2.0 mm or less relative to PWVs obtained by radiosonde or MWR observations.

3.3.2 Tsukuba GPS Dense Network Campaign Observation

Two campaign observations, using a dense network of 79 GPS antennas, were carried out at Tsukuba for 30 days in the autumn of 2000 and 51 days in summer, 2001. The main objectives of the observations were as follows:

(1) To investigate the details of local-scale variations of water vapor, which is

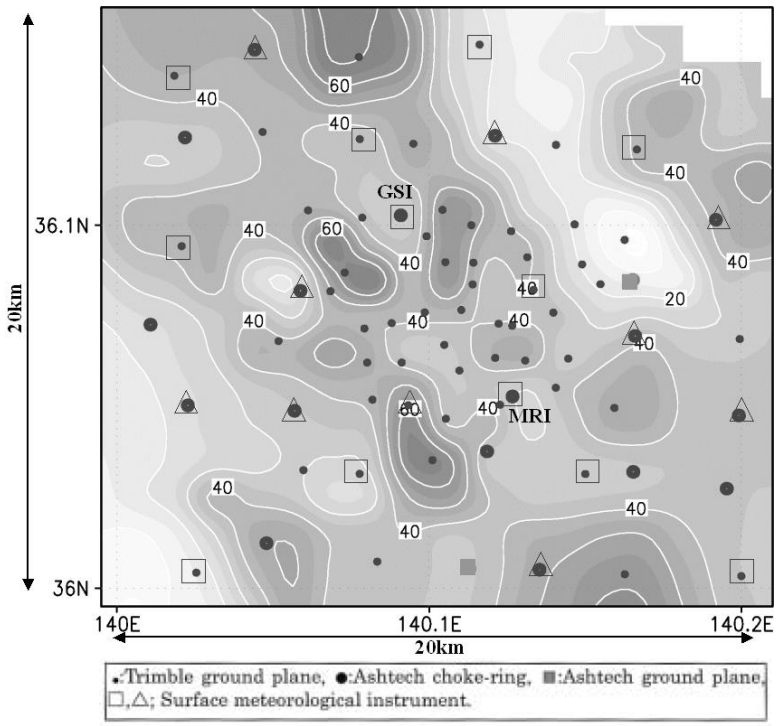

Figure 3. 6: The distribution of 79 GPS receivers in the 2000 Autumn Campaign, classified by antenna types. The area is approximately 20 km by 20 km. Contour lines represent the antenna antenna height above sea level in meters. (Adapted from Shoji et al. 2004)

important not only for meso- to micro-scale weather analysis, but also for the evaluation of GPS errors, since local-scale inhomogeneous distribution of water vapor has a great influence on the precise estimation of position and atmospheric delay;

(2) To develop meteorological usage of slant path delays (SPD), especially at low elevation angles, for various applications, such as water vapor tomography, and data assimilation into mesoscale numerical weather prediction (NWP) models; and,

(3) To reveal the 3-dimensional structure of the local-scale water vapor distribution which will be used for the development and verification of mesoscale NWP models.

The campaign observations consist of two periods; 30 days in autumn 2000 from October 14 to November 13, and 51 days in summer 2001 from July 14 to September 2. Both campaigns were carried out at Tsukuba, Japan (60 km north-east of Tokyo) over a 20 km by 20 km area, with intervals of 1 to 3 km between adjacent sites (Figure 3.6).

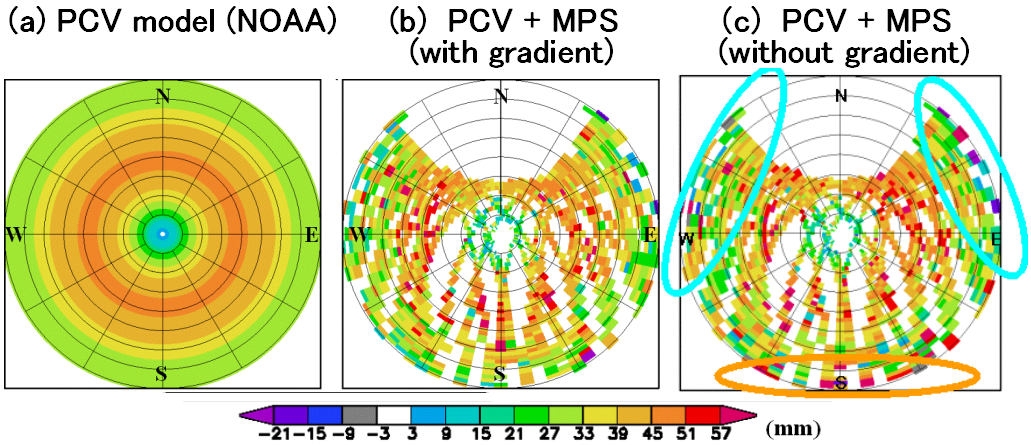

Figure 3. 7: Examples of the PCV model and the constructed MPS map. (a) PCV model of the Trimble ground plane (TRM22020) antenna. (b) PCV model + MPS of site GM58 which is made from residuals from a GPS analysis with atmospheric gradient estimation. (c) Same as (b) except that the map is made from an analysis without gradient estimation. The enclosed areas indicate biases in the MPS maps when gradient estimation is ignored. (Adapted from Shoji et al. al. 2004)

Seventy-nine GPS receivers were installed at 75 sites, in addition, ten surface meteorological observation instruments for pressure, temperature, relative humidity, rain, sunshine, wind direction and speed were also set up in the area. Of the 79 GPS receivers, ten GPS receivers were equipped with meteorological instruments that measured pressure, temperature, and relative humidity simultaneously.

The GPS equipment consisted of four types; 58 Trimbles with ground plane and microstrip antenna, 17 Ashtechs with choke-ring antenna (14 of those with hemisphere-shaped radomes and the other 3 with conical shape radomes), 2 Ashtechs with ground plane, and 2 AOA Turbo Rogue receivers with Dorne Margolin choke-ring antenna. Three types of GPS receivers, excluding the Ashtech ground plane, were co-located at the reference sites of the Meteorological Research Institute (MRI) and the GSI.

Rawinsonde observations were executed on a 3-hourly basis in the 2000 Autumn Campaign, and on a 6-hourly basis in the 2001 Summer Campaign. In both campaigns, two to four WVRs were installed over the campaign area to measure the total amount of water vapor in GPS satellite directions, or vertical profiles of water vapor and temperature.

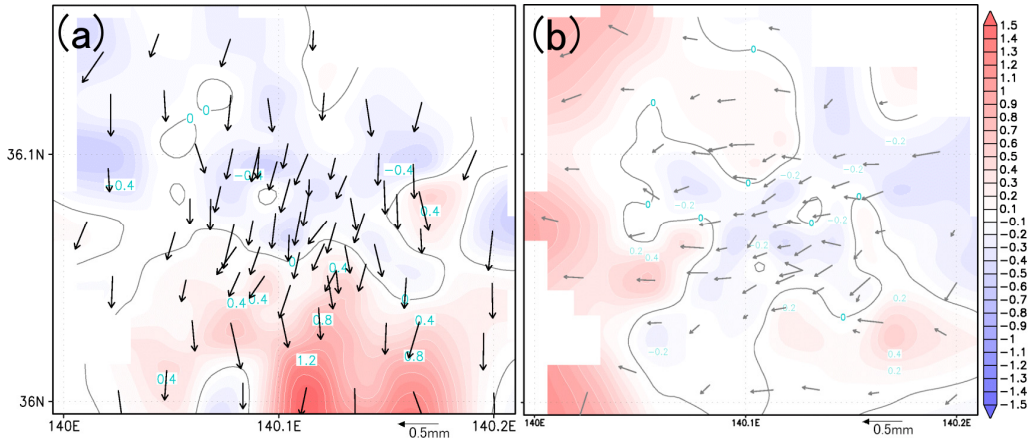

Figure 3. 8: Distribution of time averaged PWV anomalies of (a) the 2000 Autumn Campaign and (b) the 2001 Summer Campaign. The contour interval is 0.1 mm. The height dependency of PWV anomaly was corrected according to the regression formula given by height dependencies of time averaged PWV anomalies for all GPS stations. The vectors show the size and the direction of the averaged atmospheric gradient parameters from the GPS analysis. (Adapted from Shoji et al. 2004)

3.3.3 Construction of Multipath Stacking (MPS) map

We constructed PCV correction maps for each GPS site, by stacking one-way postfit phase residuals over the entire campaign period using the following procedure:

(1) We started by selecting the PCV models calibrated and provided by NOAA. The model considers the ‘‘DORNE MARGOLIN T’’, an antenna constructed by Allen Osborne Associates, as the reference antenna, and relative PCV values of other antennas to the reference antenna are given. The model describes PCVs as a function of only the elevation angle. We analyzed the GPS data during the entire campaign period, with a coordinate constraint of 999 m. The postfit residuals of each GPS site were stacked in boxes of 2 degrees in elevation and 5 degrees in azimuth, and then the stacked postfit residuals of each box were averaged. The PCV models were added to the averaged residuals to give renewed correction maps; and,

(2) We repeated the GPS analysis several times using the renewed correction maps with the coordinate constraint gradually tightened from 100 m to 10 m, then 1 m and finally to 1 mm. The averaged postfit residuals were then added to the PCV correction maps to improve them. Thus, coordinate solutions, and the PCV correction maps, were updated four times.

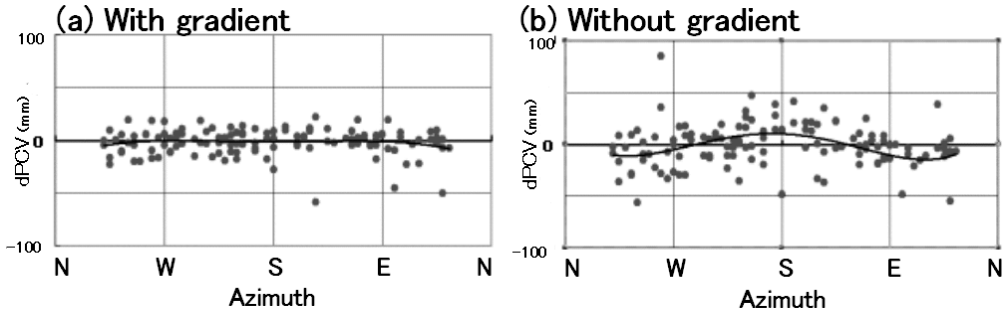

Figure 3. 9: Azimuth dependencies of MPS map using data below the 20-degree elevation angle. (a) PCV + MPS of site GM58 made from a GPS analysis with gradient estimation. (b) Same as (a) except that the map is made from an analysis without gradient estimation. The values are normalized by Niell's wet mapping function. When gradient parameters are not estimated in the GPS analysis (b), azimuth dependency in the MPS map has amplitude of about 20 mm. When gradient parameters are estimated (a), no strong azimuth dependency is seen. (Adapted from Shoji et al. 2004)

The new correction maps will include not only the intrinsic PCV from the antenna itself, but also any stationary noise, which regularly occurs at a given elevation and azimuth, such as phase multipath from surrounding objects and PCV induced, for example, by the antenna mount structure (Hurst and Bar-Sever 1998). In this paper, the new correction maps are referred to as ''Multipath Stacking'' (MPS) maps.

Figure 3.7 shows an example of the difference between the PCV model and the constructed map. These three maps show similar elevation dependency of PCV. However, the high frequency PCV is apparent in the PCV model + MPS maps ((b) and (c)), while it is not present in the PCV model. It seems that site dependent multipath effects are seen in the PCV model + MPS map.

It is necessary to estimate atmospheric gradient parameters for the GPS analysis used to construct the MPS map, because of an average atmospheric gradient that shows seasonal variations. Figures 3.8 represent distributions of averaged gradient parameters, and PWV anomalies from their mean area value for the 2000 Autumn Campaign and 2001 Summer Campaign. In order to derive PWV from ZTD, the ZHD at each GPS site was calculated using the interpolated surface pressure observation value according to Davis et al. (1985). ZHD was subtracted from ZTD to derive ZWD. Finally, PWV was estimated from ZWD using a conversion coefficient estimated from the surface temperature observation by means of the formula proposed by Bevis et al. (1992). It is understood that water vapor increases from north to south in autumn on average. On the

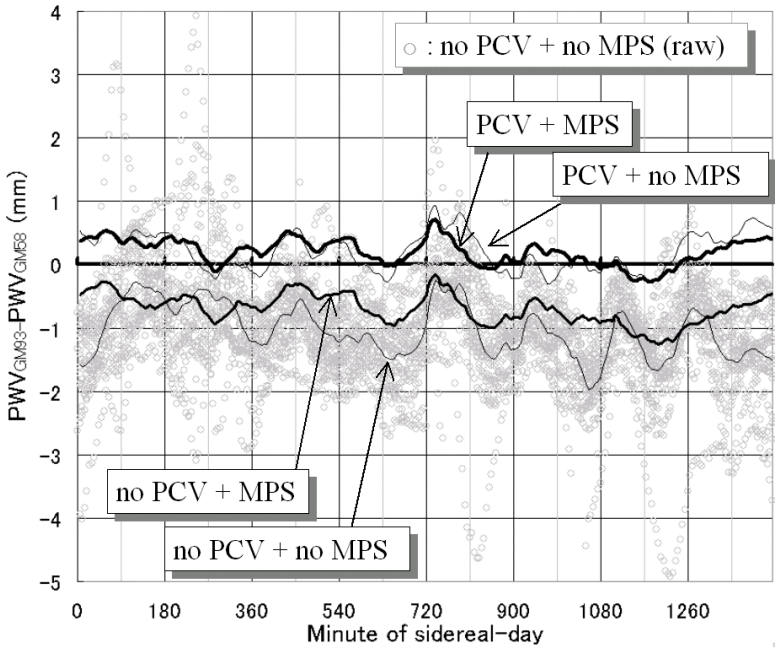

Figure 3. 10: Composite time series of the difference between PWVs derived from two GPS antennas at MRI from 14 Oct.–13 Nov. 2000. PWVs of the Ashtech choke-ring antenna (GM93), corrected by the MPS map, are assumed to be the reference value. GM58 is the Trimble ground plane type antenna. The distance between the two GPS antennas was several meters. (Adapted from Shoji et al. 2004)

other hand, an increase in water vapor from east to west is noticeable in summer. It can also be seen that the gradient parameters show the same feature, though the gradient parameters not only include the water vapor gradient, but also the gradient of dry atmosphere. Aonashi et al. (2000) found that GPS derived gradient parameters correlate positively with the MWR derived water vapor gradient in Japan. In autumn, the temperature gradient in the northsouth direction is large around Japan. In summer, the Japan Islands tend to be covered with the Pacific high atmospheric pressure system, and the temperature gradient decreases. In that season, thermally induced local circulation becomes active and water vapor tends to gather in the mountain region that is located to the west of the campaign area.

In Japan, the atmospheric gradient shows this seasonal variation. If the gradient parameter is not estimated, the gradient component of the SPD will be interpreted as a residual and stacked into the MPS map, and the seasonal atmospheric delay gradient pattern will be included in the MPS maps, such as those in Figure 3.7 (c) and Figure 3.9 (b). Correction of GPS SPD based on the MPS maps that include these gradients will causes this systematic atmospheric signal to be overlooked when analyzing the SPDs.

Table 3. 4: Comparison of GPS derived PWV with radiosonde observed PWV at MRI during the observation period from October 14 to November 13, 2000. (Adapted from Shoji et al. 2004)

Antenna	PCV correction	Bias (mm)	Bias free RMS (mm)	Inclination of regression line	Y-intercept of regression line (mm)
Trimble GP (GM58)	no PCV + no MPS	-1.73	1.78	0.986	-1.380
	PCV + no MPS	-0.09	1.68	0.979	0.460
	no PCV + MPS	-1.33	1.54	0.975	-0.680
	PCV + MPS	-0.14	1.55	0.976	0.482
Ashtech CR (GM93)	PCV + no MPS	-0.47	1.85	0.960	0.549
	PCV + MPS	-0.36	1.60	0.971	0.391

3.3.4 Accuracy Improvements in GPS derived PWV

Figure 3.10 shows the averaged PWV differences between two GPS antennas set up at the MRI site. Since PCV and the multipath strongly depend on the incidence angle of the GPS carrier wave, the PWV differences were rearranged with a cycle of one sidereal day (the repeating period of the GPS satellite constellation), and the differences averaged. Without PCV corrections, there seems to be a negative bias of about 1.5 mm in the Trimble ground plane antenna relative to the Ashtech chokering antenna (no PCV + no MPS), and the bias varies with about 1.5 mm amplitude and a cycle of several hours. When the PCV model was used (PCV + no MPS), the negative bias disappeared.

As a result of the MPS correction (no PCV + MPS), the amplitude of the time variation of the differences was reduced, but negative biases still remained. Correction by PCV model + MPS map (PCV + MPS) resulted in the best result. The bias is less than 0.5 mm, and the amplitude of the time variation was reduced. It is thought that the azimuth dependence of PCV and the influence of the multipath, which the PCV model cannot correct, were corrected by the MPS map.

The same thing can be concluded from comparison between the GPS derived PWV, and the PWV of rawinsonde observations. The results are summarized in Table 3.4 and support the conclusions above. As a result of correction by the PCV model, the biases of the GPS derived PWV (especially large for the Trimble ground plane) were reduced considerably. As for the reduction of the RMS difference, improvements were seen following correction by the MPS. In addition, it was the PCV + MPS analysis that again gave the best result. If the antenna phase characteristics and multipath errors are corrected, GPS can derive PWV with an accuracy of about 1.5 mm RMS errors and very small biases.

3.3.5 Summary

GPS dense net campaign observations were carried out at Tsukuba in autumn 2000 and summer 2001 to investigate local-scale water vapor distributions. The GPS PWVs were improved by introducing the antenna PCV model and MPS corrections. It has been proved that GPS can derive PWV within 2-mm accuracy without biases from different types of antennas. The averaged PWV fields indicated seasonal changes on the Kanto Plain. Seasonal gradients revealed by the analysis suggest that it is necessary to estimate gradient parameters when constructing MPS maps.

The improvement of the postfit residuals using both the PCV model and the MPS map had a positive impact on the estimation of slant path delay (SPD). The details of the same are described in Appendix-B.

3.4 Correction of Satellite Clock Error for Near Real-Time Analysis

3.4.1 Introduction

Several studies have shown that the water vapor information retrieved from GEONET has positive impacts on numerical weather prediction (NWP) (e.g., Nakamura et al. 2004; Koizumi and Sato 2004; Seko et al. 2004c). Such previous studies conducted in Japan mainly used postprocessed GPS PWV data that was retrieved from a GPS analysis using a precise final ephemeris (orbits and clocks). The latency of a final ephemeris is approximately 2 weeks; however, for example, to input the GPS PWV data into an operational mesoscale four-dimensional variational data assimilation system (Meso 4D-VAR) of the Japan Meteorological Agency (JMA), the retrieval of GPS PWV must be completed within 50 min after the observation. Hence, the construction of a highly accurate GPS NRT analysis system is necessary for the operational use of GPS data in weather monitoring and forecasting.

Numerous studies have already been conducted on several different approaches to NRT GPS analysis for meteorology (e.g., Flores et al. 2000; Gendt et al. 2004; and Gutman et al. 2004). In Japan, Hatanaka (1998) summarized the problems to be solved for NRT analysis. However, no study on NRT PWV retrieval for meteorology has been reported thus far. One of the reasons for this may be the large number of GPS stations in Japan: over 1,200. However, the three abovementioned studies were aimed at analyzing at most 200 GPS stations. Considering this, our research is designed to employ the large

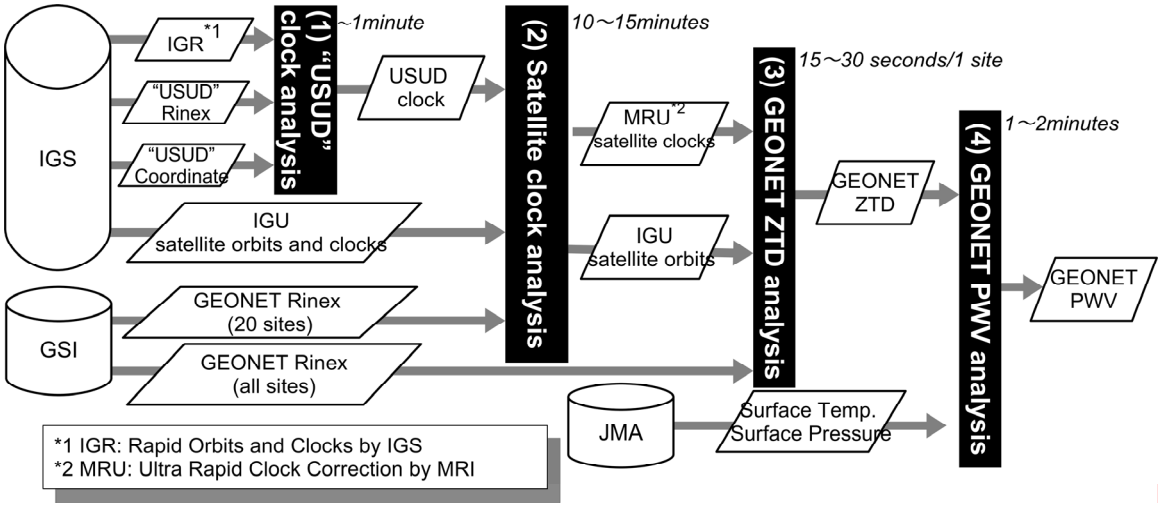

Figure 3. 11: Schematic diagram of NRT GPS analysis used in this study. Column: data server; lozenge: data file; open letters on black filled square: analysis. (Adapted from Shoji 2009)

number of GPS receivers in Japan as operational weather instruments.

3.4.2 Double difference (DD) procedure and precise point positioning (PPP) procedure

There are two major GPS analysis procedures for unknown parameter estimation, the double difference (DD) procedure (e.g., Hofmann et al. 2000) and the precise point positioning (PPP) procedure (e.g., Zumberge et al. 1997). As described in sub-section 2.1.1, these two procedures differ in the treatment of the effects of the clock offsets of GPS satellites and receivers. In view of computational burden to analyze more than 1,200 GPS stations, we decided to adopt the PPP procedure in this study.

The basic concepts of our NRT system are the same as those demonstrated by Gendt et al. (2004) and Flores et al. (2000). Both studies first analyzed satellite orbits and clocks and then estimated the unknown parameters at each GPS station using the PPP procedure. In these studies, hydrogen-maser atomic clocks, which were installed at several GPS stations, were used as the reference clocks to analyze the clock offsets of GPS satellites. Gendt et al. (2004) employed the GPS analysis software EPOS.P.V2 at the Geo Forschung Zentrum Potsdam (GFZ). Flores et al. (2000) used the GIPSY OASIS II software package (Webb and Zumberge1993).

3.4.3 Outline of the NRT Analysis Procedure

In the PPP analysis, satellite clock offsets are treated as known parameters. One

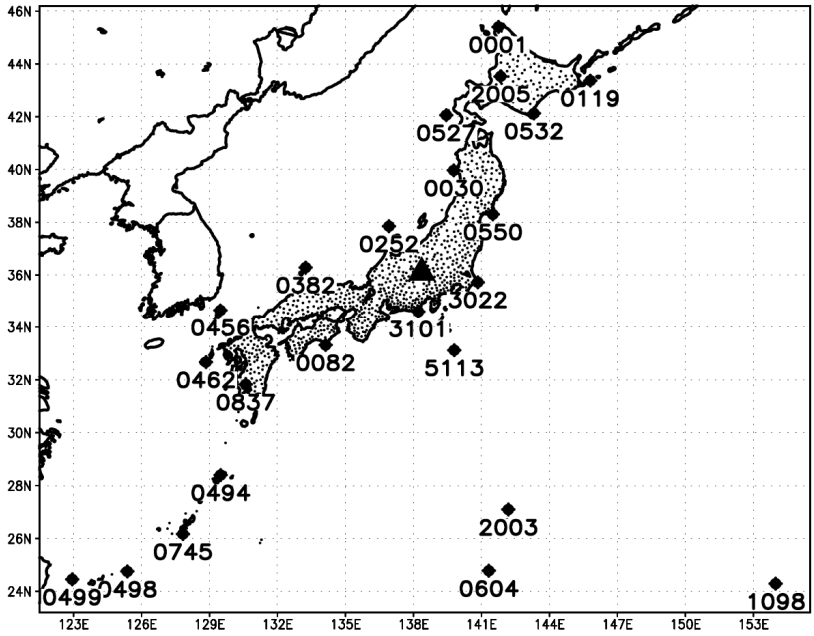

Figure 3. 12: Locations of GEONET GPS stations. Small dots (●): GEONET stations; large diamonds (◆): GEONET station used for the analysis of satellite clock offsets; filled triangle (▲): USUD IGS station. The four digits under the large diamonds represent the last 4 digits of the GEONET station ID. (Adapted from Shoji 2009)

simple approach to acquire those data is to use final ephemerides of IGS (IGF). In this study, we selected an IGS station ‘‘USUD,’’ which has been equipped with hydrogen maser atomic clock, as a reference station to analyze the clock offsets of GPS satellites. This station was installed in July 1990, on the building roof of the Usuda Deep Space Center of the Japan Aerospace Exploration Agency (JAXA) in Saku city, Nagano Prefecture. The outline of our procedure is shown schematically in Figure 3.11. Firstly, the clock offset of USUD was analyzed by using the IGS rapid orbit (IGR), and then, the offset was extrapolated for the next two days. Secondly, the offsets of GPS satellite clocks were analyzed while the extrapolated offsets of the USUD clock were kept fixed as a time reference. In this step, 23 GEONET stations (large dots in Figure 3.12) were analyzed simultaneously while the satellites positions were kept fixed at orbits in IGU. Thirdly, the coordinates and atmospheric delay parameters of each GEONET station were estimated using the PPP method. A detailed description is provided in the next subsection. We use GPS software GIPSY OASIS II version 4.03 (GIPSY) on a Linux-based PC with an Intel Xeon processor (CPU clock: 3.06 GHz) and a memory of 2 GB.

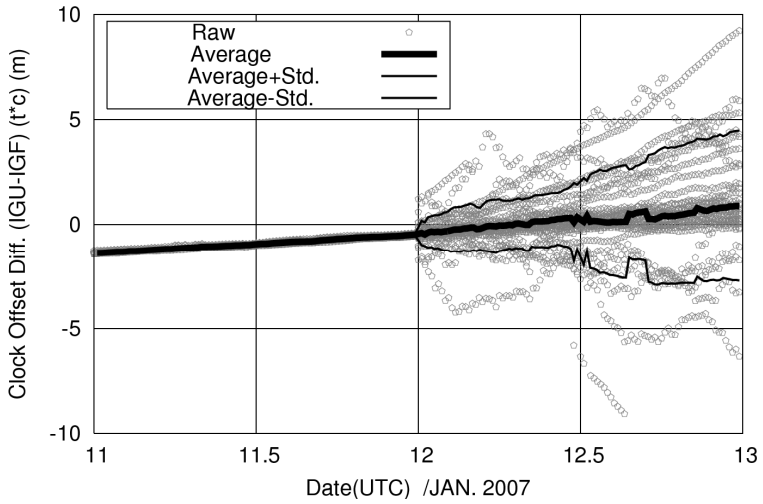

Figure 3. 13: Clock offset differences of IGU from IGF for all GPS satellites for two days (from 00 UTC, 11 Jan. to 00 UTC, 13, Jan., 2007) expressed in the unit of length (m). The gray open circles represent each difference; the black thick line, the average; and the two black thin lines, the average plus positive (negative) standard deviations. (Adapted from Shoji 2009)

3.4.4 Clock Offsets

Figure 3.13 shows differences between the clock offsets for all GPS satellites stored in the IGU and the IGF. It can be observed that the error suddenly increases at the beginning of the predicted clocks (00 UTC 12th Jan., 2007) and increase with time. The PPP procedure requires accurate relative clock differences of GPS satellites. The time variation of relative clock differences shown in the figure exhibit the necessity of correction for the clock offsets stored in IGU in the NRT analysis.

Figure 3.14 shows the USUD clock offsets, estimated by following the PPP strategy using IGF (gray thick line) and IGR (black thick line) for the same period as that employed in Figure 3.13. In Figure 3.14, the USUD clock offsets estimated by linear extrapolation of the IGR results (black dashed line) are also plotted. It can be observed that the USUD clock offsets exhibit a linear trend. In the unit of length, the USUD clock had been showing an offset variation of about 20 m in one day as compared to GPS time. Further we can see that the linear extrapolation of the clock offset (black dashed line) predicted the real trend (gray thick line) well. In the second experiment, we applied this linear extrapolated clock offset to the USUD clock and estimated satellite clock offsets.

Hereafter we refer this experiment as ‘‘IGU.usud.IGR.’’ Also, we performed another experiment that did not consider this linear trend. Hereafter we call this experiment ‘‘IGU.usud.’’

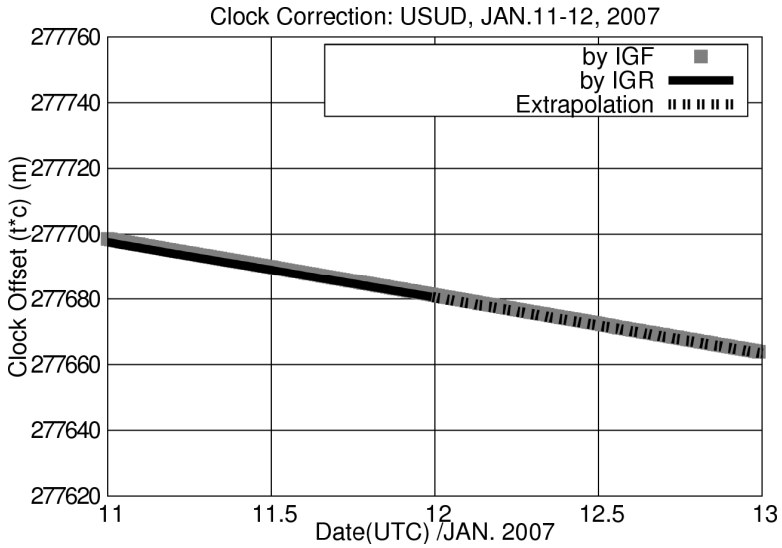

Figure 3. 14: Clock offsets of the "USUD" IGS station from 11 to 12 Jan., 2007 (unit of length is m). The offsets are estimated by the PPP strategy by using GIPSY OASIS II. The gray thick line represents the offsets estimated by fixing the satellite orbits and clocks for the IGF. The black line represents those estimated by fixing the satellites orbits and clocks for the IGR. The black dashed line is a linear extrapolation of the black line. (Adapted from Shoji 2009)

3.4.5 PWV Retrieval Experiments

Figure 3.15 shows the comparison of the PWV retrieved at MRI with nearby radiosonde observation. Four types of retrieved results are shown in the figure. In the GPS analysis performed using the final orbit provided by Jet Propulsion Laboratory (hereafter referred to as ''JPF'' experiment), we used 36-h span of data for both the satellite orbit and observation data, and analysis was performed on a daily basis. For the PWV comparison, we used only the mid 24-h PWV sequence, while the first and last 6-h data were neglected. This treatment allows us to reduce the degradation of accuracy near the data edge of each time window. It can be observed that the PWVs retrieved from the experiments IGU and IGU.usud have substantial errors. On the other hand, the IGU.usud.IGR trial yielded results that are comparable to those obtained from the JPF experiment. IGU.usud.IGR experiment resulted in bias growth in each satellite clock offset, though they resulted in remarkable improvement in PWV retrieval. The satellite clock offset bias in IGU.usud.IGR should be hidden in other unknown parameters in Eq. (2.3), for example the ambiguity term ($N_i^l\lambda$) or receiver clock offset (δ_i). However, the causes and effects of such constant clock offset biases have not been studied so far. If we can estimate satellite clock offset precisely, we might improve the accuracy of the retrieved PWV. Further investigation is required to confirm this possibility.

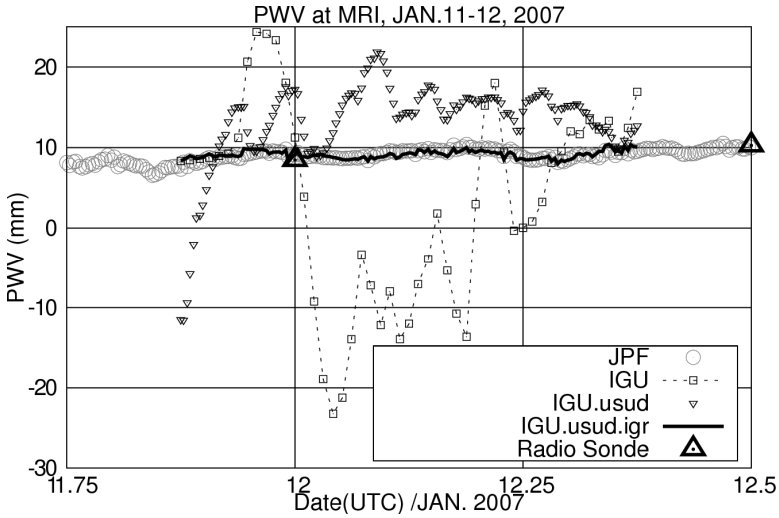

Figure 3. 15: PWV sequence at MRI observed by radio-sonde observation and GPS analyses. Open large triangles (△); Radio-sonde observation, Gray open circles (○); PWV data retrieved by "JPF" experiment, Open squares (□); those retrieved by "IGU" experiment, Open upside-down triangles (▽); those retrieved by "IGU.usud" experiment, and Solid line (-): those retrieved by "IGU.usud.IGR" experiment. (Adapted from Shoji 2009)

Table 3.5 summarizes the comparison with radiosonde observation. The PWV retrieved from the IGU and the IGU.usud experiments exhibit large error with more than 10-mm R.M.S difference. In addition, the IGU.usud experiment resulted in large positive bias of more than 8 mm both in winter and summer. On the other hand, the IGU.usud.IGR experiment exhibited a good agreement with radiosonde observation with an R.M.S difference of 1.64 mm in winter and 3.36 mm in summer. This result is almost comparable with that of the JPF experiment. In Table 3.5, we also show the results of the IGU.usud.JPR experiment. This experiment is similar to the IGU.usud.IGR experiment, except for the use of rapid orbit provided by the JPL (JPR) instead of the IGR. The results suggest that the JPR can be an alternative to the IGR.

3.4.6 Summary

NRT processing of GPS data from a dense GPS network in Japan is introduced.

The linear extrapolation of the clock offsets of a highly accurate, stable hydrogen maser atomic clock at the USUD IGS station indicated that this clock has good accuracy and can be used as a reference clock. The precise point positioning analysis, which uses the IGU orbit and satellite clock offsets estimated from the extrapolated USUD clock time, can retrieve PWV data with an accuracy comparable to those retrieved using final

Table 3. 5: Comparison of GPS derived PWV with radio-sonde observed PWV in Japan (Reproduced from Shoji 2009)

Orbit	Clock	01,12utc-29,00utc, Jan. 2007			01,12utc-29.00utc, Jul. 2007		
		Bias	R.M.S	Count (total 1120)	Bias	R.M.S	Count (total 1072)
IGU	IGU	5.96	14.11	843	0.33	10.67	1041
	IGU.usud	9.67	10.92	1094	8.63	12.16	1053
	IGU.usud.IGR	0.29	1.64	1094	0.22	3.36	1056
	IGU.usud.JPR	0.30	1.64	1094	0.22	3.36	1057
JPF	JPF	0.65	1.53	1115	0.86	3.37	1054

orbits and clocks.

This system heavily relies on the accuracy of the USUD IGS station. Therefore, to make the system more reliable, the combined use of other stations that are equipped with atomic clocks may be required.

3.5 Concluding Remarks

Using final precise ephemerides for GPS satellite orbits and clocks, Ohtani and Naito (2000) analyzed PWV data derived from GPS analysis and compared them with those obtained from 10 nearby radiosonde stations in Japan. Based on a one-year comparison, they summarized that the GPS PWV had a mean bias of -2.7 mm and a standard deviation of 2.6 mm against radiosonde observations. They also found that GPS PWV agrees well with the PWV obtained from morning launches (08:30 JST; 23:30 UTC) of radiosondes by the JMA; however, it had a negative correlation with increasing PWV for nighttime launches (20:30 JST; 11:30 UTC) of the same. They suggested that the day and night differences in the bias may be caused by site displacement due to OTL. Their GPS analysis did not consider the antenna PCV.

It has been confirmed that Shwiderski's OTL model (Shwiderski, 1981) reduces the amplitude of the day and night bias difference by one-half or one-third the original value. Matsumoto et al. (2001) developed a high-resolution (1/12°) regional ocean tide model around Japan by assimilating both the TOPEX/POSEIDON data and the data of 219 coastal gauges. Further improvements in GPS PWV accuracy can be expected from the use of these precise tide models.

Introducing an antenna PCV model that is specific to the antenna type can eliminate most of the antenna-specific bias in GPS PWV. Hatanaka et al. (2001a, b) considered not only the antenna PCV but also the multipath effect of the antenna pillar. They constructed a new PCV model for each type of antenna-pillar pair for GEONET. We constructed a multipath correction table by stacking post-fit phase residuals. This

method allows us to include not only the effect of the antenna pillar but also site-specific multipath effects. The multipath correction table also allows us to reproduce the signal delay along the ray path (slant path delay, SPD). Shoji et al. (2004) estimated the horizontal scale of SPD using correlation distributions. As a result, the horizontal scale of the zenith total delay, gradient component, and post-fit residual may be roughly considered to be 644 ± 120 km, 62 ± 23 km, and 2–3 km, respectively (APPENDIX-B).

The NRT processing of GPS data from a dense GPS network in Japan has been introduced.

The linear extrapolation of the clock offsets of a highly accurate, stable hydrogen maser atomic clock at the USUD IGS station indicated that this clock has good accuracy and can be used as a reference clock. The precise point positioning analysis, which uses the IGU orbit and satellite clock offsets estimated from the extrapolated USUD clock time, can retrieve PWV data with an accuracy comparable to that of data retrieved using final orbits and clocks. Shoji et al. (2009a, 2010) expanded the NRT analysis area from Japan to East Asia, and also globally. On October 28, 2009, JMA started the operational use of GPS PWV for a mesoscale DA system called JNoVA (Honda and Sawada, 2009). The GPS PWV can now contribute to both mesoscale and global-scale weather analysis and forecasting.

Chapter 4

Impact of GPS PWV on Mesoscale NWP

4.1 Introduction

This chapter focuses on DA experiments involving GPS-derived PWV. JMA's operational four-dimensional DA system (Meso 4D-Var) was used for all the experiments. GPS PWV values were retrieved by an NRT procedure, as described in Section 3.4.

In Section 4.2, we describe the outline of the Meso 4D-Var system and the procedure for GPS PWV DA. Results of statistical analyses of precipitation forecasts obtained by the assimilation of PWV data derived from the nationwide Japanese GPS network "GEONET" are presented in Section 4.3. Our NRT procedure is applicable not just in Japan but also globally. In Section 4.4, we present the results of a case study on the assimilation of GPS PWV data obtained from GEONET and GPS stations in East Asia. Section 4.6 provides a summary of this chapter.

4.2 Data Assimilation Procedure

4.2.1 Meso 4D-Var

We used JMA's Meso 4D-Var (Ishikawa and Koizumi 2002; Koizumi et al. 2005) system for our DA experiments. Meso 4D-Var is a four-dimensional data assimilation system developed at JMA, which was used as the operational mesoscale data assimilation system from March 2002 to April 2009. The dynamical core of this system is based on the hydrostatic spectral model of JMA (hydrostatic mesoscale model; MSM), and the system consists of a nonlinear forward model and a simplified adjoint model with a horizontal resolution of 20 km. An incremental approach is employed, where the analysis field is made by an outer model with a horizontal resolution of 10 km. Figure 4.1 shows the analysis domain of JMA's original Meso 4D-Var, and Table 4.1

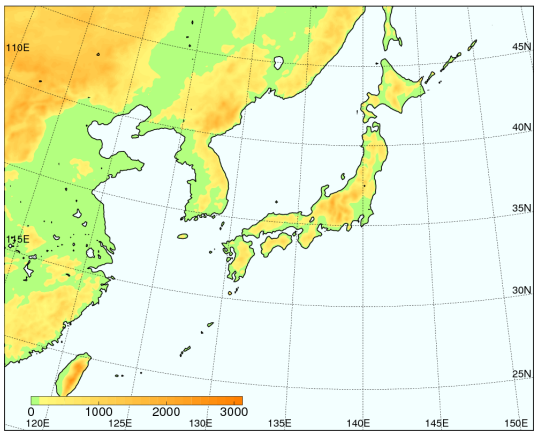

Figure 4. 1: Domain of JMA Meso 4D-Var system. The system uses the Lambert conformal projection.

summarizes how the Meso 4D-Var system used in the experiments for this thesis differs from the original specifications.

4.2.2 GPS Analysis and PWV Retrieval

NRT GPS analysis refers to the retrieval of the PWV within several tens of minutes after the observation, in order to facilitate NWP. We followed Shoji's procedure (2009) and retrieved the zenith tropospheric delay (ZTD) every 10 min. In order to calculate the PWV from the ZTD, we required the values of the pressure and the column mean temperature weighted by water vapor (T_m) at the GPS antenna position. For GEONET sites, we first obtained the pressure and temperature at the GPS stations by interpolating JMA's surface meteorological observations. Then, T_m was estimated from the interpolated surface temperature using the linear relation between T_m and the surface temperature, which was based on one-year statistics of radiosonde observations in Japan. For GPS stations outside Japan, the pressure and T_m values were calculated using model first guesses because of the lack of surface observations and statistics. We used GSIGEO2000 (Kuroishi et al. 2002) for GEONET and EGM96 (Lemoine et al. 1998) for International GNSS Service (IGS) as a geoid model to calculate the altitudes of the GPS stations. Shoji (2009) compared GEONET-derived PWVs with those obtained from radiosondes and calculated the root mean square errors to be 1.6 mm in winter and 3.4 mm in summer. Our statistical comparison of IGS-derived PWV values and radiosonde observations in East Asia showed a comparable agreement (2.0 mm).

The PWV of a numerical model is calculated in a rather simple manner from the model variables as follows:

$$PWV = \frac{1}{g}\int_{p_s}^{p_t} q dp \,, \tag{4.1}$$

where q, p, p_t, p_s, and g are the specific humidity, pressure, model top pressure, model surface pressure, and gravitational acceleration, respectively.

Table 4.1: Specifications of Meso 4D-Var. Comparison between original specifications and those used in the experiments in this thesis.

		Original	Section 4.3	Section 4.4
Method		Incremental method		
Forward model		A hydrostatic spectral model with a horizontal resolution of 10 km and 40 vertical levels up to 10 hPa. Three types of precipitation scheme; a large-scale condensation scheme, amoist convective adjustment scheme for mid-level convection and a prognostic Arakawa-Schbert scheme for deep cumulus convection		
Adjoint model		Same dynamical process as the forward model but has only a few physical processes: simplified vertical diffusion, simplified long-wave radiation, grid-scale condensation and moist convection adjustment.		
Lateral boundary condition		Forecast of Global Spectral Model (GSM; TL959L60)		
		1 hourly original data (0.1875 degree gausian grid, 60 model planes)		
Assimilation window		6 hours	3 hours	
Observation data *All observation data are treated as observed hourly. That is all data between -30 and +29 minutes to the clock time are regarded as observation s at the clock time.		Radio-sonde, synop (surface), ship, buoy, aircraft,wind and PWV fields retrieved from satellite-based microwave scatterometer/radiometer, tropical cyclone bogus. Wind-profiler, doppler-radar radial wind, Radar-AMeDAS analyzed rainfall.		
		Tropical cyclone bogus. Wind-profiler, doppler-radar radial wind, Radar-AMeDAS analyzed rainfall.		
			GPS PWV ・GEONET	GPS PWV ・GEONET ・IGS
Observation error of GPS PWV			5 mm	
Map projection		Lambert conformal projection		
Horizontal grid resolution (grid size)	Outer model	10 km (361 x 289)		
	Inner model	20 km (181 x 145)		
Assimilation period			12 days from 00 UTC 31 Aug. to 00 UTC 13 Sept., 2006	30 hours from 18 UTC 26 to 00 UTC 28 July, 2008
Forecast model		MSM / NHM	MSM	NHM
Forecast time			18-h	18-h
Number of forecasts			48 (every sixth hour from 00 UTC 1 Sept., 2006)	1 (Init. = 00 UTC 28 July, 2008)

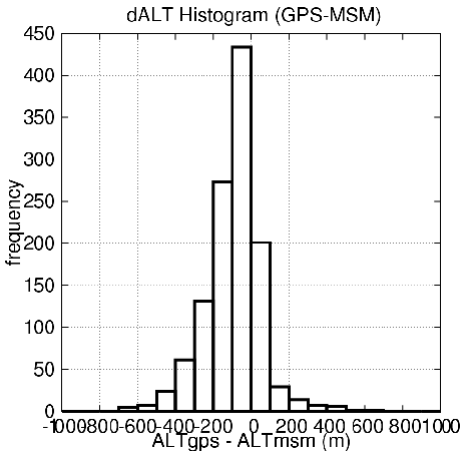

Figure 4. 2: Height difference histogram of GPS sites against model surface of Meso 4D-Var inner model.

4.2.3 Height Correction

As Japan has steep mountains and the NWP model employs a smoothed orography for determining the actual terrain surface, large differences exist between the GPS antenna height and the corresponding MSM surface height, particularly in mountainous areas. In order to adjust for the difference in PWVs between the first guess and the GPS, the first guess PWV is interpolated or extrapolated from the model surface to the actual terrain surface using a method by Mannoji et al. (1998) as follows:

(1) If the model surface is higher than the actual terrain surface, the model PWV is extrapolated to the actual terrain surface by assuming that the specific humidity between the model surface and actual terrain surface is equal to that in the lowest model layer.

(2) If the model surface is lower than the actual terrain surface, the model water vapor between the actual terrain surface and the model surface is subtracted from the model PWV.

4.3 Statistical Evaluation of Impact of GPS PWV DA

4.3.1 Introduction

The impact of GPS-derived water vapor information on mesoscale NWP has been investigated in several studies (e.g., Nakamura et al. 2004a; Koizumi and Sato 2004; Seko et al. 2004c). However, these studies mainly used GPS PWV data retrieved by GPS

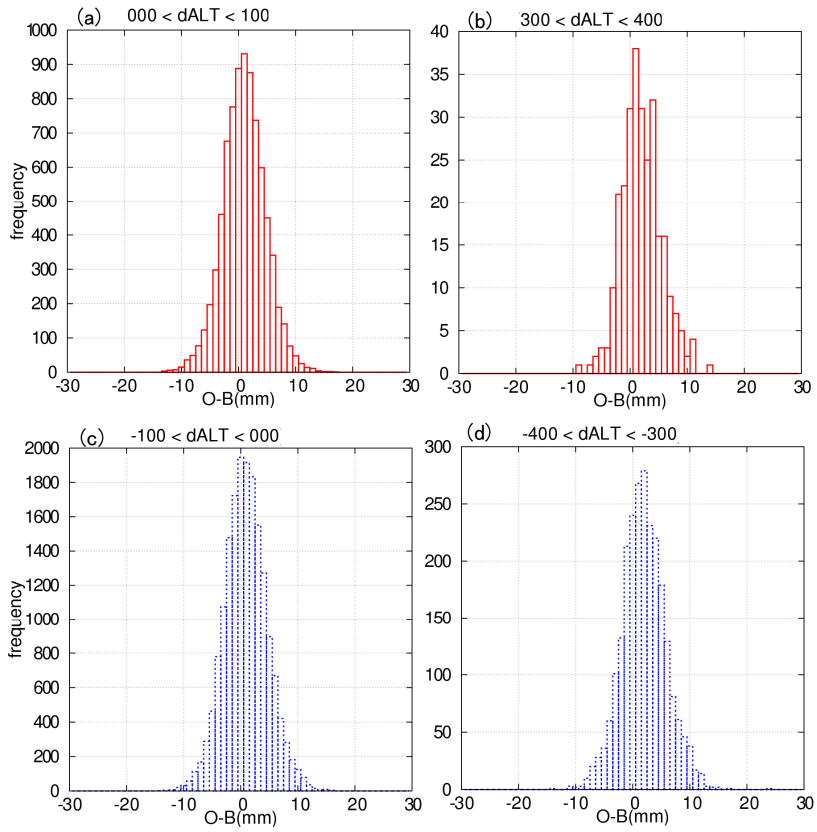

Figure 4. 3: Histogram of PWV departure for 10 days from August 31 to September 9, 2006. The height difference (GPS-Model) is (a) more than 0 m and less than 100 m, (b) more than 300 m and less than 400 m, (c) less than 0 m and more than -100 m, and (d) less than -300 m and more than -400 m.

analyses using IGS's precise final ephemerides (IGF). IGF cannot be applied to operational weather forecasting because its latency is about 2 weeks. Shoji (2009) developed an NRT PWV analysis system that enables PWV to be determined in time for the operational mesoscale DA of JMA. To statistically evaluate the impact of the NRT-retrieved GPS PWV on precipitation forecasting, a DA experiment was conducted using data collected over 12 consecutive days from September 1 to 12, 2006. We used JMA's Meso 4D-Var system for the DA experiments, essentially following Nakamura et al. (2004). In this section, we describe the procedure and results of the experiment. In subsection 4.3.2, the design of the experiment is explained. In subsection 4.3.3, the NRT PWV departure statistics are discusses. The results and summary are presented in subsections 4.3.4 and 4.3.5, respectively.

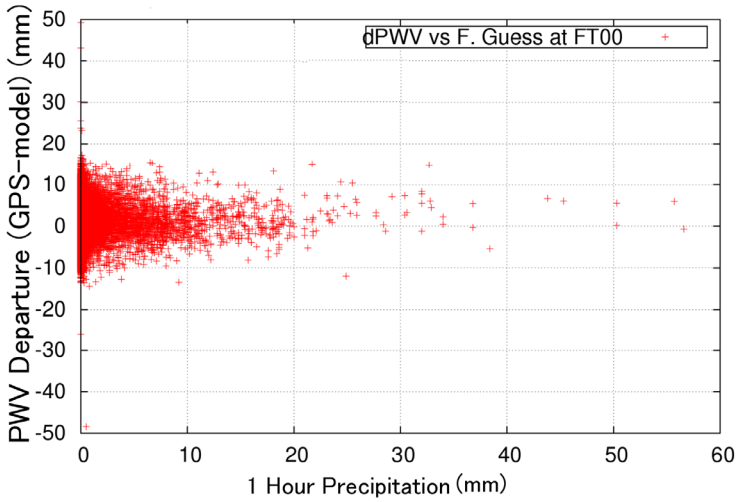

Figure 4. 4: Differences in GPS PWV against analysis field generated by “CNTL” experiment as a function of 1 h precipitation.

4.3.2 Experiment Design

In this study, we performed the following two continuous assimilation experiments. These experiments were different in terms of their assimilated observation data, as follows.

(1) Control (CNTL)

The following observations were assimilated: radiosonde, synop (surface), ship, buoy, aircraft, wind-profiler, Doppler-radar radial wind, wind and PWV fields retrieved from a satellite-based microwave scatterometer/radiometer, Radar-AMeDAS-analyzed rainfall data, and typhoon bogus data. These data were normally assimilated by the operational Meso 4D-Var. The observation error of the satellite-based PWV was set to 5 mm. Data thinning with a 40 km spacing was applied. For the purposes of quality control, the satellite-based PWV data acquired over land, over dense cloud cover, and over areas undergoing precipitation were discarded.

(2) GPS

In this experiment, in addition to the normal data used in the “CNTL” experiment, GPS-derived PWV values from GEONET stations were also assimilated. Shoji (2009) found that the error related to NRT-analyzed GPS PWV data increases with increasing PWV values. In the present study, the observation error for the

GPS-derived PWV data was set to 5 mm on the basis of a comparison between GPS and radiosonde observations. The other settings were the same as those in the "CNTL" experiment.

At the beginning, we performed a pre-run of 24-h sequential DA from 00:00 UTC August 31 to 00:00 UTC September 01, 2006. The JMA-hydrostatic MSM with a horizontal resolution of 10 km was employed as the forecast model to perform 18-h prediction.

4.3.3 Departure Statistics and Quality Control

Figure 4.2 shows a histogram of the height differences between GPS sites and the model surface of the Meso 4D-Var inner model. In mountainous areas, GPS antennas tend to be set up in valleys rather than on mountain slopes or crests. The NWP model surface expresses a smoothed topography; therefore, the model height is greater than the actual surface for about 80% of the GPS stations. This height difference exceeds several hundred meters for about 10% of the GPS stations.

Figure 4.3 shows a histogram of the differences in the GPS PWV values against the mesoanalysis fields generated by the "CNTL" experiment for 10 days from August 31 to September 9, 2006. Most of the departures are within ±10 mm, and in cases where the absolute height difference is less than 100 m ((a) and (c)), the differences show characteristics of a Gaussian distribution. In cases where the absolute altitude difference is larger than 300 m ((b) and (d)), small positive biases can be seen. This may express the limitation of the height correction scheme described in subsection 4.2.3. On the basis of this result, to avoid introducing biased data in the DA, we decided to use GPS stations that had an absolute height difference from the inner model of Meso 4D-Var of less than 200 m.

Figure 4.4 shows the dependence of the PWV difference on the precipitation intensity. It can be seen that the GPS PWV values tended to be larger than the analysis field generated by the "CNTL" experiment in the case of heavy rain. We attributed this result to the fact that especially under heavy rain conditions, the GPS PWV shows a water vapor increase associated with precipitation whereas the model tends to underestimate the same.

	Observed	Not observed
Predicted	Hits	Misses
Not predicted	False alarms	

Figure 4. 5: Contingency table for calculating threat score and bias score. Usually, the case of no precipitation for both observation and prediction has the highest ratio in the table. To focus on the NWP performance for a precipitation forecast, such cases were excluded from the evaluation target.

The quality check was mainly based on the method proposed by Mannoji et al. (1998). However, the threshold value was changed according to the departure statistics as follows. The observed GPS PWV data were discarded if the following conditions were not satisfied:

(1) Absolute value of height difference between model surface and actual surface was less than 200 m.

(2) The observed GPS PWV was between 1 mm and 80 mm.

(3) The absolute value of the PWV D-value was less than 8 mm after height correction.

4.3.4 Data Assimilation Results

(1) Precipitation Forecast Score

A precipitation forecast result is often evaluated by a threat score and bias score. Figure 4.5 shows the concepts of these scores. First, the precipitation forecasts at each grid point are sorted according to the conditions of the two-by-two contingency table. Then, the scores are calculated by using the number of data in each contingency box as follows.

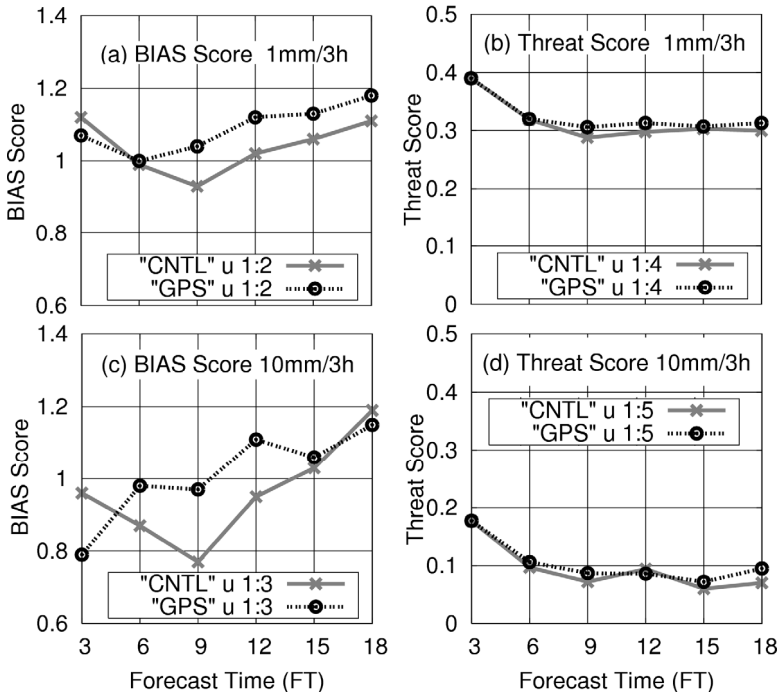

Figure 4. 6: Precipitation forecast score calculated from 48 forecasts from 00:00 UTC September 1 to 18:00 UTC September 12, 2006. (a) Bias score (1 mm/3 h), (b) threat score (1 mm/3 h), (c) bias score (10 mm/3 h), (d) bias score (10 mm/3 h). Thick gray line: "CNTL," dotted black line: "GPS." (Adapted from Shoji and Kunii 2007)

$$\text{Threatscore} = \frac{\text{Hits}}{\text{Hits} + \text{Misses} + \text{FalseAlarms}}, \tag{4.2}$$

$$\text{Bias score} = \frac{\text{Hits} + \text{False Alarms}}{\text{Hits} + \text{Misses}}. \tag{4.3}$$

Figure 4.6 shows the comparison results for precipitation forecasts using Radar-AMeDAS-analyzed rainfall, which was estimated by meteorological radars and calibrated using surface rain gauge observations. The bias score of the "CNTL" experiment reaches a minimum at around the 09 hour forecast (FT = 09), whereas the "GPS" experiment shows a tendency to gradually increase. In contrast, the bias score of "GPS" for heavy (10 mm/3 h) rain reaches a minimum at around FT = 03 with values less than 0.8. The Radar-AMeDAS-analyzed rainfall is also assimilated in both the "CNTL" and the "GPS."

The bias score of nearly 1 against the Radar-AMeDAS-analyzed rainfall in the

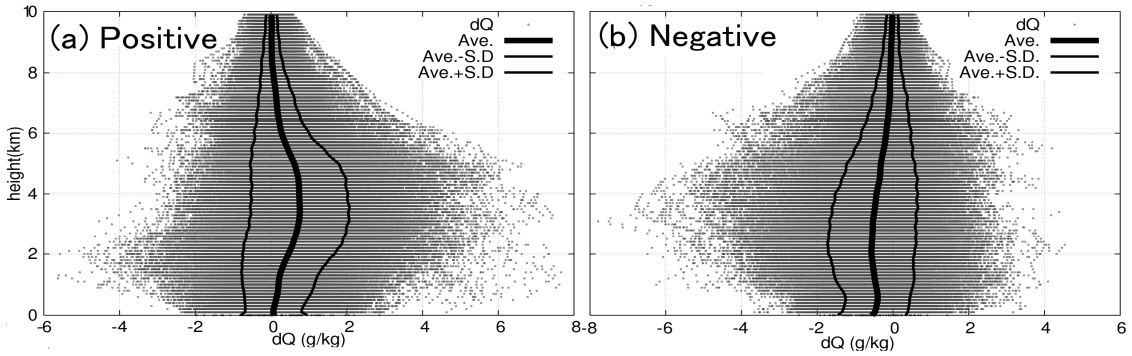

Figure 4. 7: Change in analyzed specific humidity profile by GPS PWV assimilation for entire assimilation period. The grids nearest to each GPS station between the northern latitudes of 31–36° were selected for comparison. (a) Positive increment case, (b) negative increment case. The small gray dots represent raw data, whereas the thick black line represents the average and the thin black lines represent the average ±standard deviation. (Reproduced from Shoji and Kunii 2007)

"CNTL" experiment might indicate that the assimilation of the Radar-AMeDAS itself results in the prediction of a comparable amount of precipitation for the first 3 h of the NWP. Further, the depression of the bias score toward FT = 09 might have been caused by an underestimation of the water vapor in the analyzed initial field of the MSM. In the "GPS" experiment, the water vapor increase might play a role in inhibiting the development of a strong precipitation system at an early stage of each prediction.

The threat score of the "GPS" experiment is almost neutral or slightly higher than "CNTL" throughout the forecast time for both light (1 mm/3 h) and heavy (10 mm/3 h) rains. At FT = 03 h, the threat score of "GPS" is almost the same as that of "CNTL," even though the bias score is small. This may imply that the positional lags of predicted precipitations are improved by the DA of GPS PWV.

(2) Change in Water Vapor Vertical Profile

Because PWV is a vertically integrated value and possesses no information about the vertical structure of the atmosphere, it is important to determine how the GPS PWV modifies the vertical structure of the water vapor.

Figure 4.7 shows the changes in the specific humidity profile in the analysis field generated by GPS PWV assimilation for the entire assimilation period. The grids nearest to each GPS station in the northern latitudes of 31–36° were selected for comparison. In a case where the increment of PWV was positive (a), an increase in specific humidity

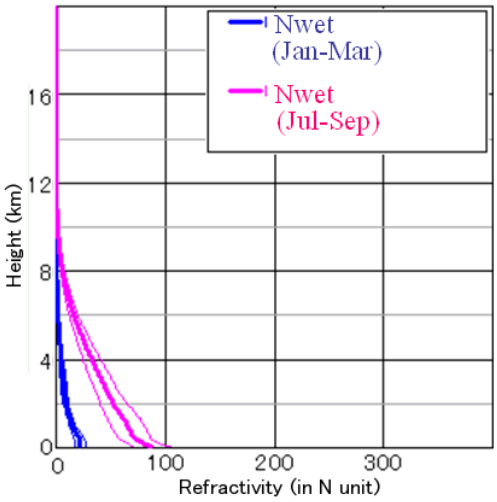

Figure 4. 8: Vertical structure of variation in water vapor refractivity (sum of the second and third terms on the right-hand side of equation (2.15)) observed by radiosonde at Tsukuba, Japan, in 2001. The peach colored thick line and thin lines represent the average and variation in summer, respectively (July–September). The thick blue line and thin lines represent the average and variation in winter, respectively (January–March).

occurs, mainly at altitudes of 3–5 km. At altitudes below 1 km, the average changes are neutral and the variability is smaller than those at 3–5 km. In a negative increment case (b), the average changes at altitudes of less than 1 km are negative, whereas the maximum change occurs at altitudes of 3–5 km. As shown in Figure 4.8, the water vapor variation is large in the lowest layer of the atmosphere. The results shown in Figure 4.7 express different characteristics. The altitudes where a large variability in humidity increments is observed (3–5 km) correspond to the altitudes with relatively large background error. The statistical tendency of the water vapor increments shown in Figure 4.6 might reflect the vertical structure of the background error. Therefore, as Nakamura et al. (2004a) mentioned, PWV DA might result in a misleading vertical profile analysis, particularly in cases where the departure of the GPS PWV from the model first guess is large.

4.3.5 Summary of Continuous DA Experiment

To statistically evaluate the impact of the NRT-retrieved GPS PWV on a precipitation forecast, a continuous DA experiment was conducted for 12 days, from September 1 to 12, 2006.

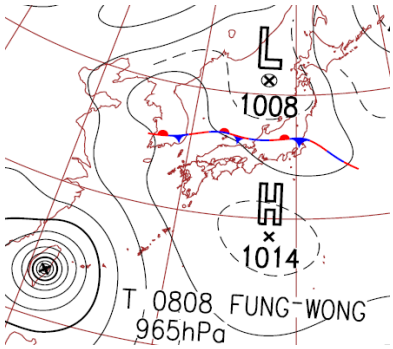

Figure 4. 9: Surface weather map at 09 JST on July 28, 2008.

The NRT-retrieved GPS PWV data showed good agreement with the MSM initial field obtained from DA without the GPS PWV data. After height correction, the GPS PWV data showed little bias against the MSM initial field, except for a large height difference (more than 600 m) and in a heavy rain case.

The DA of the GPS PWV data resulted in no effect or a slight improvement in the precipitation forecast. A tendency of inhibition of a strong precipitation prediction in the first 3 h forecast was seen to some extent for the DA of GPS PWV. The bias score gradually increased as the forecast time advanced. The bias score of the "CNTL" experiment was nearly 1 at the first 3 h forecast, but this score decreased and reached a minimum at FT = 09.

A statistical comparison of the change in the humidity profile revealed that the DA of PWV caused a relatively large change at altitudes of around 3–5 km.

These results show both the usefulness and the limitation of the DA of GPS PWV.

4.4 Importance of Windward Water Vapor Information

In this section, we introduce a DA experiment using GPS PWV data for a heavy rainfall case that occurred in the Hokuriku and Kinki districts on July 28, 2008. The JMA operational mesoscale NWP system (MSM) could not predict the strong precipitation. Therefore, to examine the performance of GPS-derived PWV data for heavy-rain prediction, a DA experiment was conducted. The results strongly support the usefulness of the GEONET-derived PWV. The importance of water vapor information in the windward direction is also highlighted.

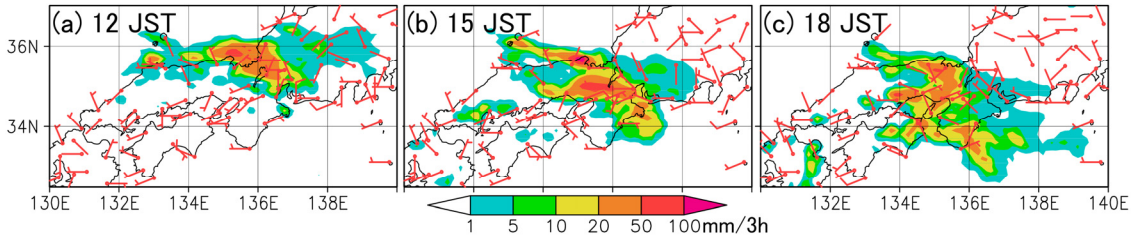

Figure 4.10: 3-h accumulated Radar-AMeDAS analyzed rainfall at (a) 12 JST, (b) 15 JST, and (c) 18 JST on July 28, 2008. The arrows show the observed surface horizontal winds. (Adapted from Shoji et al. 2009a)

In subsection 4.4.1, the meteorological case is described. The design of the experiment is explained in subsection 4.4.2. In subsection 4.4.3, the results of the experiment are provided, and in subsection 4.4.4, the experiment is summarized.

4.4.1 Meteorological Case

On July 28, 2008, a local heavy rainfall occurred over the Hokuriku and Kinki districts, in central Japan. A stationary front existed near the heavy rainfall areas, and the atmospheric instability was increased by the inflow of upper-level cold air. In the surface weather map for that day (Figure 4.9), a stationary front was analyzed in the east-west direction across the central part of Honshu Island. There was a cold low-pressure system approximately 500 km north of the front. The western part of Japan was covered by a high pressure system, and Typhoon 0808 (Fung-Wong) hit Taiwan. These synoptic patterns suggest inflows of low-level humid air around the western part of Japan. Figure 4.10 shows the 3-h accumulated Radar-AMeDAS analyzed rainfall, which was estimated by meteorological radars and calibrated using surface rain gauge observations. Before 12 JST, a strong rainfall system was observed along the San-in and Hokuriku districts. This precipitation system developed as it moved southwestward. JMA's operational mesoscale model (MSM) could not predict the heavy rainfall.

The IGS operates a continuous global network of ground-based GPS stations for GPS satellite tracking and provides GPS observation data via their ftp server. Though the spatial distribution is rather sparse compared to that of the GEONET stations, some of the IGS stations are located in East Asia (Figure 4.11). In this study, we analyzed the PWV data obtained from the IGS stations and assimilated these with the GEONET-derived PWV by using Meso 4D-Var in order to validate their usefulness.

Figure 4.12 shows the time variation in the precipitation system and the GPS-derived

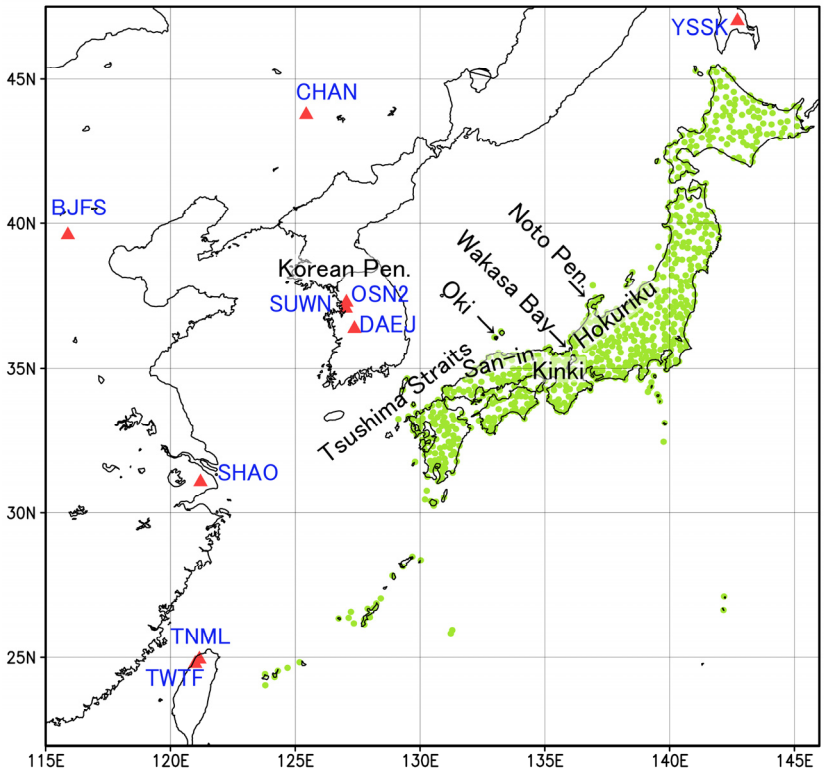

Figure 4.11: GPS stations around Japan. Green filled circles (●): GEONET stations used in 4D-Var experiments “GEONET” and “GEONET + IGS” and red filled triangles (▲): IGS stations used in 4D-Var experiment “GEONET + IGS.” The four blue characters near each IGS station denote the IGS station ID. The names of the places referred to in this paper are represented using black characters. (Adapted from Shoji et al. 2009a)

PWV from 03 to 09 JST on July 28. At 03 JST, a line-shaped precipitation system was observed from the northeast through the Noto Peninsula to the southwest (Figure 4.12(a)). This precipitation system developed over time as it moved southward. At 09 JST, the western part of the rain came close to the coast of the San-in region (Figure 4.12(b)). The GPS-derived PWV exceeded 60 mm along the San-in district and Wakasa Bay (Figure 4.12(c)). The change in PWV from 03 JST to 09 JST clearly shows an increase on the south side of the rainfall system and a decrease on the north side (Figure 4.12(d)). The PWV increase in the San-in district was limited to the coastal region.

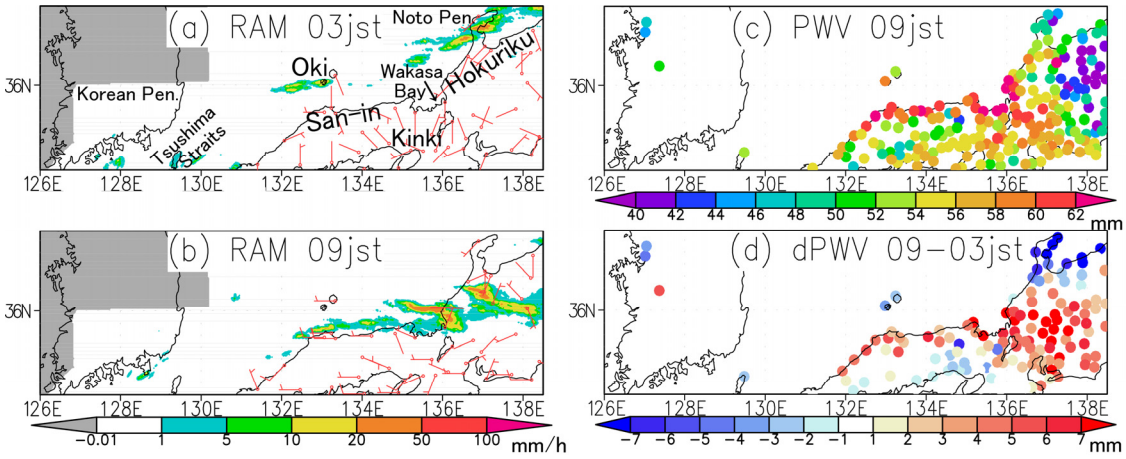

Figure 4.12: 1-h accumulated Radar-AMeDAS analyzed rainfall at (a) 03 JST and (b) 09 JST. (c) GPS derived PWV at 09 JST, and (d) differences in GPS-derived PWV between 09 JST and 03 JST. (Adapted from Shoji et al. 2009a)

This suggests that most of the humid air was concentrated at the lowest level of the troposphere. Further, it is noticeable that in the Korean Peninsula, the PWV decreased at the north-side stations (SUWN and OSN2) whereas it increased at the south-side point (DAEJ). This contrast may affect the forecast of the numerical model if PWV values derived from IGS stations are used in addition to those observed at GEONET stations.

4.4.2 Design of Experiments

In this study, we performed the following three continuous assimilation experiments. These experiments differed in terms of their assimilated observation data as follows:

(1) CNTL

The following data were used: radiosonde, synop (surface), ship, buoy, aircraft, wind profiler, Doppler-radar radial wind, wind and PWV fields retrieved from a satellite based microwave scatterometer/radiometer, Radar-AMeDAS analyzed rainfall, and typhoon bogus data. These data are normally assimilated in the operational Meso 4D-Var. The observation error for the satellite-based PWV was set to 5 mm. Data thinning with a 40 km spacing was applied. For quality control, the satellite-based PWV data were discarded in areas over land, covered by dense cloud, and with precipitation.

(2) GEONET

The data used in this experiment were the normal data and GPS-derived PWV values at GEONET stations. Since the horizontal grid spacing of the Meso 4D-Var system is 20 km, the spatial density of the GEONET stations was higher than that in some places. In order to avoid over-fitting, GEONET station thinning was performed to make the spatial density of the GPS observations coarser than 20 km.

The observed GPS PWV data were discarded if the following conditions were not satisfied:

・The absolute value of the height difference between the model surface and the actual surface was less than 500 m.

・The observed GPS PWV was between 1 mm and 80 mm.

・The absolute value of the PWV D-value was less than 10 mm after height correction.

Shoji (2009) found that the error related to NRT-analyzed GPS PWV increases with an increase in the PWV value. In the present study, the observation error for the GPS-derived PWV was set to 5 mm on the basis of a comparison between GPS and radiosonde observations. The other settings were the same as those in the case of "CNTL."

(3) GEONET + IGS

The GPS-derived PWV was added at both the GEONET and the IGS stations shown in Figure 4.11. The other settings were the same as those in the case of "CNTL."

Our target was to improve the forecast at the initial time of 09 JST (July 28, 2008). In each experiment, we performed a pre-run of 30-h sequential data assimilation from 03 JST (July 27) to 09 JST (July 28) with 3-h assimilation windows. The JMA-nonhydrostatic model (Saito et al. 2007) with a horizontal resolution of 10 km (10 km-NHM) was employed as the forecast model in the numerical prediction after the initial time.

4.4.3 Results of Data Assimilation

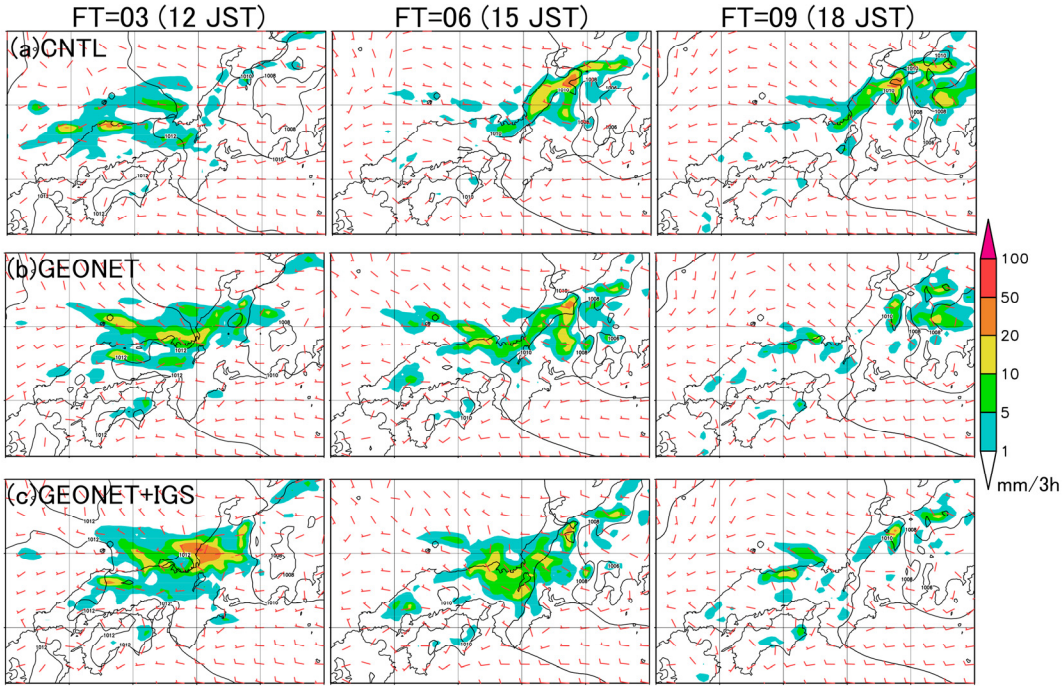

Figure 4.13: 3-h accumulated rainfall predicted by 10-km NHM for experiments: (a) CNTL, (b) GEONET, and (c) GEONET + IGS. The initial time was 09 JST on July 28, 2008. (Adapted from Shoji et al. 2009a)

Figure 4.13 shows the 3-h accumulated rainfall distribution predicted by the 10-km NHM for the following experiments: (a) CNTL, (b) GEONET, and (c) GEONET + IGS. The initial time was 09 JST on July 28, 2008. The "CNTL" experiment (Figure 4.13(a)) predicted neither the development nor the southward movement of the heavy rainfall system shown in Figure 4.10. The "GEONET" experiment (Figure 4.13(b)) predicted the line-shaped precipitation system from Wakasa Bay to the Oki islands at FT = 03; however, the system did not develop and did not move southward. The "GEONET + IGS" experiment (Figure 4.13(c)) predicted more intense precipitation around Wakasa Bay at FT = 03 and the southward development of precipitation at FT = 06. On the whole, we conclude that among these three experiments, "GEONET + IGS" provided the best forecast. The predicted rainfall was still insufficient at FT = 9. In order to elucidate the reason for this insufficiency, the DA and NHM model physics need to be investigated further.

Figure 4.14(a) describes the initial field for the PWV and surface wind of the "CNTL" experiment at 09 JST on July 28, 2008. Compared to Figure 4.12(c), this figure

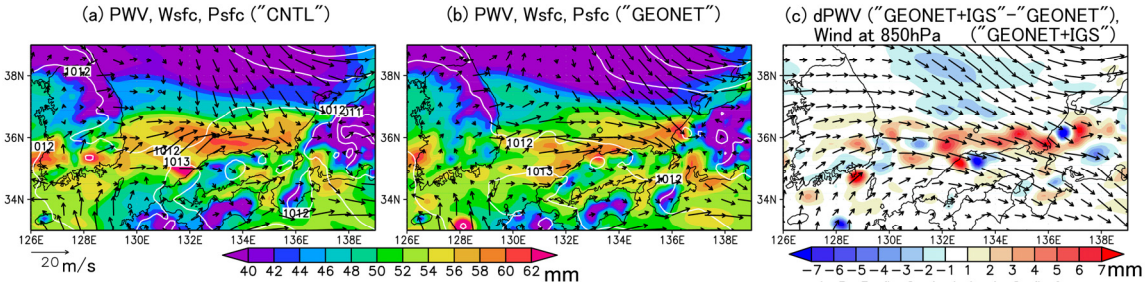

Figure 4.14: (a) Initial PWV (shaded), surface pressure (contour), and surface wind fields of "CNTL" experiment at 09 JST on July 28, 2008. (b) Same as (a) except for "GEONET" experiment. (c) Difference in initial field of PWV (shaded) between "GEONET + IGS" and "GEONET" at 09 JST on July 28, 2008. The arrows show winds at the level of 850 hPa in the case of "GEONET+IGS." (Adapted from Shoji et al. 2009a

shows a PWV overestimation around the Oki islands and an underestimation near the San-in seashore. A surface wind convergence zone is formed from Wakasa Bay toward the west-northwest, and the PWV maximum is located around the wind shear line off the north coast of the San-in district. The PWV field in the "GEONET" experiment is shown in Figure 4.14(b). The overestimation around the Oki islands and underestimation near the seashore are improved in this experiment. Northerly winds are seen around Wakasa Bay and off the coast of the San-in area. It can be said that through the assimilation of GPS-derived PWV data, the weather front was analyzed more correctly. Figure 4.14(c) shows the differences in the PWV fields between "GEONET + IGS" and "GEONET." The arrows in this figure indicate the wind field at the 850 hPa level. An eastward extension of the positive increase in PWV that has its origin near the "DAEJ" IGS station is clearly observed. In Figure 4.12(d), we see a PWV increase at "DAEJ" and a PWV decrease at "SUWN" and "OSN2." The positive increase near "DAEJ" propagated downstream and enhanced the abovementioned characteristics.

4.4.4 Experiment Summary

Data assimilation experiments using GPS-derived PWV data were performed for the heavy rainfall that occurred on July 28, 2008, in Hokuriku and Kinki districts. The PWV values derived from the nationwide ground GPS network (GPS Earth Observation NETwork: GEONET) improved both the northward position error of the low-level convergence zone and the forecast of the observed rainfall, which the operational NWP could not predict. Further improvements were obtained when the PWV data derived from the GPS stations of the International GNSS Service in East Asia were added.

The results strongly support the usefulness of GEONET-derived PWV. At the same time, the outcomes suggest the importance of water vapor observations not only in Japan but also in surrounding areas, particularly on the windward side. However, this is only one case study. To assess the impact statistically, a continuous DA experiment should be conducted over several weeks.

4.5 Concluding Remarks

The results of a continuous 12-day DA of GPS PWV data from September 2006 and a case study of GPS PWV DA for a heavy rainfall event on July 28, 2008, were introduced.

The continuous DA experiment resulted in a slight improvement in the precipitation threat score throughout the forecast period (FT = 00–18). However, a tendency was seen for the DA of the GPS PWV to inhibit a strong precipitation prediction in the first 3 h forecast and the bias score gradually increased as the forecast time advanced. A statistical comparison of the change in the humidity profile revealed that the DA of PWV caused a relatively large change at altitudes of around 3–5 km. These results show both the usefulness and the limitation of the DA of GPS PWV.

Additional studies are needed for further improvement, e.g., a closer inspection of the characteristics of the GPS PWV errors. The interpolation of the surface temperature and pressure observed at surface weather stations to GPS antennas would cause errors in the GPS PWV. The direct assimilation of ZTD may lead to better results. Ishikawa (2008) demonstrated that when ZTD was assimilated in Meso 4D-Var, there was a conspicuous improvement in the precipitation forecasts. Ishikawa also adopted a restriction for GPS use, as no GPS TZD was assimilated in rainy weather. As mentioned in subsection 4.3.4, Radar-AMeDAS-analyzed rainfall was also assimilated in the Meso 4D-Var system. Both the Radar-AMeDAS and the GPS PWV relate to atmospheric water vapor. However, their characteristics are different from each other because Radar-AMEDAS shows 1 h accumulated precipitation, whereas GPS PWV or ZTD data are momentary values calculated by averaging the signal delays of the GPS satellites in view. Further studies are needed to enable the evaluation and employment of both the Radar-AMeDAS and the GPS data without causing a conflict in the DA system.

DA experiments related to GPS-derived PWV were performed for the heavy rainfall event that occurred on July 28, 2008, in the Hokuriku and Kinki districts. These results also demonstrated the usefulness of not only the GEONET-derived PWV but also the

PWV derived from IGS stations in East Asia. These results show that it is important to use water vapor observations, not just from Japan, but also from surrounding areas, particularly on the windward side. The IGS stations can be used as a global water vapor observation network for operational NWP. We showed the considerable impact of GPS PWV data, though just for one case study. In the future, we intend to perform further statistical evaluations of quantitative forecasts.

Chapter 5

Summary and Future Aspects

5.1 Summary

The objective of this study was to contribute to mesoscale NWP by GPS remote sensing. In this thesis, we present a sequence of studies aimed at developing a practical method for PWV retrieval using GPS radio signals observed by ground-based GPS stations. We also evaluate the impact of GPS-derived PWV on mesoscale NWP. Here, we provide brief summaries of this thesis and certain aspects of GPS meteorology.

In Chapter 1, we briefly reviewed GPS meteorology, the importance of water vapor, several features of GPS remote sensing, and numerical weather predictions. Then, we explained the objective of this study.

In Chapter 2, we explained the basic principles of GPS, the effects of a neutral atmosphere on GPS radio signals, atmospheric models used in space geodesy, and the relation between GPS signal delay and water vapor. Several types of noises that can affect PWV retrieval are contained in GPS signals, such as site displacement due to tidal effects, antenna PCV, multipaths, and clock error.

In Chapter 3, we described studies directed at removing error sources from GPS-derived PWV. The results of our study can be summarized as follows:

(1) Schwiderski's OTL model (Schwiderski, 1981) is confirmed to reduce the amplitude of the day and night bias difference by almost 1/2 to 1/3.

(2) Introducing an antenna PCV model specific to the antenna type can reduce most of the antenna-specific bias in GPS PWV.

(3) We constructed a multipath correction table by stacking post-fit phase residuals. This method allows us to include not only the effect of the antenna pillar but also the site-specific multipath effect.

(4) The multipath correction table also allows us to reproduce the SPD. A detailed

explanation is provided in Appendix-B.

(5) Clock information obtained from a ground GPS station equipped with a hydrogen maser atomic clock proved useful as a reference clock for PPP analysis. This enabled the NRT retrieval of PWV from the large nationwide GPS network in Japan. By comparing GPS PWV with other water vapor sensors such as radiosonde and MWR, it was confirmed that ground-based GPS observations can be used to obtain GPS PWV with an accuracy of several millimeters under all weather conditions and in NRT.

In Chapter 4, we presented the results of DA experiments that illustrated how GPS PWV can affect mesoscale NWP. The following effects of GPS PWV were confirmed.

(1) The 12-day results for the continuous DA experiment were either neutral or contributed to some improvement in the precipitation threat score throughout the 18-h prediction period.

(2) A DA experiment on July 28, 2008, showed that assimilation of GEONET-derived PWV can lead to remarkable improvements in precipitation predictions.

(3) Assimilation of PWV derived from both GEONET and GPS over East Asia resulted in further improvements in precipitation predictions. PWV derived from GPS stations on the Korean peninsula seemed to play a significant role in the analysis of the water vapor field in the windward direction of a strong precipitation system.

(4) In the PWV DA results, we interpreted a surface wind (and also a water vapor) convergence zone extending from Wakasa Bay toward the west-northwest direction. These fields were appropriate for supplying water vapor and forming cumulus convective clouds around the observed precipitation system. The fields were analyzed by DA of GPS PWV. GPS PWV is not a dynamical element and has limited applicability on land. However, with 4D-Var and modifications to dynamic fields (such as wind), increments in water vapor can be observed not only on land but also over the ocean. Furthermore, the importance of water vapor information for the windward direction was highlighted.

5.2 Future Aspects

On October 28, 2009, JMA started the operational use of PWV derived from GEONET in its mesoscale DA system. The NRT PWV retrieval method, which is described in this thesis, was adopted in JMA's operational GPS analysis system. In this section, we describe some aspects for possible future development in GPS meteorology.

One expected development is the expansion of the PWV analysis area, e.g., over the oceans, polar regions, and the tropics. Fujita et al. (2008) demonstrated the accuracy of PWV analyzed by a ship-borne GPS receiver. Although their analysis used precise final ephemerides of GPS satellites, the results strongly suggest that ship-borne applications have good prospects. If PWV can be obtained over the ocean, it would have a great impact on both mesoscale and global-scale NWP. Despite the importance of water vapor monitoring in the polar areas and tropics, the observation density is very sparse in these areas. The water vapor variation in polar areas is very important for climate monitoring and weather forecasting. In the tropics, sparse observation sometimes causes deterioration in NWP, as in the case of our DA study on Cyclone Nargis (Shoji et al. 2010). There is a need for the establishment of water vapor observation networks in the low latitudes.

Slant path delay (SPD) or slant wet delay (SWD) data are thought to possess inhomogeneous information about the atmosphere that is neglected during the retrieval of ZTD or PWV. Several studies succeeded in reproducing the three-dimensional distribution of water vapor by using SWD (e.g., Seko et al. 2004a; Noguchi et al. 2004). These studies used SWD that was retrieved by the procedure developed by Shoji et al. (2004); in this procedure, precise final ephemerides of GPS satellites are used. Recently, Kawabata et al. (2009) conducted a DA experiment on SPD for a local heavy rainfall event in Tokyo on August 5, 2008. Their study used NRT SPD; however, the error characteristics of the data have not been well investigated thus far. It is necessary to evaluate NRT SPD/SWD for operational use.

The combined use of ground-based GPS and GPS RO methods would open up new avenues for atmospheric research. GPS PWV possesses a high time resolution. By using GEONET, we can acquire mesoscale PWV variations in Japan. However, GPS PWV does not have any vertical information. GPS RO, on the other hand, possesses high vertical resolution. Horizontal resolution varies with the height of GPS signals, which can reach several hundred kilometers in the lower troposphere. Taking advantage of each of these methods will enable the retrieval of the three-dimensional structure of water vapor. The GPS RO method is already being applied to operational NWP. Thus far, the data have mainly been used for global analysis; however, there are many studies that

have demonstrated the method's usefulness for severe weather predictions (e.g., Seko et al. 2009a; Kunii et al. 2009). As of November 2009, 1,500–2,500 atmospheric profiles have been observed by the GPS RO method. The number of observations is expected to increase with the number of GPS RO missions.

Promotion of the GPS downward-looking method is also desired. The space-based GPS RO method of observation is relatively ineffective for observations inside the planetary boundary layers, because large vertical gradients of refractivity sometimes block the penetration of the GPS signal into the boundary layer. The GPS receiver is within the boundary layer in the GPS downward-looking method. Boundary layer research is important for improving NWP, but observational data are limited. If the GPS downward-looking method comes into practice, it will surely benefit NWP.

GPS remote sensing is based on observing the phase of the radio signal. No signal intensity observation is required. This fundamental consideration provides GPS remote sensing with the unique characteristics of being calibration-free and having no age degradation. The system has great potential for monitoring the Earth's environment. The author strongly intends to continue studying GPS meteorology and to contribute toward mitigating the effects of weather disasters in Japan and throughout the world.

APPENDIX-A

Characteristics of Water Vapor Observational Systems

Here, we overview some representative water vapor observation systems. Table A1 summarizes the water vapor observation methods that are either currently used or are expected to be used in the near future for operational NWP. The values of accuracy, resolution, and height in the table are only roughly estimated values.

(1) In-Situ Observation

The importance of in-situ observation, as either a continuous monitoring tool or as a source of reference data for the evaluation of remote sensing data, is increasing.

Radiosonde observations (RA-OB) are typically used to measure atmospheric humidity. A balloon attached to meteorological sensors is launched into the atmosphere, and it measures the height profile. Though RA-OB provides valuable direct observations, the density of RA-OB is sparse due to its cost. Typically, the balloons are launched twice a day from stations that are placed mainly on land about several hundreds kilometers apart.

It is known that humidity sensors in radiosondes have type specific biases (Wang et al. 2002). The Japan Meteorological Agency (JMA) has used the static electricity capacitance humidity sensor since 1992 in the RS2-91 radiosonde. The accuracy of the static electricity capacitance sensor varies with temperature. Therefore, bias correction according to temperature is mandatory. The temperature sensor is affected by solar insolation; therefore, if the correction for insolation is insufficient, errors in temperature observations will cause errors in the humidity values. Meteolabor's Snow White model is not affected by solar insolation because it uses a mirror chilled humidity sensor. In recent years, evaluation studies of radiosonde humidity sensors have been conducted using Snow White as the reference (e.g., Nash, J. et al. 2005; Vance, A. K. et al. 2004). The humidity measurements may also be affected by liquid water from the clouds condensing on the sensor.

Low cost humidity sensors have been developed for use on small aircraft (Moninger et al. 2003). The nominal accuracy of these sensors is ±5% for aircraft speed of less than Mach 0.4 and ±10% for speeds of Mach 0.4–0.6.

(2) Geostationary Meteorological Satellite

An increase in the number of infrared channels on satellites has made quantitative water vapor observations possible. The first Japanese geostationary meteorological satellite "GMS (Himawari 1)" was launched in 1977, and it had only one channel for each visible and infrared band. The number of channels increased to 3 in "GMS-5 (Himawari 5)" and to 4 in "MTSAT-1R (Himawari 6)" and "MTSAT-II (Himawari 7)". "MTSAT-II" (launched in 2006) has 4 infrared channels, and the observed temperature in the 6.3 μm absorption band is used to image water vapor. Information regarding the amount of water vapor can be retrieved continuously by analyzing several different infrared channels (the split window method). In June 2007, JMA started brightness temperature observations in the 6.5–7.0 μm frequency bands for their operational global analysis (GANAL).

(3) Microwave Water Vapor Radiometer (MWR)

It can be said that the satellite-based MWR observation method is one of the most developed observational method in recent years.

Water vapor in the atmosphere emits and absorbs electromagnetic waves. The wavelength varies depending on the temperature of the water vapor. Liquid water and ice water in the atmosphere emit, absorb, and scatter electromagnetic waves. The radiation property differs according to the frequency of the microwave (3–300 GHz). Atmospheric water vapor amount and rainfall intensity can be retrieved by using the brightness temperatures observed at several frequencies that are sensitive to changes in the forms of water.

Space-based MWR observations have been increasing since the successful experiments with MWR in the NIMBUS and SKYLAB missions of the 1970s. At present, the technology provides practical analysis of the initial NWP field.

The MWR imager retrieves the horizontal distribution of precipitable water vapor (vertically integrated water vapor amount: PWV) using one or two frequencies. The microwave sounder analyzes the vertical water vapor profile by additional microwave frequencies. The hyper-spectrum sounder uses both microwave and infrared to enhance vertical resolution and accuracy. The limb-sounder uses microwave observations in the

direction of the Earth's limb from the satellite to resolve the water vapor height profile. Some of these data are already being used for the initial field analysis of NWP.

Ground-based MWR can retrieve both the PWV and the water vapor profiles over the sensor by using a number of frequencies. Continuous observation is possible, but the accuracy degrades under rainy conditions or thick cloud cover. If this issue were to be resolved, ground-based MWR could become an important observation tool for practical weather forecasting.

(4) Lidar

Lidar emits laser pulses and observes the intensity of backscatter caused by aerosols and molecules in the atmosphere. From these information, distribution of minor atmospheric constituents such as water vapor can be retrieved. This technology is also applied to retrieve distributions of wind, temperature, aerosols, and clouds. There are two different methods in Lidar technology. One of these is the differential absorption Lidar (DIAL), which uses the intensity differences between the backscatter of a laser (which synchronizes the absorption line of water vapor) and of frequencies not absorbed. The other method utilizes vibrational Raman scattering from molecular nitrogen and water vapor.

Though observations are restricted to the nighttime and clear skies, or at least to a sky without thick clouds (Goldsmith et al. 1994; Wulfmeyer et al. 1998), Lidar observations have better time resolution and wider height coverage compared to RA-OB.

Though Lidar is categorized as a ground method in Table A1, airborne and satellite-borne applications are being developed.

(5) Windprofiler

The wind profiling radar can observe the three-dimensional wind field with good time-height resolution. Refractivity profile analysis is conducted using turburant echo intensity and the absolute value of the vertical gradient of refractivity. Furumoto et al. (2005) developed a procedure for determining the sign of the refractivity vertical gradient using GPS derived PWV as a constraint condition. The humidity estimated by their method showed good agreement with radiosonde observations at 0.2–2.2 km, and they succeeded in capturing the rapid humidity variations, which cannot be detected by 12-h interval radiosonde observations.

Table A 1　Water Vapor Observational Systems (Reproduced from Shoji 2007)

	In situ		Remote sensing							
			Satellite-based				Ground-based			
	Surface obs.	Radio-sonde	GMS (Imager)	Polar orbiting satellite			Microwave radiometer		Lider	GPS
				Microwave radiometer	Vertical sounder	GPS Radio Occultation				
Observed element	Change in static electricity capacitance between electrodes caused by water absorption of humidity sensor		Brightness temperature in visible and infrared region	Brightness temperature in microwave region	Brightness temperature in infrared and microwave region	GPS signal phase	Brightness temperature in microwave region		Backscatter intensity of laser pulse by atmospheric molecule and aerosol	GPS signal phase
Retrieved element	Relative humidity	Vertical profile of relative humidity	Water vapor in middle to upper troposphere, PWV	PWV	Vertical profile of specific humidity	Refractive index	PWV	Vertical profile of relative humidity	Vertical profile of water vapor mixing ratio or number density	PWV
Horizontal resolution (observation density)	～100km (depends on country and region)	Several hundred km (depends on country and region)	4 km (right below satellite)	10～several tens km	15～50km	several hundred km in lower troposphere				10～several hundreds km (depends on country and region)
Observation height	Surface	Surface～30km	Middle to upper troposphere by WV channel. PWV by split window		Surface～	Surface～40km		Surface～	100m～10km	
Vertical resolution		30m			2～3km	Several tens m		0.2 ～ 0.4 km (depends on height)	100m	
Time resolution	1 hour	6, 12 hour	0.5 - 1 hour	Several hours (depends on number of satellites)		400～500profile per day by 1 satellite	1～several minutes		several minutes	several minutes
Accuracy	Relative humidity 5%		PWV 3～4mm	PWV 3～5mm	Relative humidity10～20%	Refractive index 1%	PWV 2～3mm	Relative humidity 30～50%	Mixing ratio 5～10%	PWV 2～3mm
Satellites (sensor)			GMS, MTSAT, GOES, METEOSAT	DMSP (SSM/I), TRMM (TMI), Aqua (AMSR-E)	NOAA (AMSU-A,B, MHS,HIRS), METOP (AMSU-A, MHS,HIRS,IASI), Aqua (AMSU-A, HSB,AIRS) GOES	CHAMP SAC-C FORMOSAT-3/COSMIC MetOp GRACE				
Remarks	Most stations distribute on land.		Accuracy varies depending weather and surface condition.			Negative bias in lower troposphere.	Accuracy varies depending weather and surface condition.			Most stations distribute on land.

(6) Weather Radar

Refractive index, which is obtained from Doppler radar phase data caused by reflections from fixed targets (e.g., power transmission towers), has recently been of interest as a possible information source for water vapor (Fabry 2004). Because the phase data of Doppler radar is available in a very short time, refractive index information is

expected to be useful for real-time prediction of the generation and development of thunderstorms.

As a part of the International H_2O Project 2002, Fabry (2006) estimated the refractivity fields from the phase data of Klystron type S-band radars, at a wavelength of approximately 10 cm. Temporal variations in refractive index (RI) were estimated from the phase data from the magnetron type C-band radar of the Meteorological Research Institute (MRI) (Seko et al., 2009b).

APPENDIX-B

Analysis of Slant Path Delay and its Horizontal Scale

There are several applications using GPS derived slant path delay (SPD) (e.g. Seko et al. 2004a; Noguchi et al. 2004; Kawabata et al. 2009). Here we describe how to retrieve the SPD from GPS analysis.

(1) Analysis of Slant Path Delay

In our analysis, we define the SPD by adding GPS carrier phase post fit residual for atmospheric delay model of MacMillan (1995) as.

$$dT_i^l(\theta,\phi) = m(\theta)\cdot\left[ZTD + cot\theta\left(G_n cos\phi + G_e sin\phi\right)\right] + \varepsilon\,, \tag{B1}$$

where θ and ϕ denote the elevation and azimuth angle of each satellite, respectively. m(θ) is the mapping function and ε is the postfit phase residual that would include all unmodeled phase errors that are not considered in GPS analyses. The postfit residuals contain the higher order atmospheric inhomogeneity. However, other errors that result from antenna PCV, signal scattering and multipath and satellite orbit errors are also included. It is important to remove such errors for the SPD analysis, except for those due to atmospheric inhomogeneity.

In order to estimate SPD as well as PWV, correction methods were adopted to correct for unmodeled PCV errors, specific to antenna-types, and errors due to signal scattering in combination with the GIPSY-OASIS II software package based on the simple procedure of precise point positioning strategy. Precise orbit and high rate satellite clock correction data provided by the Jet Propulsion Laboratory (JPL) of the National Aeronautics and Space Administration (NASA) were used for the analysis. Niell's mapping function (NMF) was used for m(θ) (Niell 1996). NMF contains two different mapping functions, NMFh for delay attributed to dry atmosphere (Hydrostatic delay)

and NMFw for that resulting from atmospheric water vapor (Wet delay).

In our GPS analysis, the hydrostatic delays in the zenith direction (ZHD) were calculated based on the station height by using following equation and regarded as a constant through the analysis.

$$ZHD = 1.013 \cdot 2.27 \cdot \exp\left(-0.116 \cdot 10^{-3} \cdot ht\right), \tag{B2}$$

where *ht* is the station height in meters. The wet delay in the zenith direction (*ZWD*) and gradient parameters (G_N, G_E) were modeled as random walk variables with random walk sigma of 0.17mm/s$^{1/2}$ for *ZWD* and 0.03mm/s$^{1/2}$ for G_N and G_E, and estimated every 30 seconds as time dependent parameters. The delay gradient by water vapor and that by dry air cannot be separated unless a three-dimensional atmospheric structure is used. Therefore, for convenience, we chose Niell's mapping function for water vapor (*NMFw*) for the delay gradient. The final formula for describing *SPD* in our analysis becomes as follows:

$$\begin{aligned} dT_i^j(\theta,\phi) = {} & NMFh(\theta) \cdot ZHD + \\ & NMFw(\theta) \cdot [ZWD + \cot\theta(G_N \cos\phi + G_E \sin\phi)] + \varepsilon \end{aligned}. \tag{B3}$$

The elevation cut-off angle for the GPS analysis was set at 10 degrees, because the PCV models that we used describe the PCV value only above 10 degree elevation angles. We applied 11 main tidal constituents for the ocean tidal loading effect, calculated by GOTIC software (Sato and Hanada, 1984) based on Schwiderski's ocean tidal model (Schwiderski, 1981) for all campaign sites. The effectiveness of this model in Japan is described in Shoji et al. (2000).

The postfit residual would contain clock offsets in GPS satellite clocks that commonly affect postfit residuals at all GPS stations. To remove these common modes, we averaged the residuals of each GPS satellite for all the GEONET sites, and subtracted the averaged values from the residuals of each campaign site.

(2) Horizontal Scale of SPD

In order to confirm this, we studied the distance dependency of correlation coefficients between all combinations of the SPDs obtained at different GPS sites and found that postfit residuals have a common time variation that does not depend on the distance between the sites.

At first, we divided each SPD expressed by Equation (B3) into three components and

converted into the zenith direction as follows:

(a) ZTD component: ZHD+ZWD

(b) Gradient component: $\cot\theta(G_N \cos\phi + G_E \sin\phi)$

(c) Residual component: $\varepsilon / NMF_W(\theta)$

Ten-day mean values of the ZTD component and the gradient component were subtracted from those of the original values to remove seasonal variation in water vapor. We then calculated the correlation coefficients for each of the three components.

Figure B1 shows the distance dependency of correlation coefficients for (a) ZTD, (b) Gradients, and (c) postfit residuals. Not only campaign data, but also GEONET results are plotted on the figure. ZTD (crosses) shows very high correlation within the campaign area. The gradient component (open circles) also shows high correlation when the distance is short, but decreases as the distance increases. The postfit residuals which show exponential-like increase when the distance is less than 15 km and approach to zero for distances greater than 15 km.

Some models describe distance dependency of correlation coefficients between water vapor variations observed at different points. For example, Maanen (1981) proposed the following relations:

$$\text{Corr} = \alpha \exp(-R / R0), \tag{B4}$$

where Corr is the correlation coefficients between water vapor variations observed at different points, α is a correlation coefficient when the distance is zero, R is the distance between the two points, and R0 is the horizontal scale of water vapor variation. When errors occur in observation, the correlation coefficient may not reach one even if the distance (R) is zero. In this case α is less than one.

Aonashi et al. (2004) adopted this assumption and estimated the horizontal scales of the zenith component, the gradient component, and the inhomogeneity of water vapor using observed slant path water vapor from three ground-based WVRs. They concluded that the horizontal scale of the atmospheric water vapor inhomogeneity was less than 10 km. If we also adopt the assumption of the exponential-type spatial correlation expressed in Equation (B4) for local-scale atmospheric disturbances, it is estimated from Figure 9 that the mean scale of the local-scale disturbances is about 2 to 3 km. As most of the variations in delay are attributed to water vapor, this suggests the scale of water vapor variations near the ground surface is about 2 to 3 km. Correlation

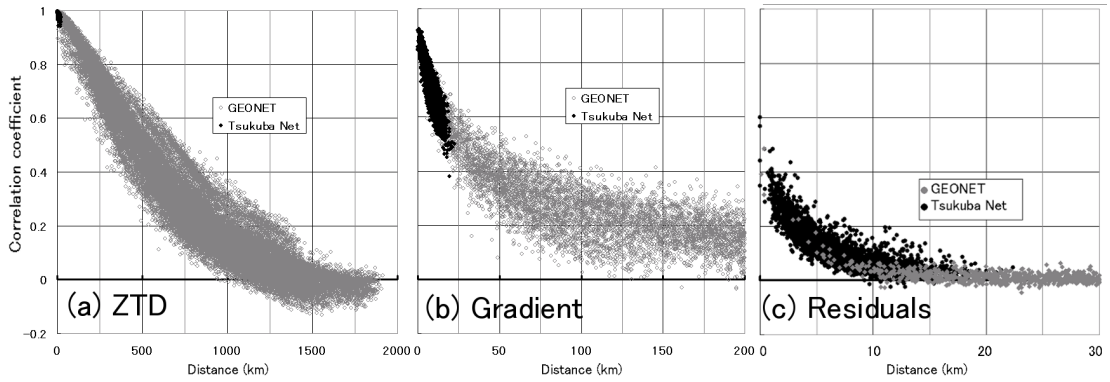

Figure B 1: Correlation coefficients as a function of distance for (a) ZTD, (b) Gradients, and (c) postfit residuals. Gray filled circles are GEONET and black filled circles are Tsukuba Net. Each data point is based on 51 days of data from July 14 to September 2, 2001. (Adapted from Shoji et al. 2004)

coefficients of both ZTD and the gradient component also show an exponential function. However, when we estimate the horizontal scale to be the distance at which the correlation coefficients become 1/e, those of the ZTD and the gradient component are 644±120 km and 62±23 km, respectively.

The standard deviation of the postfit residuals at each site was about 3 mm in the unit of distance. If the correlations are calculated only when the absolute value of the postfit residual at one site was larger than 3 mm, the correlations within a 10 km distance increase. This suggests that when a severe local weather phenomenon, such as a thunderstorm, has been generated, the degree of atmospheric inhomogeneity increases, and that GPS has ability to detect it.

Implications of the existence of correlations due to local-scale variations of atmospheric disturbances in the GPS SPD are:

(1) the conventional GPS analysis inevitably has errors due to local-scale variations in the atmosphere, even if the estimates of gradient parameters are applied. These errors appear in positioning as well as in atmospheric delays. In order to improve accuracy, the effect of local-scale atmospheric variations must be taken into account in the GPS analysis.

(2) GPS postfit residuals detect the inhomogeneous distribution of water vapor on a local-scale of less than 10 km due to weather disturbances like convective thunderstorms. GPS analysis uses a number of models for solid earth tide, ocean

tide, earth rotation and atmospheric delay. If these models are perfect, only random errors that have no spatial correlation will be included in the postfit residuals. Accordingly, spatially dependent correlation must be due to local-scale variation of atmosphere, which is not resolved by ordinary ZTD and gradient parameter analysis.

Publication List

Note: This thesis is based on articles numbered [13],[14],[15],[16],[24] and [25] of the following list.

Refereed Journals

[1] Aonashi, K., Y. Shoji, R. Ichikawa, and H. Hanado, Estimating spatial variation of humidity from GPS and WVR observation in Tsukuba. *Earth Planets Space*, **52**, 907–912, 2000.

[2] Aonashi, K., T. Iwabuchi, Y. Shoji, R. Ohtani, and R. Ichikawa, Statistical Study on Precipitable Water Content Variations Observed with Ground-Based Microwave Radiometers. *J. Meteor. Soc. Japan*, **82**, 269–275, 2004:

[3] Aoyama, Y., Y. Shoji, A. Mousa, T. Tsuda, and H. Nakamura, Temperature and Water Vapor Profiles Derived from Downward-Looking GPS Occultation Data, *J. Meteor. Soc. Japan*, **82**, 433-440, 2004.

[4] Fujibe, F., H. Seko and Y. Shoji, Relation Between Precipitation Distribution and Surface Wind Patterns in the Kanto Plain in the Afternoon of Summer, *TENKI*, **50**, 777-786, 2003 (in Japanese).

[5] Hayashi, H., J. Furumoto, X. Lin, T. Tsuda, Y. Shoji, Y. Aoyama and Y. Murayama, Validation of Refractivity Profiles Retrieved from FORMOSAT-3/COSMIC Radio Occultation Soundings: Preliminary Results of Statistical Comparisons Utilizing Balloon-Borne Observations, *Terr. Atmos. Ocean. Sci.*, **20**, 51-58, 2009.

[6] Iwabuchi, T., Y. Shoji, S. Shimada, and H. Nakamura, Tsukuba GPS Dense Net Campaign Observation: Comparison of the Stacking maps of Postfit Phase Residuals Estimated from Three Software packages, *J. Met. Soc. Japan*, **82**. 315-330, 2004.

[7] Kunii, M., Y. Shoji, M. Ueno and K. Saito, Mesoscale Data Assimilation of Myanmar Cyclone Nargis. *J. Meteor. Soc. Japan*. 2010 (in press).

[8] Nakamura, H., H. Seko, Y. Shoji, and Aerological Observatory, Dry Biases of Humidity Measurements from the Vaisala RS80-A and Meisei RS2-91 Radiosondes and from Ground-Based GPS, *J. Meteor. Soc. Japan*, **82**, 277-299,

2004b.

[9] Sakai T., T. Nagai, M. Nakazato, T. Matsumura, N. Orikasa and Y. Shoji, Comparison of Raman Lidar Measurements of Tropical Water Vapor Profiles with Radiosondes, Hygrometers on the Meteorological Observation Tower, and GPS at Tsukuba, Japan, *J. Atmos. Oceanic. Technol.*, **24**, 1407-1423, 2007.

[10] Seko, H., H. Nakamura, Y. Shoji, and T. Iwabuchi, Meso-γ scale water Vapor Distribution associated with the Thunderstorm on 1 August 2001 Estimated by the Tomography Method. *J. Meteor. Soc. Japan*, **82**, 569–586, 2004b.

[11] Seko, H., Y. Shoji and F. Fujibe, Evolution and air flow structure of a Kanto thunderstorm on 21 July 1999 (the Nerima Heavy Rainfall Event). *J. Meteor. Soc. Japan*, **85**, 455-477, 2007.

[12] Seko, H., Y. Shoji, M. Kunii, and Y. Aoyama, Impact of the CHAMP Occultation Data on the Rainfall Forecast Case study on 16 July 2004. *Data Assim. Atmos., Ocean, and Hydro. Appl.*, Springer-Verlag, 197-218, 2009a.

[13] Shoji, Y., H. Nakamura, K. Aonashi, A. Ichiki, H. Seko, and Members of GPS/MET Japan summer Campaign 1997 in Tsukuba, Semi-diurnal and diurnal variation of errors in GPS precipitable water vapor at Tsukuba, Japan caused by site displacement due to ocean tidal loading, *Earth Planets Space*, **52**, 685-690, 2000.

[14] Shoji, Y., H. Nakamura, T. Iwabuchi, K. Aonashi, H. Seko, K. Mishima, A. Itagaki, R. Ichikawa, and R. Ohtani, Tsukuba GPS Dense Net Campaign Observation: Improvement in GPS Analysis of Slant Path Delay by Stacking One-way Postfit Phase Residuals. *J. Meteor. Soc. Japan*, **82**, 301–314, 2004.

[15] Shoji, Y., A Study of Near Real-time Water Vapor Analysis Using a Nationwide Dense GPS Network of Japan. *J. Meteor. Soc. Japan*, **87**, 1-18, 2009.

[16] Shoji, Y., M. Kunii, and K. Saito, Assimilation of Nationwide and Global GPS PWV Data for a Heavy Rain Event on 28 July 2008 in Hokuriku and Kinki, Japan, *SOLA*, **5**, 45-48, 2009a.

[17] Shoji, Y., T. Iwabuchi, Y. Hatanaka, H. Seko, R. Ichikawa, R. Ohtani, and N. Mannoji, GPS Meteorology: Research on the Construction of GPS Water Vapor Information System and Application to Meteorology, Geodesy, and Hydrology, *J. Geod. Soc. Japan*, **55**, 17-38, 2009b (in Japanese).

Unrefereed Articles

[18] Kato, T. and Y. Shoji, Environment of Niigata-Fukushima and Fukui Heavy Rainfall, *Technical Report of the Japan Meteorological Agency*, **129**, 174-185, 2006 (in Japanese).

[19] Shoji, Y., K. Aonashi, H. Nakamura, H. Seko, and A. Ichiki, Retrieval of Precipitable Water Vapor Using GPS Data Observed in 1997 Summer Campaign in Tsukuba, *Chikyu Monthly*, 25, 35-40, 1999 (in Japanese).

[20] Shoji, Y., T. Kawabata, Y. Aoyama, H. Seko, T. Tsuda and M. Kunii, Data Assimilation of Mt. Fuji Observed GPS Down-Looking Occultation Data into the JMA Mesoscale Numerical Weather Prediction Model, *Remote Sensing Applications of the Global Positioning System, (ed.) M. Bevis, Y. Shoji, and S. Businger, Proc. SPIE*, **5661**, 27-36; DOI:10.1117/12.578647, 2004.

[21] Shoji, Y., Analysis of a Cold Front on 29 June 1999 using GPS derived Precipitable Water Vapor, *Kishou Kenkyuu Note (Meteorological Research Notes)*, **208**, 89-96, 2005 (in Japanese).

[22] Shoji, Y. and M. Kunii, Data Assimilation Experiment of Near-realtime GPS PWV Retrieved from Ground GPS Network, *Suuchi Yohouka Houkoku Bessatsu (Additional Volume to Report of Numerical Prediction Division*, **53**, 147-152, 2007 (in Japanese).

[23] Shoji, Y., Assimilation method considering the effect of horizontal gradient of refractivity, *Suuchi Yohouka Houkoku Bessatsu (Additional Volume to Report of Numerical Prediction Division*, **53**, 144-146, 2007 (in Japanese).

[24] Shoji, Y., Development of Water Vapor Monitoring Technology: Overview and Perspective, *TENKI*, 54, 885-888, 2007 (in Japanese).

[25] Shoji, Y. and M. Kunii, Data Assimilation of Precipitable Water Vapor Retrieved from Nationwide GPS Network, *Kishou Kenkyuu Note (Meteorological Research Notes)*, 217, 228-238, 2008 (in Japanese).

[26] Shoji, Y., Application of GPS Derived Water Vapor Information for Weather Forecast, *CHANNEL*, **29-3**, 1, 2009 (in Japanese).

References

Aonashi, K., Y. Shoji, R. Ichikawa, and H. Hanado, Estimating spatial variation of humidity from GPS and WVR observation in Tsukuba. *Earth Planets Space*, **52**, 907–912, 2000.

Aonashi, K., T. Iwabuchi, Y. Shoji, R. Ohtani, and R. Ichikawa, Statistical Study on Precipitable Water Content Variations Observed with Ground-Based Microwave Radiometers. *J. Meteor. Soc. Japan*, **82**, 269–275, 2004:

Aoyama, Y., Y. Shoji, A. Mousa, T. Tsuda, and H. Nakamura, Temperature and Water Vapor Profiles Derived from Downward-Looking GPS Occultation Data, *J. Meteor. Soc. Japan*, **82**, 433-440, 2004.

Askne, J. and H. Nordius, Estimation of Tropospheric delay for microwaves from surface weather data, *Radio Sci*., **22**, 379-386, 1987.

Beutler, G., I. Bauersima, W. Gurtner, M. Rothacher, T. Schildknecht, and A. Geiger, Atmospheric refraction and other important biases in GPS carrier phase observation, in Atmospheric Effects on Geodetic Measurements, Monograph, **12**, pp. 15–43, School of Surveying, Univ. of New South Wales, Kensington, Australia, 1988.

Bevis, M., S. Businger, T. A. Herring, C. Rocken, R. A. Anthes, and R. H. Ware, GPS Meteorology: Remote sensing of atmospheric water vapor using or estimation of the wet delay. *J. Geophys. Res.*, **97**, 15,787-15,801, 1992.

Boehm, J., B. Werl, and H. Schuh, Troposphere mapping functions for GPS and very long baseline interferometry from European Centre for Medium-Range Weather Forecasts operational analysis data, *J. Geophys. Res.*, **111**, B02406, doi:10.1029/2005JB003629, 2006.

Boudouris, G., On the index of refraction of air, the absorption and dispersion of centimeter waves by gasses, *J. Res. Natl. Bur. Stand*., *Sect*., **67D**, 631-684, 1963.

Businger, S., S.R. Chiswell, M. Bevis, J. Duan, R. A. Anthes, C. Rocken, R. H. Ware, T. VanHove, and F. S. Solheim, The Promise of GPS in Atmospheric

Monitoring, *Bull. Am. Meteor. Soc*., **77**, 5-18, 1996.

Davis, J. L., T. A. Herring, I. I. Shapiro, A. E. E. Rodgers, and G. Elgered, Geodesy by radio interferometry: Effects of atmospheric modeling errors on estimates of baseline length, *Radio Sci*., **20**, 1593–1607, 1985.

Duan, J., M. Bevis, P. Fang, Y. Bock, S. Chiswell, S. Businger, C. Rocken, F. Solheim, T. VonHove, R. Ware, S. McClusky, T. A. Herring, and R. W. King, GPS meteorology: Direct estimation of the absolute value of precipitable water, *J. Appl. Meteor.*, **35**, 830–838, 1996.

Fabry, F., Meteorological value of ground target measurements by Radar, *J. Atmos. Oceanic Technol*., **21**, 560 -573, 2004.

Fabry, F., The spatial variability of moisture in the boundary layer and its effect on convection initiation: Project-long characterization, *Mon. Wea. Rev*., **134**, 79 91, 2006.

Fjeldbo, G., A. J. Kliore, and V. L. Eshleman, The neutral atmosphere of Venus as studied with the Mariner V radio occultation experiments. *Astron. J*., **76**, 123-140, 1971.

Flores, A., A. Escudero, M. J. Sedo´, and A. Rius, A near real time system for tropospheric monitoring using IGS hourly data. *Earth Planets Space*, **52**, 681–684, 2000.

Fujita M., F. Kimura, K. Yoneyama, and M. Yoshizaki, Verification of precipitable water vapor estimated from shipborne GPS measurements, *Geophys. Res. Lett.*, **35**, L13803, doi:10.1029/2008GL033764, 2008.

Furumoto, J., S Iwai, H. Fujii, T. Tsuda, W. Xin, T. Koike, and L. Bian, Estimation of Humidity Profiles with the L-Band Boundary layer rada-RASS Measurements. *J. Meteor. Soc. Japan*, **83**, 895-908, 2005.

Gendt, G., G. Dick, C. Reigber, M. Tomassini, Y. Liu, and M. Ramatschi, Near real time GPS water vapor monitoring for numerical weather prediction in Germany. *J. Meteor. Soc. Japan*, **82**, 361–370, 2004.

Goldsmith, J. E., M., S. E. Bisson, R. A. Ferrare, K. D. Evans, D. N. Whiteman, S. H. Melfi, Raman lidar profiling of atmospheric water vapor: simultaneous measurements with two collocated systems, *Bull. Am. Meteor. Soc*., 7. 975-982, 1994.

Gutman. S. I., S. R. Sahm, S. G. Benjamin, B. E. Schwartz, K. L. Holub, J. Q. Stewart, and T. L. Smith, Rapid retrieval and Assimilation of Ground based GPS Precipitable Water Observation at the NOAA Forecast Systems laboratory: Impact on Weather Forecasts, *J. Meteor. Soc. Japan*, **82**, 351-360, 2004.

Hatanaka, Y., Problems in GPS Near Real-time Analysis. *Kishou Kenkyuu Note (Meteorological Research Notes)*, **192**, 145–158, 1998 (in Japanese).

Hatanaka, Y., M. Sawada, A. Horita, and M. Kusaka, Calibration of antenna-radome and monument-multipath effect of GEONET-Part 1: Measurement of phase characteristic, *Earth Planets Space*, **53**, 13-21, 2001a.

Hatanaka, Y., M. Sawada, A. Horita, and M. Kusaka, Calibration of antenna-radome and monument-multipath effect of GEONET-Part 2: Evaluation of the phase map by GEONET data, *Earth Planets Space*, **53**, 13-21, 2001b.

Hocke, K., and T. Tsuda, Using GPS satellites to study plasma irregularities, *GPS World*, July 2001, 34-35, 2001a.

Hocke, K., and T. Tsuda, Gravity waves and ionospheric irregularities over tropical convection zones observed by GPS/MET radio occultation, *Geophys. Res. Lett.*, **28**, 2,815-2,818, 2001b.

Hoffmann-Wellenhof, B., H. Lichtenegger, and J. Collins, *GPS theory and practice, 5th rev*. ed., Springer-Verlag Wien New York, 2000.

Honda, Y. and K. Sawada, Upgrade of the Operational Mesoscale 4D-Var System at the Japan Meteorological Agency. *CAS/JSC WGNE Res. Activ. Atmos. Oceanic Model*, 2009.

Hurst, K. J. and Y. E. Bar-Sever, In-situ GPS antenna phase center calibration, *Proceedings of the Workshop 'GPS/MET JAPAN Has Come!'*, 54–63, 1998.

Ichikawa, R., H. Seko, and M. Bevis, An evaluation of geodetic positioning error simulated using a mesoscale nonhydrostatic model, *Remote Sensing Applications of the Global Positioning System, (ed.) M. Bevis, Y. Shoji, and S. Businger, Proc. SPIE*, **5661**, 37-45; DOI:10.1117/12.578647, 2004.

Ishikawa, Y., and K. Koizumi, One month cycle experiments of JMA mesoscale 4-dimensional variational data assimilation (4D-Var) system. *Research Activities in Atmospheric and Oceanic Modeling*. **32**, WMO/TD-No. 1105,01.26-01.27, 2002.

Ishikawa, Y., Application of GPS Signal Delay Observed by Ground-based Receivers, Validation and Upgrading of Analysis-Forecast System, *Suuchi Yohou Kenshuu Text (Text for NWP Training Course)*, **41**, 53-57, 2008 (in Japanese).

Iwasaki, H., and T. Miki, Observation study on the diurnal variation in precipitable water associated with the thermally induced local circulation over the "semi-basin" around Maebashi using GPS data, *J. Meteor. Soc. Japan*, **79**, 1,077-1,091, 2001.

Iwabuchi, T., I. Naito, S. Miyazaki, N. Mannoji, Precipitable water vapor moved along a front observed by the Nationwide GPS Network of Geographical Survey Institute, *TENKI*, **44**, 765-766, 1997 (in Japanese).

Kato, T., and K. Aranami, Formation Factors of 2004 Niigata-Fukushima and Fukui heavy rainfalls and problems in the predictions using a cloud-resolving Model. *SOLA*, **1**, 1-4, doi:10.2151/sola.2005-001, 2005.

Kawabata, T., Y. Shoji, H. Seko, and K. Saito, Assimilation Experiment of a Local Heavy Rainfall Event with a Cloud-Resolving 4D-Var Assimilation System, *Proceedings of International Symposium on Radar and Modeling Studies of the Atmosphere*, Nov., 2009.

Koizumi, K., and Y. Sato, Impact of GPS and TMI precipitable water data on mesoscale numerical weather prediction model forecasts. *J. Meteor. Soc. Japan.*, **82**,453-457, 2004.

Koizumi, K., Y. Ishikawa and T. Tsuyuki, Assimilation of Precipitation Data to the JMA Mesoscale Model with a Four-dimensional Variational Method and its Impact on Precipitation Forecasts. *SOLA*, **1**, 45-48, 2005.

Kunii, M., H. Seko, Y. Shoji, and T. Tsuda, Meso-scale Data Assimilation Experiments in Low latitudes with GPS RO data, *Proceedings of the 4th FORMOSAT-3/COSMIC User's Workshop*, Oct., 2009.

Kuroishi, Y., H. Ando, and Y. Fukuda, A new hybrid geoid model for Japan, GSIGEO2000. *J. Geodesy,* **76**, 428-436, doi:10.1007/s00190-002-0266-5, 2002.

Lemoine, F. G., S. C. Kenyon, J. K. Factor, R. G. Trimmer, N. K. Pavlis, D. S. Chinn, C. M. Cox, S. M. Klosko, S. B. Luthcke, M. H. Torrence, Y. M. Wang, R. G. Williamson, E. C. Pavlis, R. H. Rapp, and T. R. Olson, Joint NASA GSFC and the National Imagery and Mapping Agency (NIMA) geopotential model EGM96,

NASA/TP- 1998-206861, 1998.

Maanen, J.V., Objective analysis of humidity by the optimum interpolation method. *Tellus*, **33**, 113–122, 1981.

MacMillan, D.S., Atmospheric gradients from very long baseline interferometry observations. *Geophys. Res. Lett*., **22**, 1041–1044, 1995.

Mannoji, N., H. Tada, Y. Hatanaka, R. Ohtani, and I. Naito, An impact study of precipitable water estimated from ground-based GPS network over Japan. *Proceedings of 12th Conference on Numerical Weather Prediction*, 77-80, 1998.

Matsumoto, K., T. Sato, T. Takanezawa, and M. Ooe, GOTIC2: A Program for Computation of Oceanic Tidal Loading Effect, *J. Geodet. Soc. Japan*, **47**, 243-248, 2001.

Moninger, W.R., R. D. Mamrosh, and P. M. Pauley, Automated Meteorological Reports from Commercial Aircraft, *Bull. Amer. Meteor. Soc*., **84**, 203-216, 2003.

Nakamura, H., K. Koizumi, and N. Mannoji, Data assimilation of GPS precipitable water vapor into the JMA mesoscale numerical weather prediction model and its impact on rainfall forecast. *J. Meteor. Soc. Japan*, **82**, 441-452, 2004a.

Nakamura, H., H. Seko, Y. Shoji, and Aerological Observatory, Dry Biases of Humidity Measurements from the Vaisala RS80-A and Meisei RS2-91 Radiosondes and from Ground-Based GPS, *J. Meteor. Soc. Japan*, **82**, 277-299, 2004b.

Nash, J., R. Smout, T. Oakley, B. Pathack, and S. Kurnosenko, *WMO intercomparison of high quality rediosonde systems, Vacoas, mauritius*, 2-25, February 2005.

Niell, A. E., Global mapping functions for the atmosphere delay at radio wavelengths. *J. Geophys. Res.*, **101**, 3227–3246, 1996.

Nishida, M., A. Shimizu, T. Tsuda, C. Rocken, and R. Ware, Seasonal and Longitudinal Variations in the Tropical Tropopause Observed with the GPS Occultation Technique (GPS/MET), *J. Meteor. Soc. Japan*, **78**, 691-700, 2000.

Noguchi, W., T. Yoshihara, T. Tsuda, and K. Hirahara (2004): Time-Height Distribution of Water Vapor Derived by Moving Cell Tomography During Tsukuba GPS Campaigns, *J. Meteor. Soc. Japan*, **82**, 561-568.

Ohtani, R., and I. Naito, Comparison of GPS-derived precipitable water vapors with radiosonde observations in Japan. *J. Geophys. Res.*, **105**, 26917-26929, 2000.

Owens, J. C., Optical Refractive Index of Air: Dependence on Pressure, Temperature and Composition, *Applied Optics*, **6**, 51-59, 1967.

Ozawa, E., GPS, *Suuchi Yohouka Houkoku Bessatsu (Additional Volume to Report of Numerical Prediction Division*, **53**, 133-139, 2007 (in Japanese).

Rocken. C., T. VanHove, J. Johnson, F. Solheim, R. H. Ware, M. Bevis, S. Businger, and S. R. Chiswell, GPS/STORM-GPS sensing of atmospheric water vapor for meteorology. *J. Atmos. Oceanic Technol.*, **12**, 468-478, 1995.

Rothachar. M., and L. Mervart, The Bernese GPS software version 4.0 user manual report, *Astron. Inst., Univ. of Bern*, Bern, Switzerland, 1996.

Sasaki, T., and F. Kimura, Diurnal Variation of Water Vapor Content over the Kanto Area during Clear Summer Days Observed through GPS Precipitable Water, *TENKI*, **48**, 65-74, 2001 (in Japanese).

Saito, K., T. Fujita, Y. Yamada, J. Ishida, Y. Kumagai, K. Aranami, S. Ohmori, R. Nagasawa, S. Kumagai, C. Muroi, T. Kato, H. Eito and Y. Yamazaki, The operational JMA Nonhydrostatic Mesoscale Model. *Mon. Wea. Rev.*, **134**, 1266-1298, 2006.

Saito, K., J. Ishida, K. Aranami, T. Hara, T. Segawa, M. Narita, and Y. Honda, Nonhydrostatic atmospheric models and operational development at JMA. *J. Meteor. Soc. Japan,* **85B**, 271-304, 2007.

Sato, T., and F. Kimura, Diurnal cycle of convective instability around the central mountains in Japan during the warm season, *J. Atmos. Sci*, **62**, 1,626-1,636, 2005.

Sato, T. and H. Hanada, A Program for the Computation of Oceanic Tidal Loading Effects 'GOTIC', *Publications of the International Latitude Observatory of Mizusawa,* **18**, 29–47, 1984.

Schwiderski, E. W., NSWC Global Ocean Tide Data (GOTD) Tape, *U. S. Naval Surface Welfare Center*, Dahlgren, Virginia, 1981.

Seko, H., H. Nakamura, and S. Shimada, An Evaluation of Atmospheric Models for GPS data Retrieval by Output from a Numerical Weather Model, *J. Meteor.*

Soc. Japan, **82**. 339-350, 2004a.

Seko, H., H. Nakamura, Y. Shoji, and T. Iwabuchi, Meso-γ scale water Vapor Distribution associated with the Thunderstorm on 1 August 2001 Estimated by the Tomography Method. *J. Meteor. Soc. Japan*, **82**, 569–586, 2004b.

Seko, H., T. Kawabata, T. Tsuyuki, H. Nakamura, K. Koizumi, and T. Iwabuchi, Impacts of GPS-derived Water vapor and Radial Wind measured by Doppler radar on Numerical Prediction of Precipitation. *J. Meteor. Soc. Japan*, **82**, 473-489, 2004c.

Seko, H., Y. Shoji, M. Kunii, and Y. Aoyama, Impact of the CHAMP Occultation Data on the Rainfall Forecast Case study on 16 July 2004. *Data Assim. Atmos., Ocean, and Hydro. Appl.*, Springer-Verlag, 197-218, 2009a.

Seko, H., H. Yamauchi., O. Suzuki, and K. Saito, Estimation of Temporal variation of Refractive Index Using C-band Doppler radar Equipped with magnetron Transmitter, *SOLA*, **5**, 145-148, 2009b.

Sengoku, A. and T. Sato, Site displacement due to Solid Earth Tide and Ocean Loading at SLR, VLBI and GPS Observation Sites in Japan, Journal of the Japan Society for Marine Surveys and Technology, **7**, 1–7, 1995 (in Japanese).

Shimada, S., H. Seko, H. Nakamura, K. Aonashi and T.A. Herring, The impact of atmospheric mountain lee waves on systematic geodetic errors observed using the Global Positioning System. *Earth Planets Space*, **54**, 425–430, 2002.

Shoji, Y., K. Aonashi, H. Nakamura, H. Seko, and A. Ichiki, Retrieval of Precipitable Water Vapor Using GPS Data Observed in 1997 Summer Campaign in Tsukuba, *Chikyu Monthly*, 25, 35-40, 1999 (in Japanese).

Shoji, Y., H. Nakamura, K. Aonashi, A. Ichiki, H. Seko, and Members of GPS/MET Japan summer Campaign 1997 in Tsukuba, Semi-diurnal and diurnal variation of errors in GPS precipitable water vapor at Tsukuba, Japan caused by site displacement due to ocean tidal loading, *Earth Planets Space*, **52**, 685-690, 2000.

Shoji, Y., H. Nakamura, T. Iwabuchi, K. Aonashi, H. Seko, K. Mishima, A. Itagaki, R. Ichikawa, and R. Ohtani, Tsukuba GPS Dense Net Campaign Observation: Improvement in GPS Analysis of Slant Path Delay by Stacking One-way Postfit Phase Residuals. *J. Meteor. Soc. Japan*, **82**, 301–314, 2004.

Shoji, Y., Assimilation method which taking into account the effect of horizontal refractivity gradient, *Suuchi Yohouka Houkoku Bessatsu (Additional Volume to Report of Numerical Prediction Division*, **53**, 144-146, 2007 (in Japanese).

Shoji, Y. and M. Kunii, Data Assimilation of Precipitable Water Vapor Retrieved from Nationwide GPS Network, *Kishou Kenkyuu Note (Meteorological Research Notes)*, **217**, 228-238, 2008 (in Japanese).

Shoji, Y., A Study of Near Real-time Water Vapor Analysis Using a Nationwide Dense GPS Network of Japan. *J. Meteor. Soc. Japan*, **87**, 1-18, 2009.

Shoji, Y., M. Kunii, and K. Saito, Assimilation of Nationwide and Global GPS PWV Data for a Heavy Rain Event on 28 July 2008 in Hokuriku and Kinki, Japan, *SOLA*, **5**, 45-48, 2009a.

Shoji, Y., T. Iwabuchi, Y. Hatanaka, H. Seko, R. Ichikawa, R. Ohtani, and N. Mannoji, GPS Meteorology: Research on the Construction of GPS Water Vapor Information System and Application to Meteorology, Geodesy, and Hydrology, *J. Geod. Soc. Japan*, 55, 17-38, 2009b.

Shoji, Y., M. Kunii, and K. Saito, Mesoscale Data Assimilation of Myanmar Cyclone Nargis Part II : Assimilation of GPS Derived Precipitable Water Vapor, *J. Meteor. Soc. Japan,* 2010 (submitted).

Syndergaard, S, E. R. Kursinski, B. M. Herman, E. M. Lane, D. E. Flittner, A refractive index mapping operator for assimilation of occultation data. *Mon. Weather. Rev*. **133**, 2650–2668, 2005.

Thayer, D., An improved equation for the radio refractive index of air, *Radio Sci.*, **9**, 803-807, 1974.

Tsuda. T., M. Nishida, C. Rocken, and R. H. Ware, A global morphorogy of gravity wave activity in the stratosphere revealed by the GPS occultation data (GPS/MET), *J. Geophys. Res.*, **105**, 7,257-7,273, 2000.

Vance, A. K., J. P. Taylor, T. J. Hewison, and J. Elms, Comparison of in situ humidity data from aircraft, dropsonde, and radiosonde. *J. Atmos. Oceanic. Technol*., **21**, 921-932, 2004.

Wang. J., H. L. Cole, D. J. Carlson, E. R. Miller, K. Beierle, A. Paukkunen, and T. K. Laine, Correlations of humidity measurement errors from the Vaisala RS-80 radiosonde – Application to TOGA-COARE data. *J. Atmos. Oceanic*

Technol., **19**, 981-1002, 2002.

Ware, R., M. Exner, D. Feng, M. Gorbunov, K. Hardy, B. Herman, Y. Kuo, T. Meehan, W. Melbourne, C. Rocken, W. Schreiner, S. Sokolovskiy, F. Solheim, X. Zou, R. Anthes, S. Businger, and K. Treberth, GPS Sounding of the Atmosphere from Low Earth Orbit: Preliminary Results, *Bull. Amer. Meteor. Soc.*, **77**, 19-40, 1996.

Webb, F. H., and J. F. Zumberge, An introduction to the GIPSY/OASIS-II, *JPL Publ*., D-11088, 1993.

Wulfmeyer, V. and J. Boesenberg, Ground-based differential absorption lidar for water-vapor profiling: Assesment of accuracy, resolution, and meteorological applications, *Applied Optics*, **37**, 3825-3844, 1998.

Yoshihara, T., N. Fujii, S., Saito, Y., Sakai, Y., Matsunaga, O., Hoshino, T., Tsuda, Y. Aoyama, and S. Danno, Airborne-Based Downward-looking GPS Occultation Experiments, *J. IEICE,* **J89-B**, 1233-1241, 2006 (in Japanese).

Zumberge, J. F., M. B. Heflin, D. C. Jefferson, M. M. Watkins, Precise point positioning for the efficient and robust analysis of GPS data from large networks, *J. Geophys. Res.*, **102(B3)**, 5005–5017, 1997.